Real-time Sub-carrier Adaptive Modulation and Coding in Wideband Orthogonal Frequency Division Multiplexing Wireless Systems

by

Farinaz Edalat

B.S., Computer Engineering
University of Illinois Urbana-Champaign, 2001
and
M.S., Electrical Engineering and Computer Science
Massachusetts Institute of Technology, 2003

Submitted to the Department of Electrical Engineering and Computer Science
in partial fulfillment of the requirements for the degree of

Doctor of Philosophy

at the

MASSACHUSETTS INSTITUTE OF TECHNOLOGY

February 2008

Author .....
Department of Electrical Engineering and Computer Science
December 13, 2007

Certified by .....
Charles G. Sodini
Professor of Electrical Engineering and Computer Science
Thesis Supervisor

Accepted by .....
Terry P. Orlando
Chairman, Department Committee for Graduate Students

Real-time Sub-carrier Adaptive Modulation and Coding in Wideband Orthogonal Frequency Division Multiplexing Wireless Systems

by

Farinaz Edalat

Submitted to the Department of Electrical Engineering and Computer Science
on December 13, 2007, in partial fulfillment of the
requirements for the degree of
Doctor of Philosophy

Abstract

The increasing demand for high speed wireless connectivity at low cost proposes new challenges for communication systems designers to implement solutions that increase the data rate by utilizing the limited radio resources more efficiently at a low additional complexity. *Sub-carrier Adaptive Modulation and Coding (AMC)* exploits the high frequency diversity in wideband Orthogonal Frequency Division Multiplexing (OFDM) channels to obtain higher data rates. While prior work has discussed the value of sub-carrier AMC from a theoretical perspective, this work presents the design and performance of a real-time sub-carrier AMC system.

We describe our OFDM transceiver prototype, which implements real-time sub-carrier AMC for a wideband wireless channel. We discuss how our design achieves accurate and consistent Signal-to-Noise Ratio (SNR) estimates, which are critical for the success of AMC. We compare the performance of sub-carrier AMC with a non-adaptive scheme that assigns the same modulation and channel coding to all sub-carriers that can support that modulation and coding for the target Bit Error Rate (BER). For a conservative comparison, we compare against the uniform modulation/coding assignment that achieves the highest data rate. Our experiments over the wireless channel show that for a target coded BER of 10^{-5}, our system achieves average data rates of 308.3 and 237.1 Mbps across a variety of Line-of-Sight (LOS) and Non Line-of-Sight (NLOS) locations respectively, which result in *34%* and *40%* gain over the best non-adaptive scheme. Equivalently, such data rate gain from AMC translates to an SNR improvement of 3 dB. Finally, our implementation of AMC incurs a low overhead of *1.1%* of the data rate, and a reasonable complexity, occupying *9.95%* of the total transceiver gates on the Field Programmable Gate Array (FPGA).

Thesis Supervisor: Charles G. Sodini
Title: Professor of Electrical Engineering and Computer Science

Acknowledgment

There are many people that I would like to thank without whom the completion of this thesis would have not been possible.

First and foremost, I would like to express my whole-hearted gratitude to my advisor, Prof. Charlie Sodini, for his invaluable guidance, insight, and encouragement throughput this thesis work. Charlie thought me how to think critically about a problem and how to present effectively. I also learned the importance of balancing between my work and personal life for success and happiness. Indeed, my best experience at MIT was working with Charlie, who I believe prepared me well for the professional life after.

I would like to thank my committee members professors Muriel Medard and Gregory Wornell for their invaluable time and guidance throughout this thesis, particularly on the system issues.

My special appreciation goes to the entire WiGLAN team: Jit Ken Tan, Nir Matalon, Khoa Nguyen, Hariharan Rahul, and Yun Wu. In fact, without the RF Front-End and Data Converters design by Nir and the digital baseband transceiver implementation by Ken, and the numerous helps from Khoa, our transceiver prototype would have not existed and this work would have not been possible. I would like to thank Ken for his continuing consultation support after graduating from MIT.

Furthermore, other individuals whose expert advise was significant to the success are Prof. Muriel Medard, Prof. Dina Katabi and Manish Bhardwaj. In particular, Manish Bhardwaj, with expertise in both communications theory and practice, offered invaluable recommendations. I would also like to thank Manish Goel and Anuj Batra from Texas Instruments for offering expert discussions on digital and RF implementations.

My tremendous thanks go to all my officemates for their technical support and continuing friendship (even after gradation). I am grateful to my caring cubiclemates: Matthew Guyton, Sungah Lee and Mariana Markova. I would like to thank Todd Sepke and Mark Spaeth for helping with the computing issues. Also, having an

expert skier, John Fiorenza, helped me to learn skiing on Moguls more aggressively. Special thanks go to Kevin Ryu for organizing birthday lunches and offering unique birthday cards. My thanks go to the rest of the group who made the office a fun and comfortable environment to work: Pablo Acosta-Serafini, Albert Chow, Jack Chu, Jeff Feng, David He, Albert Jerng, Lunal Khuon, Kevin Lu, Ivan Nausieda, Johnna Powell, and Andy Wang.

My gratefulness is extended to Debroah Hoghes-Pabon for her always loving and caring support, and to Rhonda Maynard and Marilyn Pierce for their exceptional work to speed-up all the administrative processes. I am very thankful of Bob Richards, at MIT Career Office, for his invaluable instructions during the job hunting process.

I would like to thank all my other friends and colleagues for their warmth and laughters that made MIT a truly fun and memorable place to be. I am also fortunate to have had wonderful roommates, Miriam Bruhn and Shuyin Sim, who made home a truly cozy and relaxing place.

Finally, I would like to thank my family for always being there for me. I thank my fantastic sister and brother for their love and support. I thank my mom for her unconditional love and wisdom that helped me survive the difficult times, and my dad for his always brilliant advises and continuing supervision which provided me confidence and strength to always take one step further and challenge myself. I would like to dedicate this thesis to my mom and dad.

This work is sponsored, in part, by the National Science Foundation under Grant No. ANI-0335256, the Center for Integrate Circuits and Systems, and the Texas Instruments Leadership in Microelectronics Graduate Women Fellowship.

Contents

List of Figures

List of Tables

Chapter 1

Introduction

The explosive demand for seamless wireless connectivity of all types of services - particularly multimedia applications, such as voice, data and video - over a resource-limited radio justifies the need for a wireless communications system that utilizes the available bandwidth efficiently and provides data rates close to the channel capacity. We propose to meet the demand for high data rate in the wireless fading environment by using:

- Wide Bandwidth
- Orthogonal Frequency Division Multiplexing (OFDM) Technology
- Sub-carrier Adaptive Modulation
- Adaptive Error Correction Coding

These will be introduced in the following sections. In addition, other means to improve the data rate include spatial diversity and multiplexing using Multiple-Input Multiple-Output (MIMO), adaptive antenna (such as beamforming), and power adaptation techniques. These techniques are used in the high throughput mode of the new Wireless Local Area Network (LAN) IEEE standard 802.11n [1] and WiMAX (Worldwide Interoperability for Microwave Access) that is based on the Wireless Broadband Access IEEE 802.16 standard [2]. For instance, in the 802.11n standard, the data

rate can be increased from a 1x1 antenna maximum rate of 150 Mbps (Mega bits-per-second) to a 4x4 antenna maximum rate of 600 Mbps.

Furthermore, to quantify the increased data rate achievable from sub-carrier Adaptive Modulation and Coding (AMC) in a real environment, we implement this technique on a wideband OFDM transceiver prototype for the *Wireless Giga-bit Local Area Network (WiGLAN)* system at MIT.

1.1 Wideband Channel

By the fundamental principles of communications, wider transmission bandwidth results in a higher **channel capacity**.

Definition 1.1.1. *Channel capacity* is the maximum rate of information for which an arbitrary small error probability can be achieved [3].

The capacity of an additive white Gaussian noise (AWGN) channel , C_{awgn}, with a received Signal-to-Noise Ratio, SNR, is proportional to the transmission bandwidth, W, as given by Claude Shannon's well-known formula [4]:

$$C_{awgn} = W\, log_2(1 + SNR) \quad bits/s \tag{1.1}$$

Moreover, over a wider bandwidth, the **frequency diversity** is higher. In a wideband channel, the transmitted signal - reflected, scattered and diffracted from various objects in the environment - arrives over multiple symbol times, and frequency diversity is achieved by the ability to resolve the multipaths at the receiver [3]. Equivalently, in the frequency domain, channel fading is no longer flat over the transmission bandwidth; instead, it is *frequency selective.* The high frequency diversity of a wideband channel can be exploited to increase the data rate by using OFDM and adaptive transmission techniques, which will be described next.

1.2 OFDM Technology

Orthogonal Frequency Division Multiplexing (OFDM) has been proven as an efficient multi-carrier modulation technique to transmit at high data rate over the hostile multipath wireless channel. Multi-carrier modulation divides the frequency-selective wideband channel into multiple non-interfering narrowband flat-fading sub-channels, each modulated on a separate sub-carrier. Equivalently, in the time domain, the high data rate stream is converted into multiple lower rate streams that are sent in parallel. Fig. 1-1 [5] indicates the difference between single-carrier modulation and OFDM on transmitted and received signal in the time and frequency domain. In addition, Fig. 1-1b shows that OFDM replaces the complex equalizer that is needed in single-carrier systems with significantly simpler one-tap equalizers. OFDM is an efficient version of multi-carrier modulation because it utilizes the available spectrum more efficiently by allowing sub-carriers to overlap without causing *Inter-Carrier Interference (ICI)*. This is due to the orthogonality of its sub-carriers. For the presentation clarity, Fig. 1-1 does not show the interference-free overlap of the OFDM sub-carriers. Finally, OFDM provides an efficient implementation through Inverse Fast Fourier Transform (IFFT) and Fast Fourier Transform (FFT) at the transmitter and receiver respectively.

The first OFDM wireless system was the European Digital-Audio-Broadcasting (DAB). Later, it was used in the European Digital-Video-Broadcasting (DVB)-T (Terrestrial), DVB-H (Handheld) and Digital-Multimedia-Broadcasting (DMB). Today, many of the high data rate wireless standards have adopted OFDM as the preferred technology of choice, including:

- Wireless LAN: IEEE 802.11a and 802.11n in the U.S., and High Performance LAN (HIPERLAN)/2 in Europe.
- Broadband Wireless Access Networks: IEEE 802.16-2004 and 802.16e-2005, which are adopted by Fixed and Mobile WiMAX respectively.

Discrete-Multi-Tone (DMT), a more popular terminology for OFDM in wired systems, has been proven to be an excellent method to deliver high speed data to customers

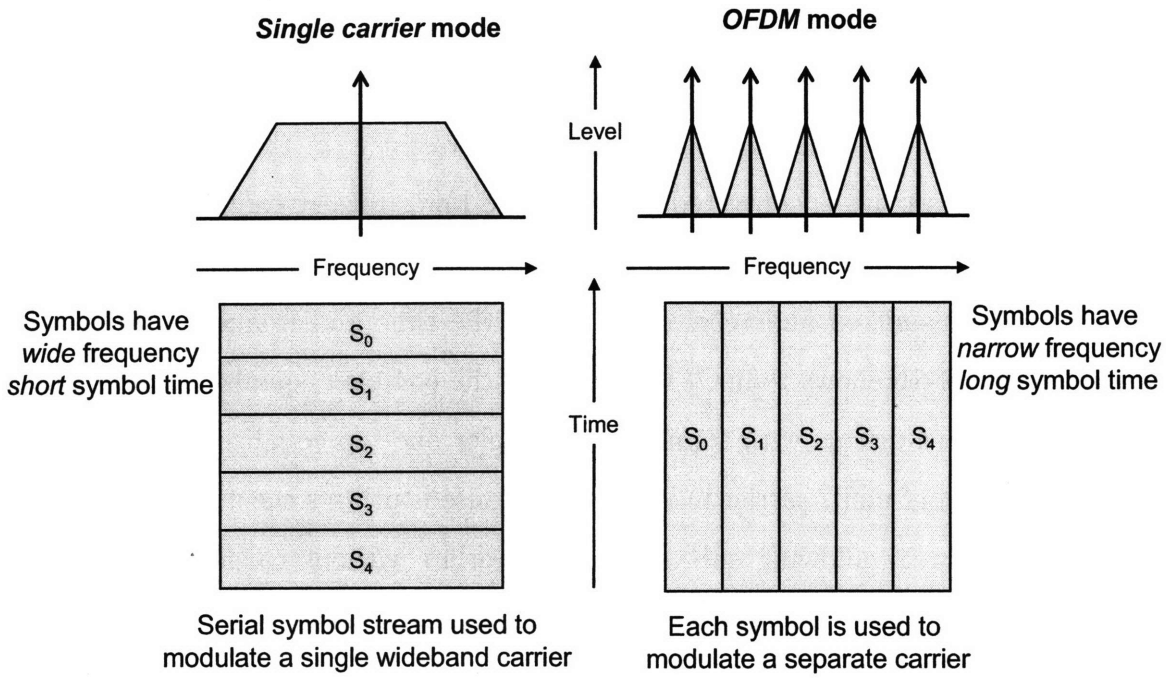

(a) Single carrier and OFDM *transmitted* signals

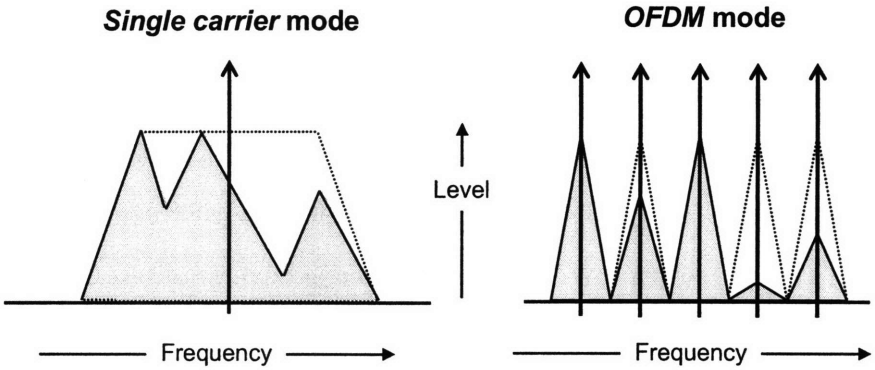

(b) Single carrier and OFDM *received* signals

Figure 1-1: Comparison between using a single carrier and OFDM modulation on transmitted and received signals (adopted from [5]).

at a low cost for Asymmetric Digital Subscriber Line (ADSL) (1.536 Mbps), High bit-rate DSL (HDSL) (1.6 Mbps), and Very high-speed DSL (VDSL) (100 Mbps) [6, 7].

In addition to mitigating multipath fading of the wireless channel, OFDM enables exploitation of the channel's frequency diversity to increase the data rate by adapting the modulation type and channel coding of each sub-carrier independently. The next two sections introduce the sub-carrier Adaptive Modulation and Coding schemes, and provide background information on these topics.

1.3 Sub-carrier Adaptive Modulation

Adaptive transmission techniques enable a spectrally efficient transmission over frequency-selective channels. The basic premise is to estimate the channel at the receiver and feed this estimate back to the transmitter, so that the transmission scheme can be adapted relative to the channel characteristics. In the case of not adapting to the fading conditions, the error probability is dominated by the sub-carriers in deep fade. Thus, a fixed link margin is required to maintain an acceptable performance under worse-case channel conditions. This results in an inefficient use of the channel.

Adapting to the channel fading can increase the average throughput, reduce required transmit radio-frequency (RF) power, or reduce average Bit Error Rate (BER) by taking advantage of favorable channel conditions to send at higher data rates or lower RF power; in contrast, as the channel degrades, it reduces the data rate or increases the RF power [8]. **Sub-carrier Adaptive Modulation** is a form of adaptive transmission technique that assigns to each sub-carrier the most efficient modulation that is supported by the sub-channel at a given target BER.

1.3.1 Work in the Literature

The principle of adapting transmission parameters to the channel conditions in narrowband fading channels was recognized by Hayes [9] as early as 1968, and by Cavers [10] in 1972. In 1989, Kalet [11] proposed adaptive *modulation* over OFDM, and later

Czylwik [12], Chow, Cioffi and Bingham [13] further developed this idea. These pioneer works on sub-carrier adaptive modulation suggest the benefits of this adaptation scheme in frequency-selective channels.

It is well-known that when the channel conditions are available to both the transmitter and the receiver, the channel capacity is achieved if the modulation of individual sub-carriers as well as power are optimally adapted to the sub-channel fading conditions, where the optimal power allocation is the *"water-filling"* (see Section 4.3.2) [14]. However, while "water-filling" yields the optimal solution, it is computationally expensive and assumes infinite granularity in constellation size, which is not realizable. There are many theoretical works that propose practical (but sub-optimal) adaptive loading (modulation and/or power) algorithms. The most well-known algorithms are:

- *Hughes-Hartogs [15, 16] algorithm:* minimizes the transmit RF power for a fixed BER and a fixed data rate. It achieves this by allocating bits one by one, each time selecting the sub-carrier that can transmit the additional bit with the least additional transmit power for a target BER. However, this comprehensive sorting strategy is too complex for a practical implementation in high speed Wireless LAN. Its algorithmic complexity is proportional to $O(N_{BPS} \times N_{FFT})$, where N_{BPS} is the number of bits assigned to each OFDM symbol and N_{FFT} is the number of OFDM sub-carriers (which is the size of the IFFT/FFT implementing OFDM).

- *Chow et al. [13] algorithm:* proposes a bit loading algorithm with a more feasible implementation than "water-filling" but with an insignificant performance degradation (up to 1.3 dB SNR) in simulation of an ADSL system. The degradation in performance is due to constraining the constellation sizes from 2 to 10 bits. The algorithm aims to achieve a fixed total bit rate while adapting both modulation and power per sub-carrier. Its worst case algorithmic complexity is proportional to $O(I \times N_{FFT} + 2N_{FFT})$ where I is the maximum number of allowable iteration steps.

- *Fischer et al. [17] algorithm:* distributes the bits and power over the sub-carriers in order to minimize the BER at a constant total bit rate and transmit power. Although its worst case algorithmic complexity is comparable to Chow et al. algorithm, it is computationally simpler with performance superior or at least equivalent to the above two algorithms in terms of achievable BER.

- *Piazzo [18] algorithm:* minimizes the transmit power for a fixed BER and data rate. It is the most efficient of all above algorithms as it replaces the linear incremental search by a logarithmic search.

Kalet [11] simulates an OFDM system with sub-carrier adaptive modulation and power, where for each sub-carrier a Quadrature Amplitude Modulation (QAM) modulation is chosen to maximize the bit rate, and the power is distributed close to "water-filling" under the constraint of BER = 10^{-5} per sub-carrier and a fixed total transmit RF power. The performance of such adaptive OFDM system is about 9 dB worse than the channel capacity independent of the channel transfer function.

Czylwik [12] simulates an uncoded OFDM transmission system with time-variant channel transfer functions, that are measured by a wideband (6 MHz) channel sounder in an outdoor environment with fixed antennas at 1.8 GHz carrier frequency. The simulation results show that compared to non-adaptation, sub-carrier adaptive modulation with optimum power distribution results in a signal power reduction of 5 to 15 dB (depending on SNR and propagation scenario) at BER = 10^{-3}. However, the gain from power adaptation over constant power is only 1 dB, and hence, using constant power is recommended instead. The modulations are chosen among {none, Binary Phase-Shift Keying (BPSK), 4-, 8-, 16-, 32-, 64-, 128-, 256-QAM} such that the BER is minimized in order to maintain a constant bit rate. However, the simulated system ignores the feedback channel, and assumes ideal time and frequency synchronization.

Van der Perre et al. [19] simulate a high-speed (data rate of 100 Mbps) OFDM Wireless LAN system with adaptive loading based on Fischer algorithm. The multipath channel is modeled using ray-tracing of a typical corridor in an office environment at 2.4 GHz carrier frequency. Simulation results show that the adaptive loading al-

gorithm provides an SNR gain of 14 dB with respect to a fixed modulation (4-QAM) scheme at BER $= 10^{-3}$.

In Chapter 4, we compare how our measured performance results using sub-carrier Adaptive Modulation OFDM transceiver compare to the theoretical "water-filling", as well as the simulated SNR gains obtained by Kalet, Czylwik and Van der Perre et al. Our results indicate that at BER $= 10^{-3}$, the performance of our Adaptive Modulation scheme is on average 4.4 dB less than the optimal "water-filling" strategy in various NLOS and LOS locations. In addition, the average SNR gain from our Adaptive Modulation algorithm over using the same modulation (4-QAM) on all sub-carriers that can support it, is 7 dB in LOS locations and 4 dB in NLOS locations. Hence, our measured gain is less by 1 dB in LOS and 10 dB in NLOS scenarios from the theoretical predictions by Czylwik and Van der Perre et al. However, as our gain is calculated compared to a fixed modulation over the subset of supporting sub-carriers, rather than *all* sub-carriers (as it is used in obtaining theoretical gains), we expect higher gains than above. However, the lower SNR gain from our Adaptive Modulation algorithm is mainly due to:

- Our algorithm is less by 4.4 dB SNR from "water-filling," while the theoretical adaptive algorithms perform close (within 1.3 dB) to this optimal solution.

- Our algorithm takes into account practical issues in a real system such as hardware non-idealities and synchronization errors, which degrade the attainable gain from sub-carrier Adaptive Modulation.

Consequently, the significance of our work is justified as it quantifies the actual gain that is achievable in a real system, which cannot be predicated by theory without having knowledge of all the practical design issues.

1.3.2 Current Standards

Some of the current wireless OFDM standards, such as the Wireless LAN IEEE 802.11a [20] and 802.11n [1] standards, use the same modulation and coding type

across all sub-carriers, and adapt the modulation and coding scheme to the temporal variations in the channel rather than its frequency variations. However, in the multiple antenna implementation of 802.11n, different modulations (but same coding rate) can be sent on different spatial streams (up to 4) [1].

On the other hand, some other standards use a form of Adaptive Modulation and Coding (AMC) similar to the sub-carrier AMC. The closest standard is the IEEE 802.16e with Orthogonal Frequency Division Multiple Access (OFDMA) that has been selected by the WiMAX Forum as the basic technology for portable and mobile applications. In this standard, to keep the signalling overhead low, the sub-carriers are grouped into a small number of blocks (*e.g.* 10) and different modulation and coding modes are used across different blocks, while a single single mode is used across all sub-carriers within a block. In WiMAX, the FFT-size can vary from 128 to 2,048 depending on the available bandwidth, but the sub-carrier spacing is fixed at 10.94 kHz [21].

Wired cable modem standards, such as ADSL, HDSL, and VDSL [22], use sub-carrier adaptive modulation technique, but as these systems have very stable channel characteristics, they are quite different from the wireless case. In particular, during the initialization phase of each session, they can spend a long time to acquire accurate SNR estimations. However, the overhead from such protocol cannot be afforded by the changing wireless channel. Thus, the design and performance of real-time adaptive modulation in wireless systems is still open.

1.3.3 Current State-of-Art

Few papers [23, 24] investigate the hardware implementation details of sub-carrier adaptive modulation. However, these papers do not implement the adaptive modulation in real-time, and hence, they do not address the design issues and performance of such schemes.

For instance, Wouters et al. [23] implement a sub-carrier adaptive modulation and power using the Fischer's algorithm [17] on Xilinx Virtex 2 XC2V6000 FPGA. However, the performance is studied in simulation using channel models and pro-

grammable time and frequency offsets without a feedback path. Their implementation of adaptive loading (sub-carrier power estimation and recursive bit assignment) occupies 25% slices of the OFDM modem.

Veillcux et al. [24] implement a sub-carrier adaptive modulation algorithm on the same FPGA as above, and study the performance in simulation using channel models with feedback channel and assuming perfect time synchronization.

Consequently, the lack of reports on the performance of sub-carrier Adaptive Modulation in a real environment - *i.e.* over the wireless channel and under the non-idealities from hardware and synchronization algorithms, motivates our work.

1.4 Adaptive Error Correction Coding

Fundamentally in all communications systems, *Forward Error Correction (FEC)* coding techniques are incorporated to reduce the system SNR requirements at low required BER values. In some systems, an Automatic Repeat reQuest (ARQ) mechanism is used, which re-sends the data packet when the FEC cannot correct the errors.

In addition, in an OFDM system with frequency-selective fading channel, coding by itself provides an alternative technique to combat the channel's fading. In other words, in the absence of adaptive modulation, coding combined with frequency and time interleaving protects the data transmitted on sub-carriers in deep fades.

To increase the data rate, **adapting modulation and coding per sub-carrier** would perform better than adapting only one of them. Hence, we focus on coding in the presence of adaptive modulation in OFDM systems.

1.4.1 Work in the Literature

One of the most popular channel coding methods in the OFDM systems is *Coded OFDM (COFDM)*. COFDM does not adapt the data rate of each sub-carrier due to differing SNRs. Instead, it uses the same high-order modulation on all sub-carriers and uses coding to correct for the errors [25]. One of the most effective COFDM

techniques in frequency-selective fading channels is the Trellis Coded Modulation (TCM) [26]. In addition, Punctured Convolutional Codes are favorable due to their good performance and ease of implementation [27].

However, neither TCM nor Convolutional codes perform well with burst noise. In general, transmission errors have a strong time and/or frequency correlation. In this case, *interleaving* plays a crucial role in channel coding by providing diversity in the time and/or frequency domain. Interleaving breaks the correlation within each sub-carrier and across all sub-carriers, and enables the decoder to eliminate or reduce local fading throughout the band and in time over the whole depth of interleaving.

In the work of [28], an adaptive TCM per sub-carrier is proposed in which the objective is to minimize the overall transmit power at a constant data rate and BER by optimizing the power distribution, code rate and modulation scheme in each sub-carrier. The simulation results indicate that their adaptive scheme can achieve more than 7 dB power reduction compared to OFDM in non-adaptive TCM. However, the implementation feasibility of adaptation per sub-carrier is not addressed, and can be expected to be quite complex.

A more feasible implementation of TCM is the *pragmatic* TCM [29], where the different coded modulation types (one for each sub-carrier) can be combined into one codeword. In fact, pragmatic TCM is the version of TCM that is well-suited for practical high data rate systems since it is simpler, more flexible and offers performance close to the best Ungerboeck code [30] that implements TCM. Moreover, the adaptive pragmatic TCM system is shown to be robust to the inaccuracies of channel gain estimations that are fed back to the transmitter [31], which is a desirable property for practical implementation.

1.4.2 Current Standards

As mentioned in Section 1.3.2, among the wireless OFDM standards, 802.11n does not adapt the channel coding with sub-carrier. However, it exploits the channel frequency diversity by using COFDM, where a higher-order modulation type is used across all sub-carriers and the errors are corrected by coding across the sub-carriers. On the

other hand, WiMAX has more flexibility and can adapt the channel codes on a limited subset of sub-carriers in an OFDM symbol. In addition, other OFDM standards such as DAB, DVB, ADSL and VDSL do not implement adaptive coding per sub-carrier. Table 1.1 tabulates channel FEC codes that are chosen (as mandatory or optional) in various OFDM standards [1, 2, 32, 33]. The following abbreviations are used:

- CC: Convolutional Code
- CTC: Convolutional Turbo Code
- BTC: Block Turbo Code
- LDPC: Low-Density Parity-Check code
- RS: Reed-Solomon code
- TCM: Trellis Coded Modulation code
- Π: Interleaver
- r: Code rate
- ν: Constraint length (= number of memory elements + 1)
- BL: Block Length

In most cases, channel coding at the transmitter consists of three main blocks in the following order. The complementary operations are applied in reverse order at the reception.

- *Randomizer*: of the data bit sequence.
- *Forward Error Correction (FEC) Encoder + Puncturer* (see Section 5.1.1) to obtain higher rates.
- *Bit-Interleaver*: is a two-step process to ensure that: (1) adjacent coded bits are mapped onto non-adjacent sub-carriers, and (2) adjacent coded bits are mapped alternatively onto less and more significant bits of constellation (to avoid long runs of low reliable Least Significant Bits (LSB)).

Standard	Channel FEC Code	
	Mandatory	*Optional*
802.11n	CC (r=1/2, ν=7, $(133,171)_8$) Zero-tailing Puncture to r={2/3, 3/4}	LDPC: BL ={648, 1296, 1944} r = {1/2, 2/3, 3/4, 5/6}
mobile WiMAX (OFDMA)	CC (r=1/2, ν=7, $(171,133)_8$) Tail-biting Puncture to r={2/3, 3/4}	(1) CC with zero-tailing (2) CTC (r=1/3) (3) BTC (4) LDPC: BL ={576 - 2304}, with r={1/2, 2/3, 3/4, 5/6}
DAB	RS	
DVB	RS + convolutional Π(outer) + Punctured-CC + Π(inner)	
ADSL (G.DMT)	RS: GF(2^8) + convolutional Π	+ TCM (Wei's 16-state 4-Dimensional)
VDSL2	RS + Π + TCM	

Table 1.1: Mandatory and optional channel FEC coding schemes in OFDM standards.

1.4.3 Current State-of-Art

Recently, there has been numerous interest on the design of capacity-approaching codes, particularly Low-Density Parity-Check (LDPC) codes, that are better suited for OFDM systems [34, 35, 36, 37]. This is due to the higher data rate that is attainable from the higher coding gain of LDPC codes. In high data rate wireless OFDM systems, the challenge is to design LDPC codes with reasonable block length (on the order of 1000) with feasible encoding and decoding complexity and overhead delay.

Authors in [34] use a higher constellation on all sub-carriers, and compensate for the loss in performance by using stronger error correction codes such as LDPC and/or antenna diversity. Another work [35] optimizes the irregularity profile of the LDPC encoder to the channel conditions. The simulation results indicate a 1.2 dB improvement by the LDPC (r=1/2, BL=1024) that is optimized to ADSL channel over the interleaved optimized code to AWGN channel. One of the advantages of this method is that it does not require a perfect a priori knowledge of channel conditions,

which makes it suitable for practical systems where there are errors in the channel estimation.

The work of [36] shows that the number of iterations needed in the Sum-Product decoding algorithm of LDPC depends on the SNR - where higher number of iterations are needed at lower SNRs. They indicate that for $SNR > 2$ dB , 20 iterations is enough for LDPC-COFDM over an AWGN channel.

Finally, the authors in [38] provide an excellent analysis on the performance of practical capacity-approaching codes, LDPC and Turbo Codes, compared to TCM in Digital Subscriber Line (DSL) system with DMT. They use a class of LDPC codes, called *array-based* LDPC, which are shown to be very well-suited for practical systems [37]. These codes offer:

- *Flexibility*: they can be constructed efficiently for any code rate and block size.
- *Good performance*: that is as good as or better than randomly constructed LDPC for comparable rates and lengths. In addition, they do not suffer from error floors at significantly high BERs.
- *Feasible implementation*: they have linear-time encodability.

However, as mentioned with prior works on adaptive modulation, there are no reports on real-time performance of adaptive coding in OFDM systems with sub-carrier adaptive modulation. This motivates our work in implementing sub-carrier AMC on a wideband OFDM transceiver prototype to quantify performance benefits and design issues in the real environment.

1.5 Thesis Contributions and Outline

The main contributions of this thesis are:

- Design and implementation of a real-time sub-carrier Adaptive Modulation and Coding (AMC) on a wideband OFDM transceiver system.

- Discussion of the importance of consistent and accurate SNR estimates to guarantee the success of AMC with the corresponding design solutions.
- Performance results quantifying the benefits of sub-carrier AMC in a real system.

Chapter 2 reviews the specifications of our WiGLAN wideband OFDM transceiver prototype. Chapter 3 and 5 describe the implementation and design issues of our sub-carrier Adaptive Modulation and AMC respectively. Chapter 4 and 6 document the measured results and analyze them. Finally, Chapter 7 concludes and provides directions for future work.

Chapter 2

WiGLAN Transceiver Specifications

To examine performance benefits and implementation complexity of sub-carrier Adaptive Modulation and Coding (AMC) in a wideband OFDM wireless system, a transceiver prototype is built, as shown in Fig. 2-1. In this chapter, We will first introduce the building blocks of an OFDM system. Next, an overview of our WiGLAN prototype specifications is provided. The transceiver prototype consists primarily of two parts, the Digital Baseband Modem and the RF Front End. We will review the WiGLAN Digital and RF implementations.

2.1 An OFDM System Block Diagram

As indicated in Fig. 2-2, the key steps in an OFDM communications system are as follows [21]:

- First, we group every N_{FFT} data samples into an *OFDM symbol.* With a sampling period T_s, an OFDM symbol has duration $T_{FFT} = N_{FFT}\ T_s$. In the frequency domain, the wideband signal with bandwidth W, is broken into N_{FFT} narrowband sub-channels, each with bandwidth $\Delta_f = \frac{W}{N_{FFT}}$. To ensure that each sub-carrier experiences flat fading, $\Delta_f < W_{coh}$ must be chosen, where W_{coh} is the channel *coherence bandwidth.*

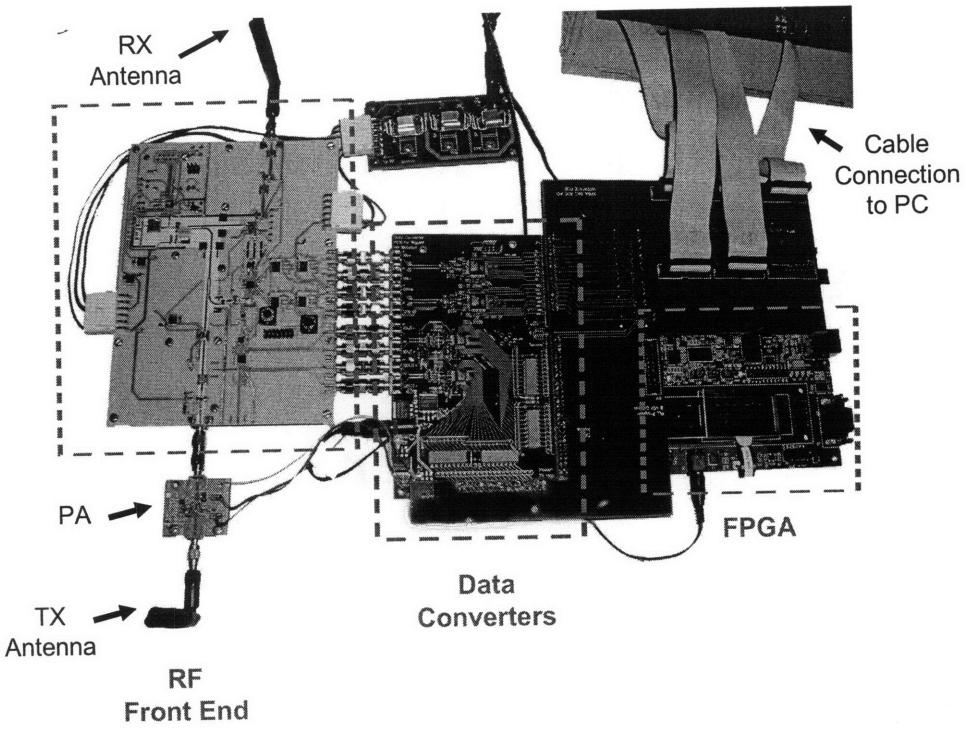

Figure 2-1: Photo of the WiGLAN transceiver prototype.

- Next, each OFDM symbol is transformed to the time-domain by N_{FFT}-point *IFFT*.

- For an Inter-Symbol Interference (ISI)-free transmission, a *Cyclic Prefix (CP)* of length $T_{CP} > \tau$ (τ = channel *delay spread*) must be appended after the IFFT operation. The resulting symbols are sent serially through the wideband channel.

- At the receiver, CP is discarded. The received OFDM symbols are transformed back to the frequency-domain by an *FFT* operation, which results in N_{FFT} data samples: $Y_{i,k} = H_k X_{i,k} + N_{i,k}$, $k = \{0, ..., N_{FFT} - 1\}$ for the i^{th} OFDM symbol.

- The received data, $Y_{i,k}$, on the k^{th} sub-carrier is then equalized by a *one-tap frequency-domain equalizer*: $\hat{X}_{i,k} = Y_{i,k}/H_k$.

In the subsequent sections, we will explain how flat-fading sub-channels and an ISI-free transmission are obtained in an OFDM system.

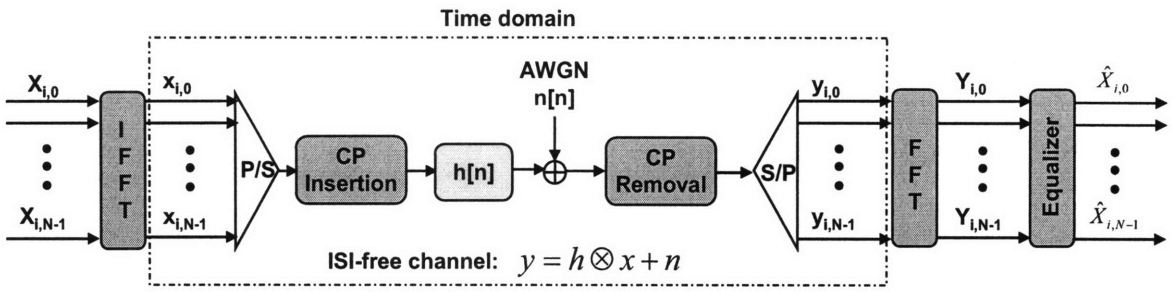

Figure 2-2: An OFDM system block diagram showing i^{th} OFDM symbol with N (= N_{FFT}) sub-carriers. Upper case letters, X and Y, denote frequency-domain samples, while lower case letters, x and y, represent time-domain samples.

2.1.1 Flat-fading Sub-channels

To ensure flat-fading in each sub-channel, we need:

$$\Delta_f < W_{coh} \ , \tag{2.1}$$

where Δ_f is the **sub-carrier frequency spacing**, and W_{coh} is the multipath channel *coherence bandwidth* defined below.

Definition 2.1.1. Channel coherence bandwidth, W_{coh}, is a statistical measure of the range of frequencies over which the channel can be considered flat - *i.e.* when the channel passes all spectral components with approximately equal gain and linear phase. Coherence bandwidth with frequency correlation above 0.9 is approximated as [39]:

$$W_{coh} \approx \frac{1}{50\sigma_\tau} \ , \tag{2.2}$$

where σ_τ is the root-mean-square (rms) delay spread that characterizes multipath in the time-domain, and is given by [39]:

$$\sigma_\tau = \sqrt{\bar{\tau^2} - (\bar{\tau})^2} \tag{2.3}$$

$$\bar{\tau^2} = \frac{\sum_k |h(\tau_k)|^2 \tau_k^2}{\sum_k |h(\tau_k)|^2} \tag{2.4}$$

$$\bar{\tau} = \frac{\sum_k |h(\tau_k)|^2 \tau_k}{\sum_k |h(\tau_k)|^2} \ , \tag{2.5}$$

where $|h(\tau_k)|^2$ is the power level of the k^{th} path with τ_k delay.

Thus, by choosing $\Delta_f < W_{coh}$, each sub-carrier experiences flat-fading.

2.1.2 ISI-free Transmission

The reason that OFDM is suitable for high data rate transmission in multipath channel is because a high data rate system generally has sampling period $T_s \ll \tau$(channel delay spread) , which results in severe Inter-Symbol Interference (ISI). By transmitting the high rate data in multiple simultaneous low-rate transmissions with symbol period $T_{FFT} \gg \tau$, OFDM efficiently achieves an ISI-free transmission in such highly dispersive channels.

In an indoor environment where channel fading is quasi-stationary, the wireless channel can be assumed time-invariant over a number of OFDM symbols. In this case, the multipath effects can be modeled as a linear and time-invariant (LTI) system - *i.e.* the discrete-time output, $y[n]$, is related to the input, $x[n]$, and multipath channel, $h[n]$, through linear convolution as below:

$$y[n] = x[n] * h[n] \tag{2.6}$$

To avoid ISI *between* OFDM symbols after going through the wireless channel, a guard time, $T_g > \tau$, must be introduced between OFDM symbols, as shown in Fig. 2-3a. However, with guard interval, although ISI *between* OFDM symbols is removed, there is still ICI *within* each OFDM symbol. Thus, to maintain the orthogonality of sub-carriers, the OFDM symbol is made periodic by adding a **Cyclic Prefix (CP)** - which is the last N_{CP} samples of the OFDM symbol - to its beginning (see Fig. 2-3b) that will act as a guard interval as well. With the channel input, $x[n]$, being periodic, its linear convolution with the channel, $h[n]$, becomes a *circular* convolution [21], *i.e.*,

$$y[n] = x[n] \otimes h[n] = \sum_{k=0}^{N_{FFT}-1} h[k]x[n-k]_{N_{FFT}} , \tag{2.7}$$

where the circular function $x[n]_{N_{FFT}} = x[n \ mod \ N_{FFT}]$ is a periodic version of $x[n]$ with period N_{FFT}. In the case of circular convolution, the Discrete Fourier Transform

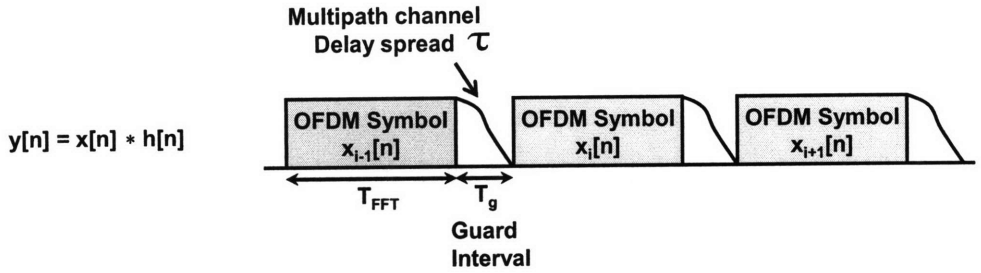

(a) Guard interval ($T_s > \tau$) removes ISI *between* OFDM symbols from channel delay spread, τ

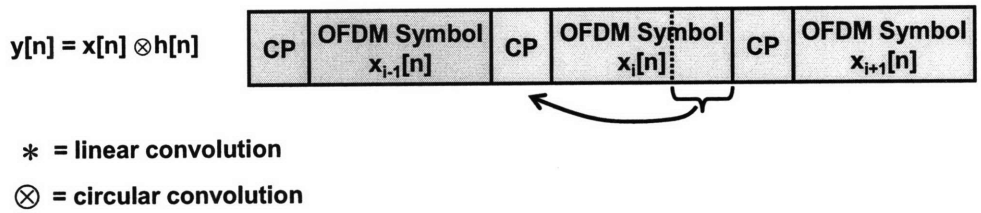

(b) CP prevents ISI and maintains orthogonality of sub-carriers.

Figure 2-3: Cyclic Prefix (CP) is needed to combat ISI from multipath channel in an OFDM system.

(DFT) of the channel output $y[n]$ becomes:

$$DFT\{y[n]\} = DFT\{h[n] \otimes x[n]\} \tag{2.8}$$

$$Y[k] = H[k]X[k] \tag{2.9}$$

$$DFT\{x[n]\} = X[k] = \frac{1}{\sqrt{N_{FFT}}} \sum_{n=0}^{N_{FFT}-1} x[n] e^{-j\frac{2\pi nk}{N_{FFT}}} \tag{2.10}$$

$$IDFT\{X[k]\} = x[n] = \frac{1}{\sqrt{N_{FFT}}} \sum_{k=0}^{N_{FFT}-1} X[k] e^{j\frac{2\pi nk}{N_{FFT}}} \tag{2.11}$$

Equation 2.9 describes an ISI-free channel in the frequency-domain, where each input symbol, $X[k]$, on k^{th} sub-carrier is simply scaled by a complex channel gain, $H[k]$. So, by estimating the channel frequency-response, $\hat{H}[k]$, at the receiver, it is trivial to recover the input symbol by a *one-tap frequency-domain equalizer*, as below:

$$\hat{X}[k] = \frac{Y[k]}{\hat{H}[k]}, \tag{2.12}$$

which corrects for both amplitude and phase distortions on the transmitted symbol. It must be noted that although CP mitigates the ISI, it entails a data rate and power

loss according to:

$$\frac{N_{FFT}}{N_{FFT}+N_{CP}}, \tag{2.13}$$

where $N_{CP} = T_{CP}/T_s$. To reduce this overhead, $N_{FFT} \gg N_{CP}$ is desirable. However, larger N_{FFT} is inferior to Carrier Frequency Offset (CFO) and Peak-to-Average Power Ratio (PAPR) [21]. So picking the number of sub-carriers, N_{FFT}, involves a tradeoff between cost and required tolerances.

2.1.3 OFDM Signal Representation

The continuous-time transmitted signal, $x(t)$, can be mathematically formulated as below [40]:

$$x(t) = \frac{1}{\sqrt{T_{FFT}}} \sum_{i=-\infty}^{+\infty} \sum_{k=-K/2}^{K/2-1} X_{i,k} e^{j2\pi k\Delta_f (t-T_{CP}-iT_{SYM})} u(t-iT_{SYM}) \tag{2.14}$$

$$u(t) = \begin{cases} 1 & 0 \le t < T_{FFT}, \\ 0 & \text{else.} \end{cases} \tag{2.15}$$

$$T_{FFT} = N_{FFT}/f_s \tag{2.16}$$

$$\Delta_f = 1/T_{FFT} \tag{2.17}$$

$$T_{SYM} = T_{FFT} + T_{CP} \tag{2.18}$$

where

- i is the time symbol index.
- k is the frequency (sub-carrier) index.
- K is the number of sub-carrier used.
- $\{X_{i,k}\}$ are the data symbols.
- Δ_f is the sub-carrier spacing.
- T_{FFT} is the IFFT/FFT period.

- N_{FFT} is the number of OFDM sub-carriers.
- f_s is the sampling frequency of the system.
- T_{CP} is the length of the cyclic prefix.
- T_{SYM} is the period of an OFDM symbol including the CP - *i.e.* $T_{SYM} = T_{FFT} + T_{CP}$.

2.2 WiGLAN System Specifications

Table 2.1 summarizes the WiGLAN system specifications. For comparison, OFDM parameters for Wireless LAN High Throughput (HT) 40-MHz 802.11n [1] and Mobile WiMAX with scalable OFDMA (and $N_{FFT} = 1,024$) are provided in this table. Next, we will discuss how WiGLAN system's OFDM parameters are chosen.

(a) Frequency Bandwidth: In our prototype, the OFDM system occupies 128 MHz bandwidth around the carrier frequency at 5.247 GHz. Each OFDM symbol is generated using 128-point IFFT/FFT, which divides the 128 MHz signal bandwidth into 128, 1-MHz sub-channels. Using Equation 2.2, the channel coherence bandwidth, W_{coh}, is 10 MHz and 2 MHz for measured channel delay spread [41], σ_τ, of 2 ns and 10 ns at link distances of 1 m and 10 m respectively, in an indoor environment at 5 GHz carrier frequency. Hence, we expect fading to be flat over each 1-MHz sub-channel, as desired.

(b) Number of Sub-carriers: In a practical implementation, not all the sub-carriers are used. This is because with our sampling frequency, $f_s = 128$ MHz, equal to signal bandwidth, when all sub-carriers are used, the signal and its replica will be next to each other. Hence, a brickwall reconstruction filter is required to filter out the replicas and avoid aliasing. However, brickwall filters cannot be implemented. To relax the constraints on the filter, the separation between the signal and its replicas can be increased by not using sub-carriers at the higher frequencies. In our prototype, 27 sub-carriers at the outer frequencies are never used.

Parameter	*Value*		
	WiGLAN	802.11n	Mobile WiMAX sOFDMA
Carrier Frequency (f_c)	5.247 GHz	5 GHz/2.4 GHz	2–6 GHz
Bandwidth:			
OFDM (f_s)	128 MHz	40 MHz	11.2 MHz
Data + Pilots	100 MHz	35.625 MHz	9.19 MHz
Sub-carrier (Δ_f)	1 MHz	312.5 kHz	10.94 kHz
Number of Sub-carriers:			
OFDM (N_{FFT})	128	128	1,024
Data	92	108	720
Pilot	8	6	120
Time Period:			
IFFT/FFT Period (T_{FFT})	1 μs	3.2 μs	94.4 μs
Cyclic Prefix (T_{CP})	0.4 μs	0.8 or 0.4 μs	{2.95, 5.9, 11.8, 23.6 } μs
Symbol Period (T_{SYM})	1.4 μs	4.0 or 3.8 μs	{97.35, 100.3, 106.2, 118} μs
BER:			
Uncoded	10^{-3}	$\approx 10^{-3}$	(not available)
Coded	10^{-5}	$\approx 10^{-5}$	
Modulation per Sub-carrier	BPSK, 4-, 16-, 64-QAM	BPSK, 4-, 16-, 64-QAM	BPSK, 4-, 16-, 64-QAM
Max Link Distance (Indoor)	10 m	70 m	(not available)

Table 2.1: Summary of WiGLAN System Specifications. The specifications for 802.11n standard and WiMAX are shown for comparison.

In addition, the DC sub-carrier is not used since there are intrinsic DC offsets from the RF Front End which are removed by DC-coupling capacitors. As a result, out of the 128 OFDM sub-carriers, 100 sub-carriers are used (occupying 100 MHz) - where 92 carry data and 8 carry pilots (*i.e.* training symbols). As shown in Fig. 2-4, the 8 pilot sub-carriers are spread evenly across the 100 MHz and are used for time and frequency synchronization by the digital receiver.

(c) Time Period: In the time-domain, the 1-MHz sub-carrier frequency spacing translates to $T_{FFT} = 1$ μs OFDM symbol length, where each OFDM symbol contains 128 samples.

A cyclic-prefix of $T_{CP} = 0.4$ μs is chosen, which is the last 51 samples of each

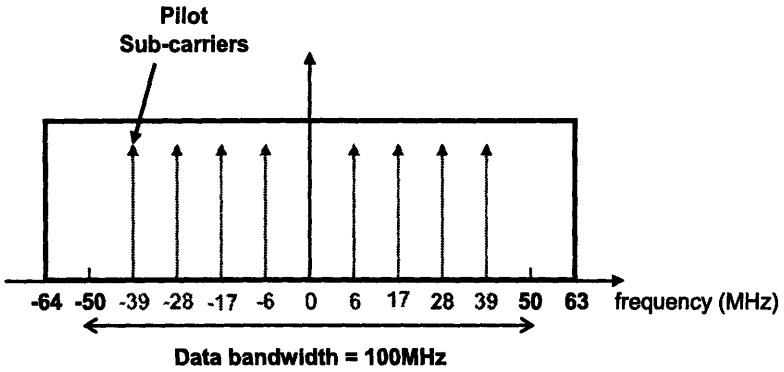

Figure 2-4: WiGLAN frequency planning and sub-carrier assignment: 100-MHz data bandwidth, 92 data sub-carriers and 8 pilot sub-carriers (as shown).

OFDM symbol appended to its beginning. As mentioned in the previous section, to combat channel-induced ISI, the CP length should be at least equal to the channel *excess delay spread* - defined as the time delay during which multipath energy falls to X dB below the maximum [39]. Conservatively, we choose X as the maximum noise floor the receiver must tolerate with its highest modulation type without violating the BER requirement. In the context of WiGLAN, we had originally chosen 256-QAM as the highest modulation type. Since 256-QAM requires minimum SNR = 28.42 dB at target BER=10^{-3}, X = 28.42 dB which is rounded to 30 dB. For X = 30 dB, the excess delay spread is around 70 ns for a link distance of 10 m at 5 GHz center frequency, as reported in [41]. This implies that the CP must be at least 70 ns. However, in practical systems, the CP length is chosen longer than the expected channel delay spread to leave room for timing estimation errors. In our prototype, we assumed 200 ns for channel delay spread, and left 200 ns margin for timing estimation errors since we do not have fine time acquisition algorithms. That is why in WiGLAN, $T_{CP} = 0.4$ μs, which is 40% of the useful OFDM symbol time, T_{FFT}. A good rule of thumb from OFDM wireless standards [1, 2, 20] is:

$$\frac{T_{CP}}{T_{FFT}} \leq 25\% \tag{2.19}$$

Hence, in WiGLAN, finer time synchronization algorithms must be implemented to reduce the size of CP to a more reasonable value, $T_{CP} \leq 0.25$ μs.

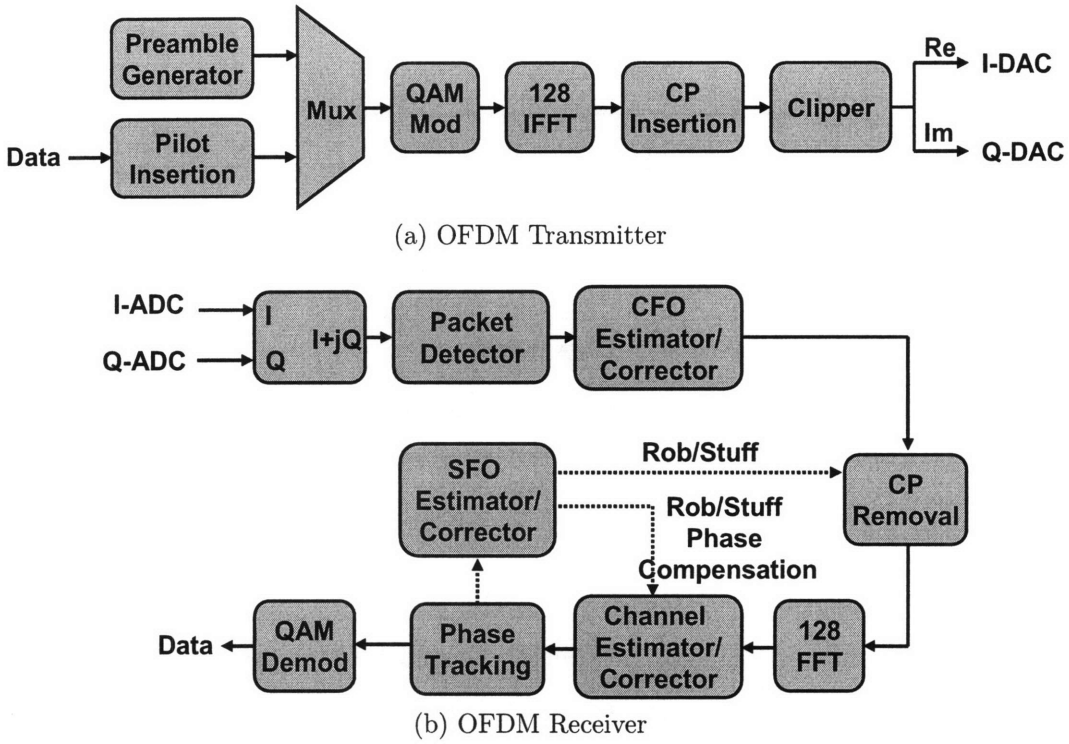

(a) OFDM Transmitter

(b) OFDM Receiver

Figure 2-5: WiGLAN Digital Baseband Modem [40].

2.3 WiGLAN Digital Baseband Modem

The entire digital baseband modem is implemented on a Xilinx Virtex 4 SX35 FPGA mounted on an Avnet Evaluation Board [42]. The System Generator software tool generates the Register Transfer Level (RTL) code for the FPGA. Our entire transceiver modem uses 439,988 2-input NAND gates clocked at 128 MHz. The digital baseband transmitter and receiver are shown in Fig. 2-5. For an extensive treatment on implementation details of the digital baseband modem, the reader is referred to [40].

2.3.1 OFDM Transmitter

At the transmitter, a random bit generator outputs the data bits. An OFDM symbol is created by grouping data bits according to the modulation per subcarrier assignment, and inserting the pilots. For a coded system, the data bits are encoded by a rate-1/2 convolutional encoder and punctured to obtain higher coding rates. As shown in Fig. 2-5a,

- First, a *Mux* selects either the Preamble or OFDM data symbols.
- Next, the *QAM Modulator* modulates each sub-carrier according to the assigned modulation. All modulations have unit average power.
- The 128 QAM symbols are fed into a *128-point IFFT*, which generates 128 time-domain complex samples.
- The *CP Inserter* adds CP to each time-domain OFDM symbol.
- To reduce the high PAPR of an OFDM symbol (PAPR > 21 dB for $N_{FFT} = 128$ [43]), the *Clipper* module clips the real and imaginary samples by a clipping amplitude, A_{CLIP}, that is read from a look-up-table based on the number of used sub-carriers. The PAPR should be reduced since such high PAPR requires high dynamic range from the DAC and ADC and high input back-off from the Power Amplifier saturation region which are not feasible. Since N_{FFT} is large (> 20 [26]), by the Central Limit theorem, $x_{i,n}$ in Equation 2.11 can be modeled as a Gaussian random variable with zero mean and variance σ_{tot}^2 expressed as:

$$\sigma_{tot}^2 = \sum_{k=0}^{N_{FFT}-1} Var(X_{i,k}) \,, \tag{2.20}$$

$$Var(X_{i,k}) = \begin{cases} 1, & \text{if sub-carrier } k \text{ is used} \\ 0, & \text{otherwise} \end{cases} \tag{2.21}$$

Furthermore, due to orthogonality of sub-carriers, $|x_{i,n}|^2$ is exponentially distributed with parameter $= \sigma_{tot}^2$. If we define, probability of Clipping, P_{CLIP}, as the probability of an event when $|x_{i,n}| > A_{CLIP}$, A_{CLIP} is obtained as below [40]:

$$1 - P_{CLIP} = Pr(|x_{i,n}|^2 < {A_{CLIP}}^2)^{N_{FFT}} \tag{2.22}$$

$$= (1 - e^{-\frac{{A_{CLIP}}^2}{\sigma_{tot}^2}})^{N_{FFT}} \tag{2.23}$$

$$A_{CLIP} = \sqrt{-\sigma_{tot}^2 \, ln(1 - (1 - P_{CLIP})^{\frac{1}{N_{FFT}}})} \tag{2.24}$$

In WIGLAN, we have chosen $P_{CLIP} = 10^{-7}$, which results in PAPR = 16 dB,

according to:

$$PAPR(dB) = 10\ log_{10}\left(\frac{max(|x_{i,n}|^2)}{Var(|x_{i,n}|)}\right) \quad (2.25)$$

$$= 10\ log_{10}\left(\frac{2{A_{CLIP}}^2}{\sigma_{tot}^2}\right) \quad (2.26)$$

$$= 10\ log_{10}\left(-2\ ln(1-(1-P_{CLIP})^{\frac{1}{N_{FFT}}})\right) \quad (2.27)$$

- Finally, the Clipper outputs are fed into the Digital-to-Analog Converter (DAC).

2.3.2 OFDM Receiver

At the receiver, the *preamble* of the transmitted packet is used to perform two important synchronization tasks as described below:

- **Time synchronization**: to estimate the timing offset of the OFDM symbol, called *symbol timing offset*, and the optimal sampling instants, *i.e. Sampling Frequency Offset (SFO)*. SFO is due to the sampling frequency mismatch between the transmitter's DAC and the receiver's Analog-to-Digital Converter (ADC).

- **Frequency synchronization**: to estimate the *CFO* in order to align the received carrier frequency as closely as possible with the transmitted carrier frequency.

Fig. 2-6 shows the structure of the Preamble, which consists of a Cyclic Prefix (CP) and 7 identical OFDM pilot symbols (T1-T7), each containing 100 BPSK sub-carriers. As indicated in the figure, the first 3 OFDM pilot symbols are used for packet detection, the next 2 OFDM pilot symbols are used for CFO estimation, and finally the last 2 are used to estimate the complex channel gain on each sub-carrier.

As shown in Fig. 2-5b, the In-phase and Quadrature-phase components at the output of the ADC are processed by the digital receiver as described below:

- *Packet Detector:* detects the transmitted packet through an energy-detection algorithm known as the *double sliding window* algorithm [44]. As shown in

Fig. 2-7, the double sliding window algorithm calculates two consecutive sliding windows, A and B, of the received energy, and forms a decision variable, M_n, as the ratio of the total energy contained inside the two windows. The received energy of $y[n]$ in windows A and B are:

$$A_n = \sum_{i=0}^{N_{FFT}-1} |y[n-i]|^2 \tag{2.28}$$

$$B_n = \sum_{i=1}^{N_{FFT}} |y[n+i]|^2 \tag{2.29}$$

The peak of M_n occurs when index n is exactly the start of the packet - *i.e.* when A_n consists of signal and noise while B_n contains noise only. Hence, locating the peak of M_n would provide the expected starting point of the packet.

- *CFO Estimator/Corrector:* estimates and corrects for CFO, $\delta f = f_{tx} - f_{rx}$, to minimize the resulting ICI in the later stages. The Maximum Likelihood (ML) CFO estimate $\hat{\delta f}$ is obtained as a function of the cross-correlation, z, between 2 repeated OFDM symbols [44] as below:

$$\hat{\delta f} = -\frac{1}{2\pi N_{FFT} T_s} \angle z \tag{2.30}$$

$$z = \sum_{n=0}^{N_{FFT}-1} y[n] y^*[n+N_{FFT}] \tag{2.31}$$

$$= \sum_{n=0}^{N_{FFT}-1} (x[n] e^{j2\pi\delta f n T_s})(x[n+N_{FFT}] e^{j2\pi\delta f (n+N_{FFT}) T_s})^* \tag{2.32}$$

$$= e^{-j2\pi\delta f N_{FFT} T_s} \sum_{n=0}^{N_{FFT}-1} |x[n]|^2 \tag{2.33}$$

At high SNR, the variance of this estimator is [45]:

$$Var(-2\pi\hat{\delta f} T_s) = Var(\frac{\angle z}{N_{FFT}}) \tag{2.34}$$

$$= \frac{1}{{N_{FFT}}^2} \cdot \frac{1}{N_{FFT}\, SNR} \tag{2.35}$$

$$= \frac{1}{{N_{FFT}}^3\, SNR} \tag{2.36}$$

A limitation of this algorithm is that since the angle of z is unambiguously defined only in the range $[-\pi, \pi]$, the estimator will be correct for the following limit:

$$|\delta f| \geq \frac{\pi}{2\pi N_{FFT} T_s} = \frac{f_s}{2} \tag{2.37}$$

Hence, in the WiGLAN system, the maximum tolerable CFO is 500 kHz. The WiGLAN carrier oscillators are specified at 50 parts-per-million (PPM), which results in maximum CFO of 524 kHz. However, using a spectrum analyzer, the measured CFO was always less than 50 kHz. Due to using cheaper oscillators in WiGLAN compared to 802.11a standard, the standard's oscillators have a superior accuracy at 20 PPM [20]. Finally, CFO is corrected by multiplying output samples, $y[n]$, by $e^{-j2\pi\hat{\delta f} n T_s}$.

- *CP Removal:* removes the CP that was inserted to guard against the ISI.
- *FFT:* transforms the time-domain OFDM samples to frequency-domain symbols.
- *Channel Estimator/Corrector*: estimates and corrects the channel-induced attenuation and phase rotation on each sub-carrier. The channel estimator is a Least Squares (LS) method (or zero-forcing), and averages over 2 identical OFDM pilot symbols to improve the estimate, as below:

$$\hat{H}_k = \frac{1}{2}\left(\frac{Y_{1,k} + Y_{2,k}}{X_k}\right) = H_k + \frac{1}{2}\left(\frac{N_{1,k} + N_{2,k}}{X_k}\right) \tag{2.38}$$

For an additive white Gaussian noise variance, $Var(N_{i,k}) = \sigma_N^2$, the variance of the above channel estimator is:

$$Var(\hat{H}_k) = \frac{\sigma_N^2}{2} \tag{2.39}$$

Finally, channel correction results in:

$$\hat{X}_k = \frac{Y_{i,k}}{\hat{H}_k} \tag{2.40}$$

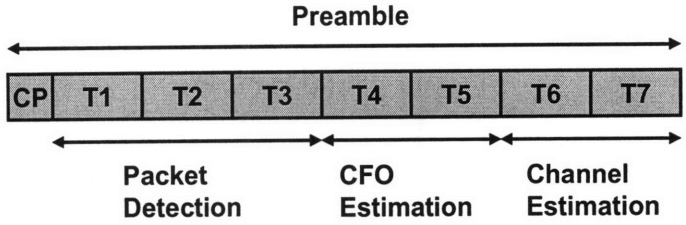

Figure 2-6: Structure of Preamble [40]. T: one OFDM pilot symbol (T1 to T7 are identical), CP: Cyclic Prefix.

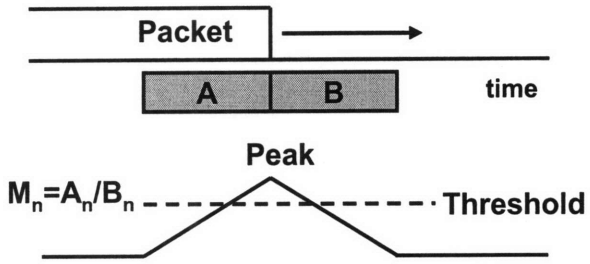

Figure 2-7: The response of the double sliding window packet detection algorithm [44].

- *Phase Tracking*: estimates and corrects for the time-variant phase rotation on the sub-carrier symbols caused by CFO, SFO, and phase noise. For each OFDM symbol, it finds the phase rotation on the 8 pilot (known) sub-carriers that are spread throughout the band. Next, it uses linear regression to estimate (and subsequently correct) for the phase rotation on the rest of the sub-carriers [46].

- *SFO Estimator/Corrector:* estimates and corrects for the SFO by processing side-products of phase tracking. In addition, it corrects for the OFDM symbol window drift caused by SFO over time by controlling the CP Removal block to advance or delay by a sample when needed. In this case, it also indicates to the Channel Corrector Block to compensate for the phase rotations on sub-carriers that result from the advance or delay of a sample.

2.4 WiGLAN RF Front End

The RF Front End is custom-made with off-the-shelf discrete components. Table 2.2 summarizes the specifications of our RF Front End, which utilizes a classical hetero-

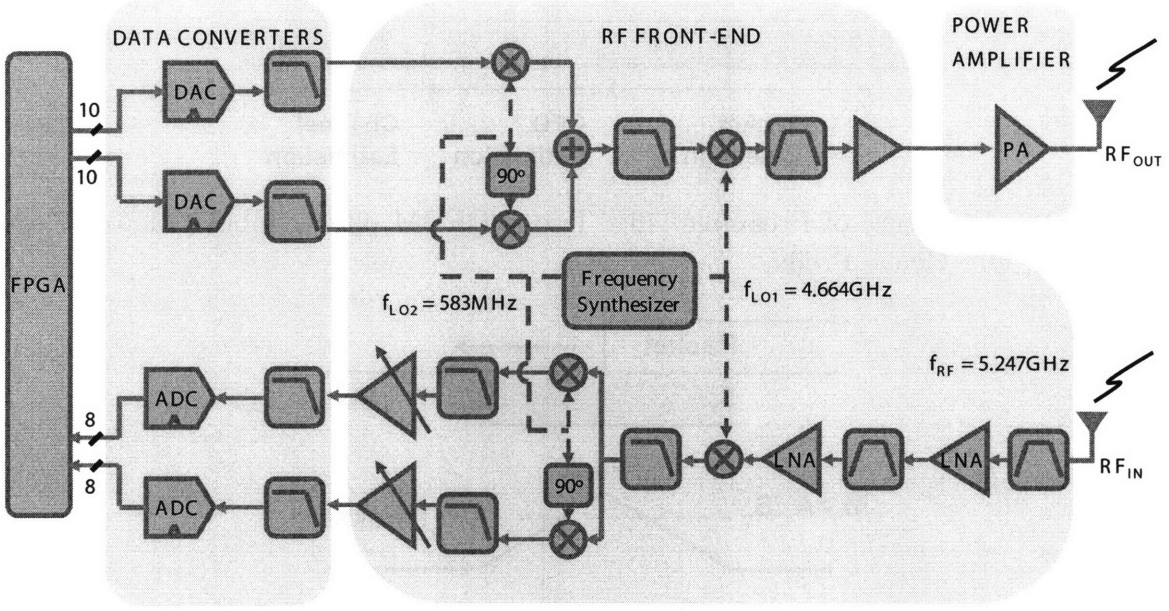

Figure 2-8: Schematic of WiGLAN RF Front End Transceiver [47].

dyne architecture with an intermediate-frequency (IF) of 583 MHz. Fig. 2-8 shows a complete block diagram of the RF Front End node consisting of 3 printed circuit boards (PCB). A PCB dedicated to data conversion contains a pair of high-speed Digital-to-Analog Converters (DACs) and Analog-to-Digital Converters (ADCs). The primary RF Front-End PCB performs almost all the analog processing at baseband and at RF frequencies. Finally, a separate Power Amplifier (PA) evaluation board (on the third PCB) is responsible for amplifying the transmitted RF signal to the desired power level. For implementation details and design justifications of the WiGLAN RF Front End, the reader is referred to [47].

We do not aim to find the maximum achievable data rate. Rather, we aim to find the relative improvement from sub-carrier AMC. Thus, we did not optimize the system to maximize its data rate. The OFDM receiver uses simple time and frequency synchronization and estimation algorithms. Also, for each experiment, the variable gain amplifier (VGA) is manually adjusted to maximize the ADC's range. By using a fine-timing acquisition and an optimized gain control algorithm, the adaptive modulation system can provide higher data rates.

Parameter	***Value***
Sampling Frequency	128 MHz
DAC and ADC:	
Number of Bits	10 and 8 bits
Effective Number of Bits	9.3 and 7.6 bits
I/Q:	
Phase Imbalance	2°
Gain Imbalance	0.2 dB
Baseband VGAs:	
Gain Range	13.5 dB to 54 dB
Gain Step	1.5 dB
Noise Figure	7 dB
PA:	
Average Output Power	7.5 dBm
1-dB Compression Point	19.6 dBm
Phase Noise:	
At Offset 1 kHz	-73 dBc/Hz
At Offset 100 kHz	-106 dBc/Hz
PLL Loop Bandwidth	20 kHz

Table 2.2: Summary of WiGLAN RF Front End Specifications.

Chapter 3

Sub-carrier Adaptive Modulation Design

Sub-carrier adaptive modulation adapts the modulation of each sub-carrier to its sub-channel fading condition. In this prototype, the Adaptive Modulation protocol occurs in a series of steps - as shown in Fig. 3-1:

- *Step 1 - Signal-to-Noise Ratio (SNR) Estimation and Modulation Assignment:* The receiver measures the SNR on each sub-carrier and assigns the most efficient modulation to that sub-carrier.
- *Step 2 - Channel State Information (CSI) Feedback:* The receiver feeds back the assigned modulation scheme to the transmitter.
- *Step 3 - Data Transmission:* Data packet is sent from the transmitter to the receiver using the assigned modulation scheme.

Such sub-carrier Adaptive Modulation protocol is suitable to implement on an OFDM system where:

- A feedback path exists between the transmitter and receiver, and
- the channel fades do not change faster than it can be reliably estimated and fed back to the transmitter.

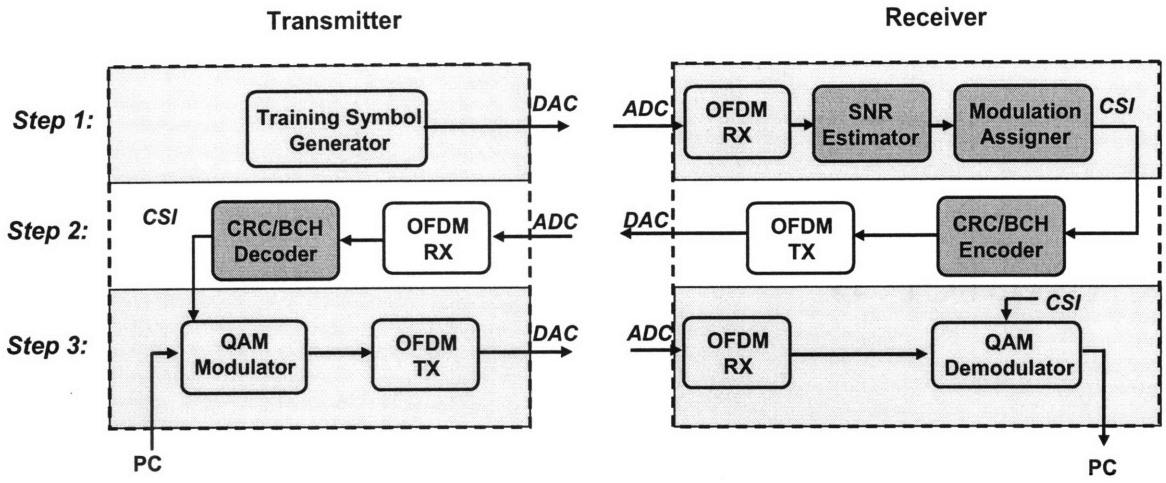

Figure 3-1: WiGLAN Adaptive Modulation Protocol.

In this chapter, first we will introduce various adaptive transmission schemes and motivate the reason for choosing the Adaptive Modulation technique. Next, we will discuss in detail the three steps in our above Adaptive Modulation protocol. Third, we will explain system design issues critical to the success of real-time sub-carrier Adaptive Modulation. Finally, we will report on the logic utilization of our implemented Adaptive Modulation protocol on the Field Programmable Gate Array (FPGA).

3.1 Adaptive Transmission Techniques

When the channel condition of each sub-carrier is known, the transmitter can vary the data rate, RF power, coding, error probability, or combinations of these parameters. Below we discuss the application of each of these adaptive transmission techniques [8]:

- *Variable-Rate:* There are two possible ways to vary the data rate: (1) fix the symbol rate but vary the modulation scheme (*i.e.* the constellation size), and (2) fix the modulation but vary the symbol rate. In practice, varying the symbol rate in the the second scheme is difficult to implement, and so the first adaptation scheme, so called **Adaptive Modulation**, is preferred.

  Depending on the application, the Adaptive Modulation technique can be opti-

mized to either maximize the data rate for a fixed error probability or minimize the error probability for a fixed data rate. The first technique can be used for data applications while the second case is better suited for delay-constrained applications, such as voice or video.

- *Variable-Power:* Adapting the transmit RF power alone is generally used to maintain a fixed BER, or equivalently a constant received SNR. The transmit power is varied per sub-carrier to invert the channel fading so that the entire channel appears as an AWGN channel to the modulator and the demodulator. However, since this technique changes the average transmit power requirements, it requires a high-linearity class-A or AB Power Amplifier which is highly inefficient.

  Furthermore, truncated channel inversion with fixed-rate transmission (fixed constellation size to maintain a fixed received SNR) has almost the same spectral efficiency as optimal variable-rate variable-power M-QAM with no restriction on constellation size.

  When variable-power scheme is used in conjunction with adaptive modulation, [12, 25, 48] show that the extra throughput achieved by power adaptation is marginal for most types of fading channels.

  In the context of WiGLAN, a unit power is allocated to all data sub-carriers which results in a fixed total average transmit RF power. However, when deeply faded sub-carriers are not used, this allocated power is wasted. Wu [49] simulates an adaptive power scheme for the WiGLAN system that re-allocates the power from null data sub-carriers (*i.e.* null-power) to useable sub-carriers selectively to optimize the data rate. This is done by placing the null-power in useable sub-carriers with SNR values close to the SNR decision threshold of the next higher modulation. Since the increase in data rate depends on the null-power available, for approximately 8 null sub-carriers (from SNR measurements), a data rate increase of 13.2% is observed. In a simplest re-allocation scheme where the null-power is re-allocated uniformly across all useable sub-

carriers, a measured data rate improvement of 4.38% is achieved for 8 null-power units. For 20 null sub-carriers (in a deeply faded system), data rate improvements of 36% and 15% are expected for the former and latter (simpler) power adaptation schemes respectively (these are obtained from linear regression of measured results).

- *Variable-Coding:* Channel codes can be varied to provide different amounts of coding gains to transmitted bits on each sub-carrier. For instance, when the modulation is fixed, a stronger error correction code may be used when SNR is small, and a weaker code or no coding when SNR is high [50].

- *Variable-BER:* One can adapt both the data rate and BER to minimize the transmit power, as it was first proposed by Hayes in [9].

Finally, we note that the performance loss from using *discrete-rate adaptive* transmission policies (as in practice) is within 3 dB of the theoretical maximum [8].

The choice of the adaptation technique depends on the system's performance objectives and implementation constraints. Since our performance objective is to maximize the aggregate bit rate over all sub-carriers, we desire an adaptive modulation and coding scheme that maintains an equal BER in all sub-channels [16]. In fact, we use ***Sub-carrier* Adaptive Modulation and Coding (AMC)** in which the modulation and coding on each sub-carrier is chosen independently based on its SNR. There is another type of adaptive modulation, called *Block* Adaptive Modulation, that divides the OFDM channel into several blocks, and uses the same modulation for all sub-carriers within a given block. In this scheme, the modulation employed by each block is based on the worst SNR among all sub-carriers within the block [51, 52]. The use of Block Adaptive Modulation is motivated by the reduced signaling overhead (in CSI Feedback Step) at the cost of reduced data rate. The adaptive modulation and coding scheme used in mobile WiMAX is of this type [2].

To quantify the performance gains from Adaptive Modulation alone, in this chapter, we discuss Adaptive Modulation with no coding. Later, Chapter 5 presents

design of Adaptive Coding with Adaptive Modulation. The next few sections justify the design choices made in each step in our Adaptive Modulation protocol.

3.2 Step1: Adaptive Modulation Algorithm

The first step in the protocol is to estimate the channel fading conditions on each sub-carrier. The modulation of each sub-carrier is then assigned based on its estimated sub-channel condition and the performance criteria. Since our performance criteria is to maximize total bit rate, for each sub-carrier, we pick the most spectrally-efficient modulation that meets our target uncoded BER of 10^{-3}.

An excellent performance metric that quantifies the fading characteristics and is related to BER is the *Signal-to-Noise Ratio (SNR)*. Hence, it is the received SNR that must be estimated. The next two sub-sections discuss how the SNR per sub-carrier is estimated, and how the SNR estimate is used to assign a modulation to each sub-carrier.

3.2.1 SNR Estimation

When the OFDM system is designed such that channel fading over each sub-carrier is flat - by choosing sub-channel bandwidth smaller than the channel coherence bandwidth, each sub-channel becomes an additive white Gaussian noise (AWGN) channel. The relation between BER and SNR for a given modulation scheme under an AWGN channel is well-known and is shown in Fig. 3-2. Thus, given the true SNR_k for a sub-carrier k, the most efficient sub-carrier modulation that yields a BER $\leq 10^{-3}$, can be selected.

The BER vs. SNR plots in Fig. 3-2 are obtained according to the following [27]:

$$P_{M-QAM} = 1 - \left(1 - P_{\sqrt{M}-PAM}\right)^2 \tag{3.1}$$

$$P_{\sqrt{M}-PAM} = 2\left(1 - \frac{1}{\sqrt{M}}\right) Q\left(\sqrt{3 \cdot \frac{SNR_b \cdot log_2(M)}{M-1}}\right) \tag{3.2}$$

$$P_{BPSK} = Q\left(\sqrt{2 \cdot SNR_b}\right), \tag{3.3}$$

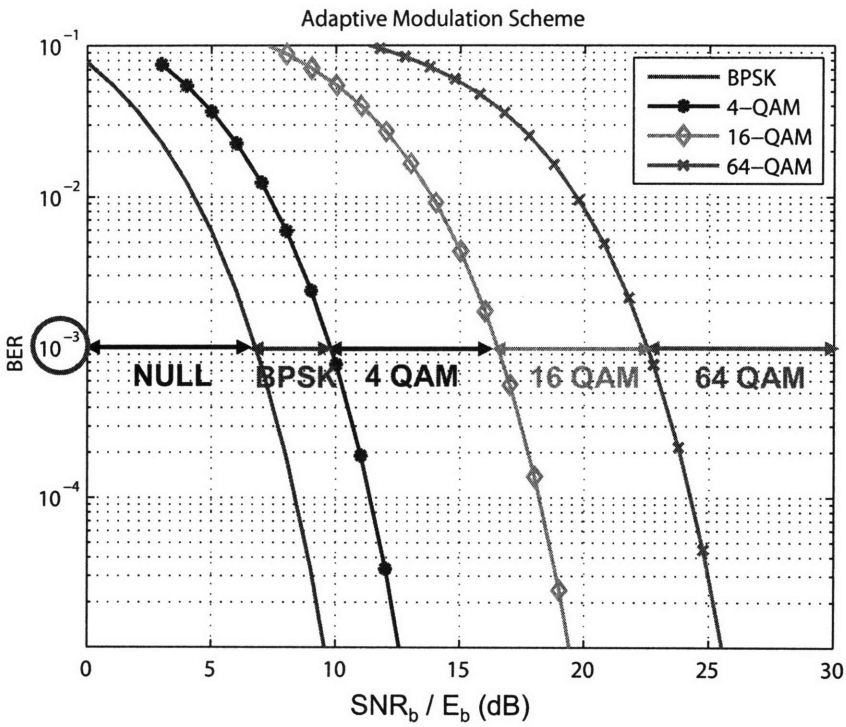

Figure 3-2: Sub-carrier modulation assignment for uncoded BER of 10^{-3} in AWGN channel. SNR_b is SNR-per-bit and is normalized by modulation Energy-per-bit, E_b. All modulations have unit average symbol energy.

where $P_{\sqrt{M}-PAM}$ and P_{BPSK} denote symbol error probabilities for $\sqrt{M}$-PAM (*i.e.* Pulse Amplitude Modulation with $\sqrt{M}$ signal points) and BPSK respectively. SNR_b is the SNR-per-bit. P_{M-QAM} is the symbol error probability of an M-QAM modulation with $M = 2^k$ - *i.e.* a rectangular constellation that can be obtained from two independent $\sqrt{M}$-PAM on In-phase and Q-uadrature channels. The BER for each modulation is approximately $P_{M-QAM}/log_2(M)$. This is a good approximation since gray-coding is used to map bits to symbols such that adjacent symbols differ in 1 bit. We note that Fig. 3-2 plots BER vs. SNR_b normalized by modulation Energy-per-bit E_b, where $E_b = 1/log_2(M)$ since all modulations have unit average symbol energy. The reason for this normalization is because our SNR estimator gives SNR normalized by signal energy. This holds for all measured SNR throughout this thesis.

To estimate the SNR on each sub-carrier, we send a training sequence that is known to the receiver. We then conservatively compute the true SNR_k that will

occur during data transmission as:

$$SNR_k(dB) = \hat{SNR}_k(dB) - SNR_{margin}(dB) \ , \tag{3.4}$$

where $\hat{SNR}_k$ is the SNR estimate from the training sequence and SNR_{margin} is a constant used to minimize the probability of overestimating the true SNR_k that will occur during data transmission.

To find $\hat{SNR}_k$, the transmitter sends M OFDM pilot symbols with equal power on all sub-carriers. Each OFDM pilot symbol contains a known training sequence, $X_k \in \{-1, 1\}$, spanning the data sub-carriers. The i^{th} received OFDM symbol at the FFT output can be expressed as:

$$Y_{i,k} = X_k H_k + N_{i,k} \ , \tag{3.5}$$

where H_k is the complex channel tap (or gain) for sub-channel k, and $\{N_{i,k}\}$ are *circularly symmetric complex Gaussian* sequences with variance σ_k^2 (as defined below). The additive white Gaussian noise is due to the thermal noise at the receiver as well as ICI due to CFO, SFO and phase-noise. Since the amount of ICI differs across the sub-carriers, the amount of the white noise N on each sub-carrier is different as well.

Definition 3.2.1. A *circular symmetric complex Gaussian* random variable, $N = Re\{N\} + j\ Im\{N\}$, has the following properties [3]:

- $N \sim CN(0, \sigma^2)$ (where $\sim$ notation denotes the phrase "is distributed as") - *i.e.* it has zero mean and variance σ^2.

- Its real and imaginary components are independent identically distributed (i.i.d.) Gaussian random variables: $Re\{N\} \sim N(0, \sigma^2/2)$ and $Im\{N\} \sim N(0, \sigma^2/2)$

- Its phase, $\angle N$, is uniformly distributed over the range $[0 : 2\pi]$.

- Its magnitude, $|N| = \sqrt{Re\{N\}^2 + Im\{N\}^2}$, is Rayleigh distributed with prob-

ability distribution function (PDF):

$$f(r) = \frac{r}{\sigma^2} \cdot exp\{-\frac{r^2}{2 \cdot \sigma^2}\}, \quad r \geq 0 \tag{3.6}$$

- The square of it magnitude, $Re\{N\}^2 + Im\{N\}^2$, is exponentially distributed with PDF:

$$f(a) = \frac{\sigma^2}{2} \cdot exp\{-\frac{a \cdot \sigma^2}{2}\}, \quad a \geq 0 \tag{3.7}$$

To compute the channel taps $\{H_k\}$, a zero-forcing channel estimator averages L received OFDM symbols and divides by the pilot symbol sent, X_k, *i.e.*,

$$\hat{H}_k = \frac{1}{L}\sum_{l=1}^{L}\frac{Y_{l,k}}{X_k} = H_k + \frac{1}{L}\sum_{l=1}^{L}\frac{N_{l,k}}{X_k} \tag{3.8}$$

Subsequently, the i^{th} output OFDM symbol is estimated as $\hat{X}_{i,k} = \frac{Y_{i,k}}{\hat{H}_k}$, and is used to calculate $\hat{SNR}_k$ by:

$$\begin{aligned}
\hat{SNR}_k &= \frac{1}{\frac{1}{M}\sum_{i=1}^{M}|\hat{X}_{i,k} - X_k|^2} && (3.9)\\
&= \frac{|\hat{H}_k|^2}{\frac{1}{M}\sum_{i=1}^{M}|Y_{i,k} - \hat{H}_k X_k|^2} && (3.10)\\
&= \frac{|H_k + \frac{1}{X_k L}\sum_{l=1}^{L} N_{l,k}|^2}{\frac{1}{M}\sum_{i=1}^{M}|N_{i,k} - \frac{1}{L}\sum_{l=1}^{L} N_{l,k}|^2} && (3.11)\\
&= \frac{|\hat{H}_k|^2}{\hat{\sigma}_k^2} && (3.12)
\end{aligned}$$

Equation 3.12 indicates that the noise-variance is estimated by:

$$\hat{\sigma}_k^2 = \frac{1}{M}\sum_{i=1}^{M}|N_{i,k} - \frac{1}{L}\sum_{l=1}^{L} N_{l,k}|^2 \tag{3.13}$$

From Equation 3.11, it is clear that the quality of SNR estimate depends on the number of OFDM pilot symbols, L and M, used for channel and noise-variance estimations respectively. The system design issues that are involved in choosing L

and M are deferred to a later section 3.5 in this Chapter.

3.2.2 Modulation Assignment

Our modulation assignment is done as follows:

1. Determine a set of modulation modes: {NULL (*i.e.* send nothing), BPSK, 4-QAM, 16-QAM, 64-QAM}.

2. From BER vs. SNR plot of each modulation (Fig. 3-2), find minimum SNR, SNR_{min}, required to meet the target BER = 10^{-3}.

3. Finally, for each sub-carrier, assign the highest supportable modulation by comparing its SNR estimate to the $\{SNR_{min}\}$.

In the modulation set, we have chosen rectangular QAM constellations with $M = 2^k$ since they can be easily generated as two PAM signals superimposed on phase-quadrature carriers, and can be easily demodulated. Gray mapping is used to map the bits to QAM symbols, which is detailed in [40]. Although rectangular M-QAM constellations are not the most energy-efficient M-QAM signal constellation for $M \geq 16$, their average power for a given minimum distance is only slightly higher than the best constellation [27]. In addition, BPSK was chosen over the more-energy efficient On-Off Keying (where either zero energy is sent (bit '0') or some energy is sent (bit '1')) since BPSK modulated training sequences result in an easier implementation of channel and SNR estimations.

Finally, our adaptive modulation scheme adapts the modulation per sub-carrier but not the power. Hence, all modulations have the same average transmit power (*i.e.* an average power of 1).

3.3 Step 2: CSI Feedback

Next, the adaptive modulation assignments, which we refer to as Channel State Information (CSI), need to be sent back to the transmitter.

This can be done by either Time Division Duplexing (TDD) or Frequency Division Duplexing (FDD). In TDD, the CSI can be sent over the data sub-carriers since a separate time is allocated to feeding back. On the other hand, in FDD scheme, CSI must be sent over dedicated control sub-carriers since the transmitter might be sending data on the data sub-carriers at the same time. We have chosen TDD scheme since we are operating in the indoor environment where the channel is quasi static. Hence, we estimate SNR and feed back CSI within the channel coherence time. FDD is useful for more mobile wireless systems where the channel conditions has to be estimated more frequently.

The CSI must be conveyed to the transmitter without error. So they are sent using a low-rate highly reliable transmission format:

- All data sub-carriers are BPSK-modulated.
- The data bits are first encoded by Cyclic Redundancy Check (CRC) (48,32) for error detection (*i.e.* 32 bits are used to form a 48-bit codeword). The implementation structure of CRC can be found in [53].
- Next, the bits are encoded by Bose, Ray-Chaudhuri, Hocquenghem (BCH) (15,5) code for error correction. Empirically, at maximum link distance of 10 m, BCH(15,5) gives no error. The implementation structure of BCH codes can be found in [27].

The number of bits required to convey the CSI is directly proportional to the number of sub-carriers in the OFDM signal and the number of modulation schemes that are chosen from. In our prototype, each sub-carrier is assigned to one of 6 modes $\in$ {PILOT, NULL, BPSK, 4−, 16−, 64 − QAM}. Thus, we need 3 bits to represent the 6 modes. Hence, the number of coded OFDM symbols sent in Step 2 are:

$$N_{Step2} = \left\lceil \frac{(3 \text{ bits/sub-carrier})(128 \text{ sub-carriers})(15/5 \text{ BCH})(48/32 \text{ CRC})}{(92 \text{ bits/OFDM})} \right\rceil = 19 \tag{3.14}$$

Fig. 3-3 shows the packet sent in Step 2, which is 30 μs long. In Step 2, the CP is 26 samples rather than 51 samples as used in steps 1 and 3. This is because the

OFDM symbols in this step are send at a low and reliable rate and can mitigate the timing estimation errors. The transmitter performs decoding on the received signal to obtain the CSI (Fig. 3-1).

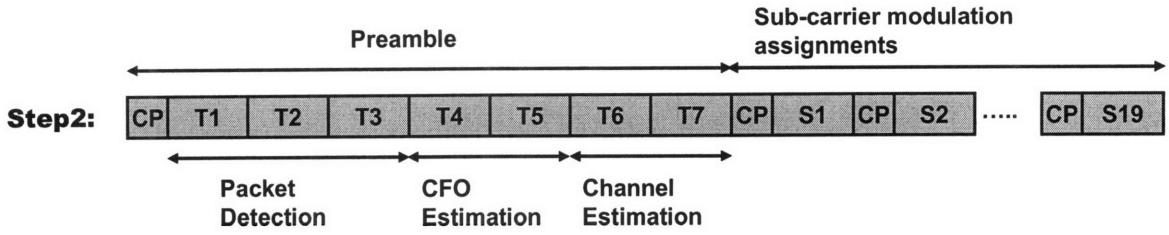

Figure 3-3: Packet structure sent in Step 2 [40]. T: one OFDM pilot symbol (T1 to T7 are identical), S: one OFDM CSI symbol, CP: Cyclic-Prefix.

3.4 Step 3: Data Transmission

After the transmitter receives and decodes the CSI, in Step 3 it uses the assigned modulation to transmit the data packet as shown in Fig. 3-1.

Finally, after completing steps 1 to 3, the assigned modulation from Step 1 remains valid until the channel changes, at which time it must be re-measured. Our system refreshes its CSI every 10 ms. This is a conservative choice compared to 17.3 ms (Equation 3.16), which is the **coherence time**, T_{coh}, for indoor environments [39], assuming an average walking speed of 5 km/h (v = 1.4 m/s) [54] and a carrier frequency of $f_c = 5.25$ GHz, obtained by:

$$T_{coh} = \sqrt{\frac{9}{16\pi {f_m}^2}} = \frac{0.423}{24.5} = 17.3\ ms \tag{3.15}$$

$$f_m = \frac{v}{\lambda} = \frac{1.4\ (m/s) \times 5.25\ (GHz)}{3 \times 10^8\ (m/s)} = 24.5\ Hz\ , \tag{3.16}$$

where f_m is the maximum Doppler shift, v is the relative speed between transmitter and receiver, and $\lambda = \frac{c}{f_c}$ is the carrier signal's wavelength, with $c = 3 \times 10^8$ (m/s) the speed of light.

Since the modulation assignments are based on SNR estimates in Step 1, the sub-carriers in Step 3 with this modulation assignment will be received without violating

the target BER if the true SNR in Step 3 is the same as SNR estimates. However, since SNR estimator has some variance, the estimates will never be exact. In addition, there are other system variables that change the true SNR between steps 1 and 3. Hence, a successful adaptive modulation requires taking these issues into account by adding a sufficient amount of margins to the true $\{SNR_{min}\}$ in Fig. 3-2, according to Equation 3.4. We discuss this in detail in the next section.

3.5 System Design Issues of Adaptive Modulation

The performance of sub-carrier adaptive modulation relies directly on the SNR estimate. The challenge is to obtain an SNR estimate that is sufficiently accurate and consistent. In this section, we first introduce how SNR accuracy and consistency affect mismatches in SNR between steps 1 and 3. We then conclude with a discussion on how to determine appropriate levels of SNR_{margin} to guarantee the success of Adaptive Modulation.

3.5.1 SNR Accuracy

In our prototype, the Adaptive Modulation algorithm assigns a modulation scheme to a sub-carrier k based on its SNR estimate, $\hat{SNR}_k$, and a target BER of 10^{-3}. If the SNR estimate is not accurate, the BER of that sub-carrier may exceed the target BER, causing poor performance.

It is important to note that even if one assumes a perfect AWGN channel model and ignores time synchronization errors and other practical issues, the SNR estimate has an **intrinsic stochastic noise** that limits our ability to measure it accurately. As can be seen from Equation 3.12, the accuracy of $\hat{SNR}_k$ depends on the k-th sub-carrier's channel fading estimate, $\hat{H}_k$, and its noise-variance estimate, $\hat{\sigma}_k^2$.

Our design problem, therefore, is to choose the number of OFDM pilot symbols, L and M, used in channel and noise-variance estimations respectively, such that the confidence that the estimated value is within an interval $[-z : z]$ (in dB) of the true value is high (*e.g.*, 99%). We discuss how we choose L and M in the next two sections.

(a) Choosing L for Channel Estimation: Using the zero-forcing channel estimator (Equation 3.8), we have $\frac{\hat{H}_k}{H_k} \sim N(1, \frac{\sigma_k^2}{L|H_k|^2})$, *i.e.,* the normalized channel estimate, $\frac{\hat{H}_k}{H_k}$, is a Gaussian random variable with mean 1 and variance $\frac{\sigma_k^2}{L|H_k|^2} = \frac{1}{L \times SNR_k}$. The confidence level in $|\hat{H}_k|^2$ is:

$$Prob\{\frac{1}{z} < \left|\frac{\hat{H}_k}{H_k}\right|^2 < z\} > 1 - \alpha\,, \tag{3.17}$$

where $1-\alpha$ is the confidence level and z is not in dB. The probability distribution of $\left|\frac{\hat{H}_k}{H_k}\right|^2$ can be derived as below:

$$\left|\frac{\hat{H}_k}{H_k}\right|^2 = \left|1 + \frac{1}{LH_k}\sum_{l=1}^{L}\frac{N_{l,k}}{X_k}\right|^2 \tag{3.18}$$

$$= \left|1 + \frac{1}{LH_k}\sum_{l=1}^{L}\frac{Re[N_{l,k}]}{X_k}\right|^2 + \left|\frac{1}{LH_k}\sum_{l=1}^{L}\frac{Im[N_{l,k}]}{X_k}\right|^2 = G_1^2 + G_2^2\,, \tag{3.19}$$

where G_1 and G_2 are independent Gaussian random variables, $G_1 \sim N(1, \frac{1}{2 \times L \times SNR_k})$ and $G_2 \sim N(0, \frac{1}{2 \times L \times SNR_k})$ respectively, since $|X_k|^2 = 1$. It can be shown (see definition below) that $|\frac{\hat{H}_k}{H_k}|^2(\frac{1}{\sigma_G^2})$ is a non-central Chi-square random variable, $\aleph^2_{2,\frac{1}{\sigma_G^2}}$, where $\sigma_G^2 = \frac{1}{2 \times L \times SNR_k}$ is the variance of each of the Gaussian random variables in the sum.

Definition 3.5.1. If $\{G_i\}$ are k independent Gaussian random variables with means $\{\mu_i\}$ and variances $\{\sigma_i^2\}$, then the random variable $\sum_{i=1}^{k}(\frac{G_i}{\sigma_i})^2$ is a **non-central Chi-square** random variable, $\aleph^2_{k,\lambda}$, with k *degrees of freedom* and *non-centrality parameter* λ, given by $\lambda = \sum_{i=1}^{k}(\frac{\mu_i}{\sigma_i})^2$ [55]. $\aleph^2_{k,\lambda}$ has PDF given by:

$$f_{\aleph}(x) = \frac{1}{2}e^{-\frac{(x+\lambda)}{2}}\left(\frac{x}{\lambda}\right)^{\frac{k}{4}-\frac{1}{2}} I_{\frac{k}{2}-2}(\sqrt{\lambda x}),\quad x \in [0, +\infty) \tag{3.20}$$

where $I(.)$ is the modified Bessel function of the first kind. $\aleph^2_{k,\lambda}$ has mean $k+\lambda$ and variance $2(k+2\lambda)$.

When the Gaussian random variables $\{G_i\}$ have zero mean and unit variance, the random variable $\sum_{i=1}^{k} {G_i}^2$ is a **Chi-square** random variable, $\aleph^2_k$, with k *degrees of*

freedom, mean k, variance $2k$, and PDF given by [55]:

$$f_{\aleph}(x) = \frac{(\frac{1}{2})^{\frac{k}{2}}}{\Gamma(\frac{k}{2})} x^{\frac{k}{2}-1} e^{-\frac{x}{2}}, \quad x \in [0, +\infty) , \tag{3.21}$$

where $\Gamma(m+1) = m!$ for positive integer m.

Since $|\frac{\hat{H}_k}{H_k}|^2 \lambda \sim \aleph^2_{2,\lambda}$, with $\lambda = 2 \times L \times SNR_k$, mean $2 + 2 \times L \times SNR_k$ and variance $4 + 8 \times L \times SNR_k$, the confidence level in $|\hat{H}_k|^2$ (in Equation 3.17) can be rearranged to get:

$$Prob\{\frac{\lambda}{z} < \aleph^2_{2,\lambda} < \lambda z\} > 1 - \alpha \tag{3.22}$$

$$Prob\{\frac{2 \times L \times SNR_k}{z} < \aleph^2_{2,2 \times L \times SNR_k} < 2 \times L \times SNR_k \times z\} > 1 - \alpha \tag{3.23}$$

In a packet-oriented wireless LAN system, we start with setting a confidence level, $1 - \alpha$, based on the target Packet Error Rate (PER). For instance, $PER < 10\%$ - which is the target value in 802.11a with packet length of 1000 bytes (8000 bits) [20] - translates to $\alpha = 0.11\%$. This is obtained by assuming that in the absence of error-correction coding, one modulation error results in one packet error. Hence, for 92 data sub-carriers, we have:

$$(1 - PER) = (1 - \alpha)^{92}. \tag{3.24}$$

Next, SNR dependency of the channel estimate accuracy suggests allowing different mismatch levels z at different $SNR_{thresholds}$ (*i.e.* SNR values at $BER = 10^{-3}$) of the modulation levels for a fixed L. Fig. 3-4a shows channel estimate mismatch levels at four $SNR_{thresholds}$ (represented by dots) when L OFDM pilot symbols are used in channel estimation, at confidence level 99.9% (or $\alpha = 0.1\%$). The 6 dashed-lines correspond to L taking values in the set {2, 4, 8, 16, 32, 64}. Similar plots but for $\alpha = 1\%$ and 10% are shown in Figs. 3-4b and 3-4c respectively. These figures show that the mismatch between the estimated and true channel power decreases with increasing SNR and L. At BPSK $SNR_{threshold} = 6.79$ dB, using $L = 2$ OFDM pilot

symbols would result in an estimate mismatch of 9.5 dB ($\alpha = 0.1\%$), 6.0 dB ($\alpha = 1\%$), and 3.3 dB ($\alpha = 10\%$). However, using same $L = 2$, at 64-QAM $SNR_{threshold} = 22.55$ dB, the resulting mismatch is significantly lower, at 1.0 dB for all confidence levels. At $SNR_{threshold} = 6.79$ dB, increasing L to 32 OFDM pilot symbols reduces the mismatch level significantly to 1.7 dB ($\alpha = 0.1\%$), 1.3 dB ($\alpha = 1\%$) and 1.0 dB ($\alpha = 10\%$).

This analysis supports using a large L to reduce inaccuracy in SNR due to errors in channel estimation. However, there is a maximum L that the system can tolerate. The measurements show that $L > 8$ is intolerable due to accumulation of uncompensated phase errors in the received OFDM symbols because channel estimation and correction are typically performed before phase-error removal (see Fig. 2-5). In addition, increasing L increases the preamble overhead of each packet by L μs. For a packet size of 8000 bits, as in 802.11a [20], and an average number of 250 bits per OFDM symbol (based on our measurements in Chapter 4 in typical indoor NLOS and LOS scenarios), each packet contains $N_{SYM} = 32$ OFDM data symbols, each with data duration $T_{FFT} = 1$ μs. The preamble contains $5 + L$ OFDM pilot symbols. Hence, using L OFDM pilot symbols reduces the data rate by:

$$\frac{L}{L + N_{SYM} \times T_{FFT}}, \tag{3.25}$$

which is 5.9%, 11%, and 20% for $L = 2$, 4, and 8 respectively. In other words, doubling L doubles the data reduction rate which is quite significant.

In our measurements using $L = 2$, channel power estimate mismatches between steps 1 and 3 never exceeded 4 dB, where higher mismatches occurred at lower SNR_k levels. Thus, to minimize this overhead, our prototype uses $L = 2$, and relies on a large M to decrease the errors in estimating the SNR, as discussed next.

(a) Choosing M for Noise-variance Estimation: Modifying Equation 3.13, the unbiased noise-variance estimation is:

$$\hat{\sigma}^2_{unbias,k} = \frac{1}{M-1} \sum_{i=1}^{M} (N_{i,k} - \frac{1}{M} \sum_{l=1}^{M} N_{l,k})^2 , \tag{3.26}$$

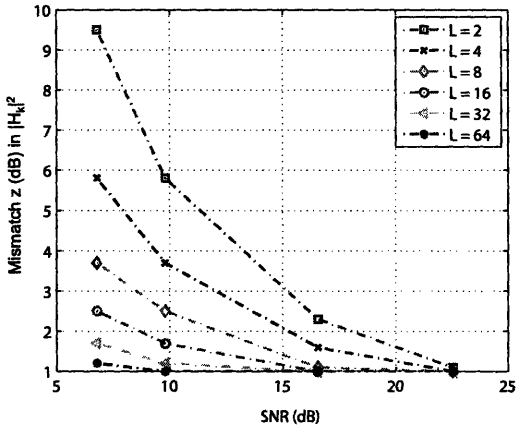

(a) z vs. SNR ($\alpha = 0.1\%$)

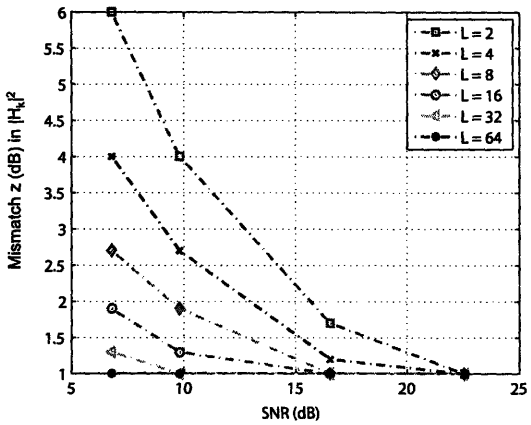

(b) z vs. SNR ($\alpha = 1\%$)

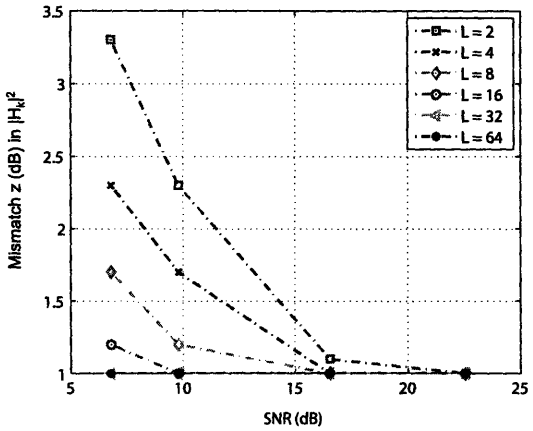

(c) z vs. SNR ($\alpha = 10\%$)

Figure 3-4: Plots of resulting z-dB mismatch in channel power estimate at $SNR(dB) = [6.79,\ 9.8,\ 16.55,\ 22.55]$ (dots) when $L = [2,\ 4,\ 8,\ 16,\ 32,\ 64]$ OFDM pilot symbols are used in the estimation. Confidence-level is (a) 99.9% ($\alpha = 0.1\%$), (b) 99% ($\alpha = 1\%$), and (c) 90% ($\alpha = 10\%$). For all confidence levels, the amount of mismatch z decreases with increasing SNR and L.

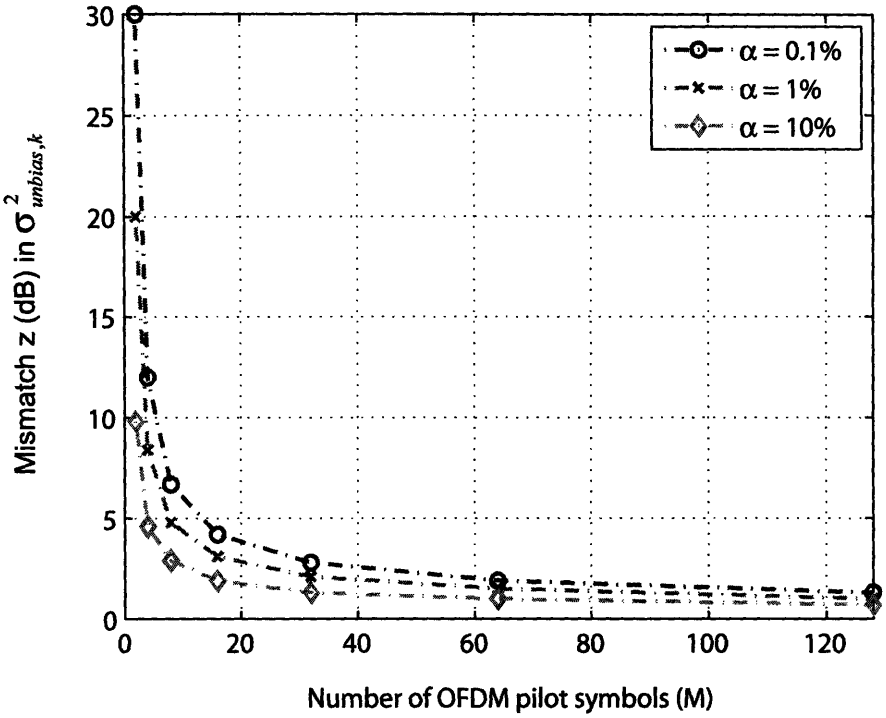

Figure 3-5: Mismatch in noise-variance estimate, z (dB), vs. M (number of OFDM pilot symbols used in noise-variance estimation) at $\alpha = \{0.1\%, 1\%, 10\%\}$. The dots represent $M = 2^{\{1:7\}}$.

with the confidence interval:

$$Prob\{\frac{2(M-1)}{z} < \frac{2(M-1)\hat{\sigma}^2_{unbias,k}}{\sigma^2_k} < 2(M-1)z\} > 1-\alpha\,, \tag{3.27}$$

where $\frac{2(M-1)\hat{\sigma}^2_{unbias,k}}{\sigma^2_k}$ is a **Chi-square** random variable, $\aleph^2_{2(M-1)}$ with $k = 2(M-1)$ degrees of freedom, mean k and variance $2k$ (Def. 3.5.1). Fig. 3-5 shows how the mismatch between the estimated and true noise variance decreases with increasing M at $\alpha = 0.1\%$, 1% and 10%, with the dots indicating M at powers of 2. At start, as M increases from 2 to 32, the mismatch level decreases sharply from 30 dB to 2.8 dB ($\alpha = 0.1\%$). The rate of decrease slows down after, with only 0.9 dB decrease from $M = 32$ to 64.

While improving SNR estimate, increasing M incurs an overhead cost of M μs during Step 1. To reduce the overhead from Adaptive Modulation protocol, it is reasonable to adopt a networking strategy that performs steps 1 and 2 once for all

the packets within the channel coherence time, T_{coh}. Assuming N_{Packet} packets can be sent within T_{coh}, using M reduces the data rate by,

$$R_{M,overhead} = \frac{M}{M + N_{SYM} \times N_{Packet}}, \tag{3.28}$$

with

$$N_{Packet} = \left\lfloor \frac{T_{coh} - T_{AdaptMod}}{T_{Packet}} \right\rfloor \tag{3.29}$$

$$T_{Packet} = \frac{N_{BPP}}{N_{BPS}} \times T_{SYM} + T_{Preamble}, \tag{3.30}$$

where we use

- $T_{coh} = 10$ ms
- $T_{AdaptMod} = (77.37 + M)\ \mu s$ which is the total time from Step 1 up to Step 3
- $N_{BPP} = 8000$ Bits per Packet
- $N_{BPS} = 250$ Bits per OFDM symbol
- $N_{SYM} = N_{BPP}/N_{BPS} = 32$ Number of OFDM symbols per Packet
- $T_{SYM} = 1.4\ \mu s$ (CP $= 0.4\ \mu s$)
- $T_{Premable} = 7.4\ \mu s$ ($L = 2$, CP $= 0.4\ \mu s$)

Table 3.1 shows the amount of data rate decrease for various M, which is as low as 0.03% for $M = 2$ and exceeds 100% for $M > 2^{14}$. We also observe that doubling M doubles the reduction in data rate.

Our SNR estimation strategy in Step 1 computes the noise variance over $M = 32$ OFDM pilot symbols. However, as shown in Section 4.4, our measurements indicate a higher throughput from using $M = 64$ OFDM pilot symbols instead. This is because the increase in throughput due to the lower mismatch level by 0.9 dB from $M = 64$ more than compensates for the loss due to the small additional overhead of 0.5%.

M	*Data Rate Decrease (%)* (Equation 3.28)	*Mismatch z (dB)*
2	0.03	30
4	0.07	12
8	0.13	6.7
16	0.26	4.2
32	0.52	2.8
64	1.05	1.9
128	2.08	1.3
256	4.12	1.0
512	8.12	0.7
1024	15.76	0.5
2048	29.77	0.4
4096	53.33	0.3
8192	88.28	0.2
16,384	131.62	0.2

Table 3.1: Decrease in data rate and mismatch (z-dB) in noise-variance estimate from using M OFDM pilot symbols for $M = 2^{\{1:14\}}$.

3.5.2 SNR Consistency

In addition to being accurate, SNR estimate in Step 1 needs to match the SNR that is actually seen by the data in Step 3. A poor match means that we cannot predict the SNR of the data based on the SNR of the training OFDM symbols, and thus we will fail to predict the right modulation for the sub-carrier. Hence, a design goal for our system is that:

$$Prob\{SNR_{mismatch} = \hat{SNR}_{Step1} - SNR_{Step3} > X(dB)\} < \alpha\,, \tag{3.31}$$

where X is a lower bound on the SNR_{margin} in Equation 3.4 and α is a small constant that defaults to 0.1% for PER = 10%.

The two major sources of $SNR_{mismatch}$ are **stochastic noise in SNR estimation**, and **timing offset**. The contribution of stochastic noise to uncertainty in SNR estimation is described in the previous section.

Timing offset results from two major sources: (1) error in estimation of start of the OFDM symbol, and (2) the mismatch in the sampling frequency of the trans-

mitter's DAC and the receiver's ADC. Hence, the different start estimations of the packet in steps 1 and 3 combined with different sampling instants can result in significant $SNR_{mismatch}$. The next two paragraphs discuss these two sources and suggest practical solutions.

The task of finding the precise moment of when individual OFDM symbols start and end - *i.e.* FFT window - is referred to as *symbol timing.* When the estimated FFT window includes samples from the next OFDM symbol, as indicated in Fig. 3-6a, symbol timing offset can introduce significant ISI (since some of the desired energy is lost and some undesired energy is added) and ICI (since the orthogonality of sub-carriers is lost) [44]. While late symbol timing is intolerable, early symbol timing when the FFT window contains samples from the previous OFDM symbol results in only rotation of sub-carriers (hence no ISI and ICI) which can be corrected for as long as it contains only insignificant samples from the channel ISI in the CP. Thus, late symbol timing is avoided by shifting the mean of symbol timing estimate inside the CP such that its PDF is entirely contained in CP, as shown in Fig. 3-6b. With such symbol timing estimator, to avoid channel ISI in CP, the CP length must include extra samples as long as the variance of the estimator. To minimize this overhead from CP, a proper system design solution is to use a fine time acquisition algorithm to minimize the variance of symbol timing estimator. Indeed, in our prototype, when we increased the CP by 0.2 μs to put enough headroom for our course timing algorithm, the levels of $SNR_{mismatch}$ reduced significantly from 10 dB down to around 3-6 dB. Hence, our system's CP length is 40% of the OFDM data symbol length which is higher than the maximum value of 25% used in practical systems [1, 2, 20]. By incorporating a fine timing algorithm, our system CP length can be reduced to 0.25 μs, which is more reasonable.

In addition to symbol timing, *Sampling Frequency Offset (SFO)* generates ICI from slightly incorrect sampling instants [44]. Due to different OFDM starting samples in steps 1 and 3, the amount of SNR losses will be different which result in mismatches in SNR. The effect of SFO can be reduced if the ADC upsamples the received signal by 2x or 4x the data frequency (128 MHz) to obtain finer sampling time estimates closer

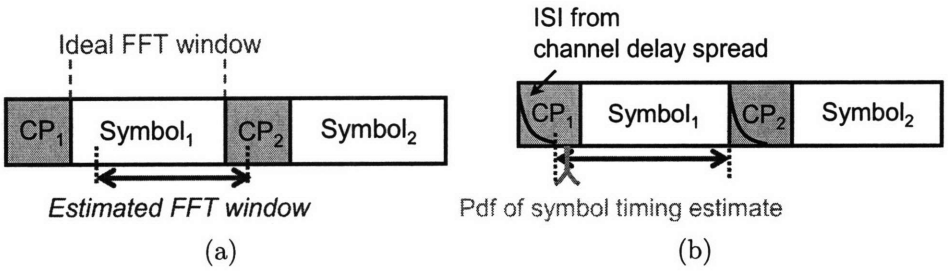

Figure 3-6: (a) Late symbol timing includes samples from the next OFDM symbol. The ideal FFT window is shown for comparison. (b) The PDF of symbol timing estimate should be contained inside CP to avoid late symbol timing in (a).

to the data points. In addition, using the same oscillator to generate the carrier and sampling frequencies can improve the accuracy of the SFO. This is in fact a requirement in the 802.11a standard [20]. We did not use a single oscillator since we were not aware of its adverse impact on AMC during initial design stages of the WiGLAN RF Front-End.

3.5.3 SNR_{margin} for Successful Adaptive Modulation

The existence of some level of $SNR_{mismatch}$ between steps 1 and 3 requires the modulation decision algorithm to include an SNR_{margin} in the SNR estimate, as in Equation 3.4.

Fig. 3-7 indicates our sub-carrier Adaptive Modulation assignment when SNR_{margin} is included in determining minimum SNR required (indicated by dashed lines) for each modulation. Hence, using $SNR_{margin} = 5.0$ dB for BPSK, SNR_{min} is shifted from 6.79 dB to 11.79 dB. The values of SNR_{margin} for all modulations are tabulated in Table 3.2. We will detail our empirical procedure to find $\{SNR_{margin}\}$ in the next Chapter.

As Table 3.2 indicates, the value of SNR_{margin} from the lowest to the highest modulation type first decreases and then increases. Higher SNR_{margin} at lower SNR values is due to the variance of estimation algorithms (such as the channel and CFO estimators) being inversely proportional to SNR. In other words, the estimations improve with increasing SNR.

However, SNR_{margin} does not continue to decrease with higher modulation because at higher modulations other non-ideality effects become dominant. In particular, during data transmission in Step 3, the uncompensated CFO before FFT as well as phase-noise cause ICI that increase the noise floor on all the sub-carriers. Similar effect is caused from clipping or saturation of the RF Power Amplifier when the data OFDM symbols have high PAPR. When clipping of peaky samples occurs, the impulse noise in the time domain corresponds to a constant noise in the frequency domain over all sub-carriers. This additional white noise imposes a higher SNR degradation on higher-order modulations where the constellation points are closer to each other. Furthermore, SNR loss of the k^{th} sub-carrier due to ICI from SFO is higher for sub-carriers with higher SNR, according to [44]:

$$SNR_{LOSS,k}^{ICI-SFO} = 10\ log_{10}(1 + \frac{1}{3} SNR_k(\pi\ k\ \frac{f_s' - f_s}{f_s}))\ , \tag{3.32}$$

where SNR_k is the SNR of the k^{th} sub-carrier, and f_s' and f_s are the sampling frequencies of the DAC and ADC respectively. This is true when all sub-carriers have the same average symbol energy as it is in our system.

Consequently, for all above reasons the higher SNR_{margin} at the lowest and highest modulation types is expected, and this is verified by our measurements.

Modulation	BPSK	4-QAM	16-QAM	64-QAM
SNR *(dB)* $@BER = 10^{-3}$	6.79	9.80	16.55	22.55
SNR_{margin} *(dB)*	5.0	3.5	3.8	6.4
SNR_{min} *(dB)*	11.79	13.30	20.35	28.95

Table 3.2: The SNR at BER of 10^{-3} as shown in Fig. 3-2, the required SNR margins, and the minimum SNR required by our algorithm to assign a modulation scheme to each sub-carrier.

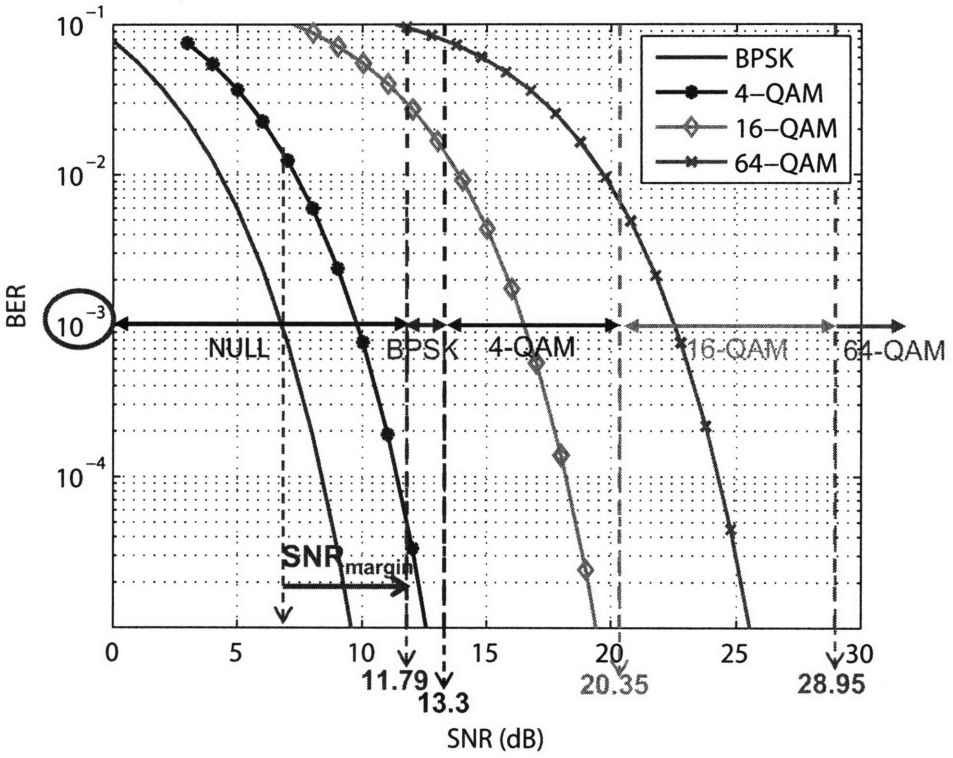

Figure 3-7: Sub-carrier modulation assignment using SNR_{min}(dashed lines) = SNR(at BER=10^{-3})+SNR_{margin} in Table. 3.2.

3.6 Logic Utilization of Adaptive Modulation Baseband Modem

The sub-Carrier Adaptive Modulation baseband modem is implemented on the Xilinx Virtex 4 FPGA. The resources available on this FPGA are as follows:

- *Flip-Flops (FF)*: These are storage elements.
- *Look-up Table (LUT)*: These are 4-input look-up tables which are capable of implementing any arbitrary defined 4-input Boolean function.
- *RAMB16*: These are 18-kbit memory blocks.
- *DSP48*: These are multipliers capable of multiplying two 18-bit numbers.

Our implementation of transmitter and receiver on a single FPGA with sub-carrier Adaptive Modulation functionality is shown in Fig. 3-1. The sub-carrier Adaptive Modulation blocks are:

- SNR estimator
- Modulation assigner
- BCH encoder and decoder
- CRC encoder and CRC check

This design runs at the desired clock frequency of 128 MHz. Table 3.3 presents the FPGA logic utilization by WiGLAN transceiver design and sub-carrier Adaptive Modulation blocks above. In addition, the FPGA synthesis and implementation tool reports the total equivalent gate count for the design which is the number of 2-input NAND gates required if all used FPGA resources are decomposed into 2-input NAND gates [42]. In terms of gate count, the sub-carrier Adaptive Modulation design occupies 9.95% of the 439,988 total transceiver gates. This indicates that our adaptive modulation scheme incurs a reasonable implementation complexity.

Resources	*WiGLAN Transceiver*	*Sub-carrier Adaptive Modulation Blocks*
FFs	17,378/30,720 (56%)	1,338/17,378 (7.7%)
LUTs	15,522/30,720 (50%)	2,090/15,522 (13.46%)
RAMB16s	179/192 (93%)	25/179 (13.97%)
DSP48s	57/192 (29%)	2/57 (3.51%)

Table 3.3: FPGA logic utilization by WiGLAN transceiver and sub-carrier Adaptive Modulation blocks.

Chapter 4

Sub-carrier Adaptive Modulation Measured Results

In this chapter, measured results from sub-carrier Adaptive Modulation will be presented. The first section will present the measurement setup conducted real-time with the WiGLAN prototype in an indoor environment. The second section will show the measured channel fading. Finally, the third section will analyze the collected data.

4.1 Measurement Test Setup

Measurements are taken in two different environments:

1. Small Line-of-Sight (LOS) environment (Room)

2. Medium Non Line-of-Sight (NLOS) environment (Lab)

As indicated in Fig. 4-1, the receiver is fixed in one location and the transmitter is moved to various locations (labeled A to J) at link distances 1.0-10.8 meters. In the medium NLOS environment, the locations include a diverse set of channel conditions from obstructed-by-lab-equipments A to D, to obstructed-by-concrete-wall E and F, and obstructed-by-metal-box G to J.

We do the measurements following steps 1 to 3 as mentioned in Chapter 3. Fig. 4-2 shows the packet sent in steps 1 and 3 from the transmitter to the receiver. In Step 1,

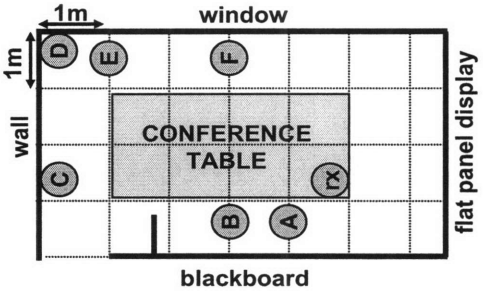

Transmitter Location	Link Distance (m)
A	1.0
B	1.8
C	4.6
D	5.3
E	3.6
F	3.1

(a) LOS

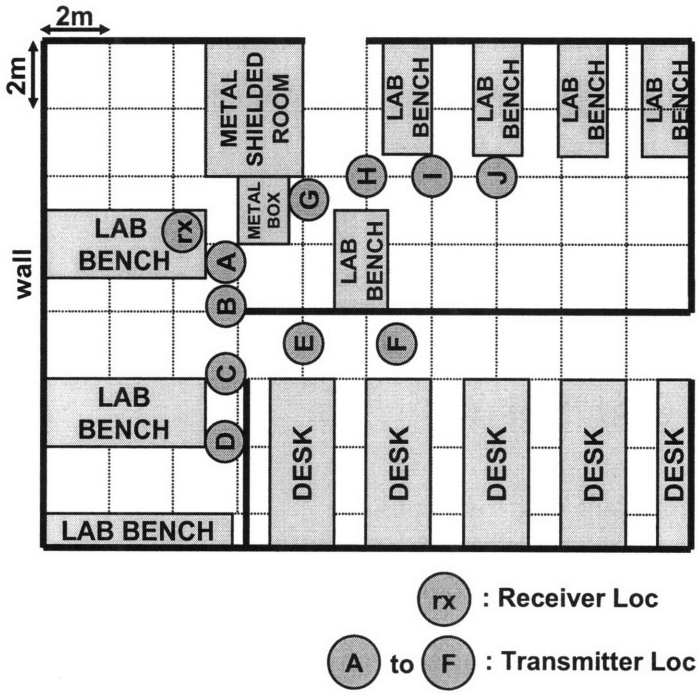

Transmitter Location	Link Distance (m)
A	1.0
B	2.8
C	4.5
D	6.3
E	4.0
F	7.3
G	5.7
H	7.2
I	8.9
J	10.8

(b) NLOS

Figure 4-1: Location of transmitter-receiver pairs in LOS (top) and NLOS (bottom) environments with corresponding link distances in the table.

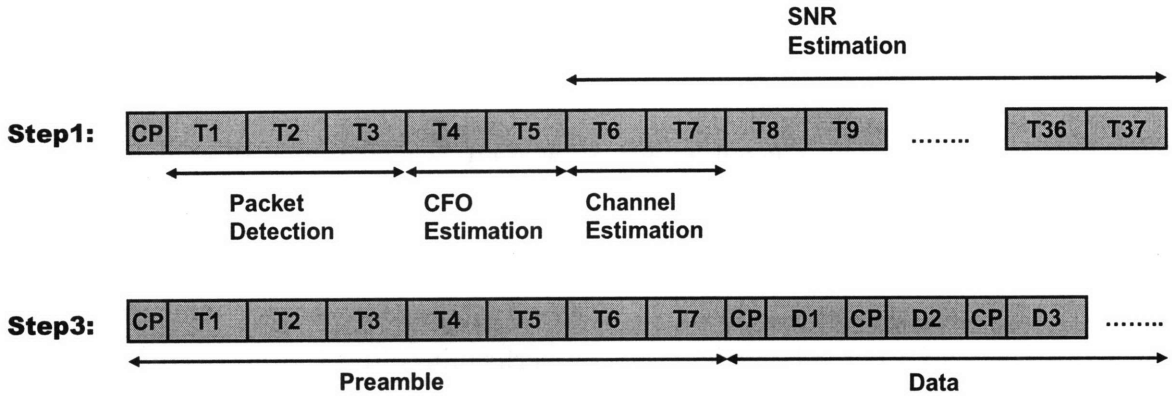

Figure 4-2: Packet structure during measurement sent in Step1 (top) and Step3 (bottom) [40]; T: one OFDM pilot symbol, D: one OFDM data symbol, CP: Cyclic-Prefix.

the transmitted packet consists of 1 CP and 37 identical OFDM pilot symbols, where OFDM pilot symbols T1 to T7 are used for Packet Detection, CFO Estimation, and Channel Estimation, as indicated in this figure. The receiver performs SNR estimation on the last 32 OFDM pilot symbols (as described in Section 3.2). In Step 2, the modulation assignments are sent back to the transmitter. Finally, in Step 3, the transmitted packet consists of a Preamble (T1 to T7), to perform time and frequency synchronization, followed by OFDM data symbols. For each OFDM data symbol, the data bits are loaded on the sub-carriers based on the sub-carrier modulation assignments. Each packet contains 4000 randomly generated OFDM data symbols. The receiver processes this packet and decodes the bits in real-time. Consequently, the receiver measures:

- Channel fade estimate $|H|^2$ per sub-carrier.
- SNR estimate per sub-carrier as described in Equation 3.9.
- BER per sub-carrier.

As explained in Section 3.5, given SNR at a BER of 10^{-3} for each modulation scheme (in Fig. 3-2), a sufficient amount of SNR_{margin} is required to ensure that the SNR in Step 3 will meet the target BER of 10^{-3}. Table 3.2 indicates the SNR_{margin} that we used for each modulation decision. The sum of the SNR at BER=10^{-3} (in

Fig. 3-2) and SNR_{margin} results in SNR_{min}, which is the minimum SNR required by our algorithm to assign a particular modulation scheme to a sub-carrier. Using these SNR_{min} thresholds, our measurements show that the BER per sub-carrier always meets the target BER.

We obtain $\{SNR_{margin}\}$ in Table 3.2 empirically by the following protocol:

- Measure SNR per sub-carrier twice by performing Step 1, Step 2, Step 1. Let us call the SNR estimates in the first Step 1-a, $S\hat{N}R_a$, and in the second Step 1-b, $S\hat{N}R_b$. Take 10 measurements in each of the various locations in the environment.

- In each measurement, for all the sub-carriers with higher assigned modulation in Step 1-a than Step 1-b, *i.e.* $\{mod_{k,a} > mod_{k,b}\}$ (since these are the ones that violate the BER), calculate how far $S\hat{N}R_a$ is from $SNR_{threshold}$ of $mod_{k,a}$: *i.e.* $\Delta SNR = S\hat{N}R_a$ - $SNR_{threshold}$ (see Fig. 4-3). Find the set of $\{\Delta SNR\}$ separately for each modulation type in Step 1-a.

- For each modulation type, find the frequency of occurrence of each ΔSNR over all corresponding sub-carriers in all measurements. Then, SNR_{margin} is the smallest ΔSNR that occurs less than 0.1%, *i.e.*

$$\text{Prob}_{\{k \mid mod_{k,a} > mod_{k,b}\}}\{\Delta SNR > SNR_{margin}\} < 0.1\% \tag{4.1}$$

The resulting set of $\{SNR_{margin}\}$, one for each modulation, is used in the Adaptive Modulation protocol. Note that for a general wireless transceiver, a similar protocol could be performed by the network during the initialization phase to calibrate its $\{SNR_{margin}\}$ for that wireless link.

4.2 Channel Measurements

The measured channel fading estimates, $|H|^2$, and SNR estimates for locations A to J (in NLOS) are shown in Figs. 4-4, 4-5, 4-6, and for locations A to F (in LOS) in

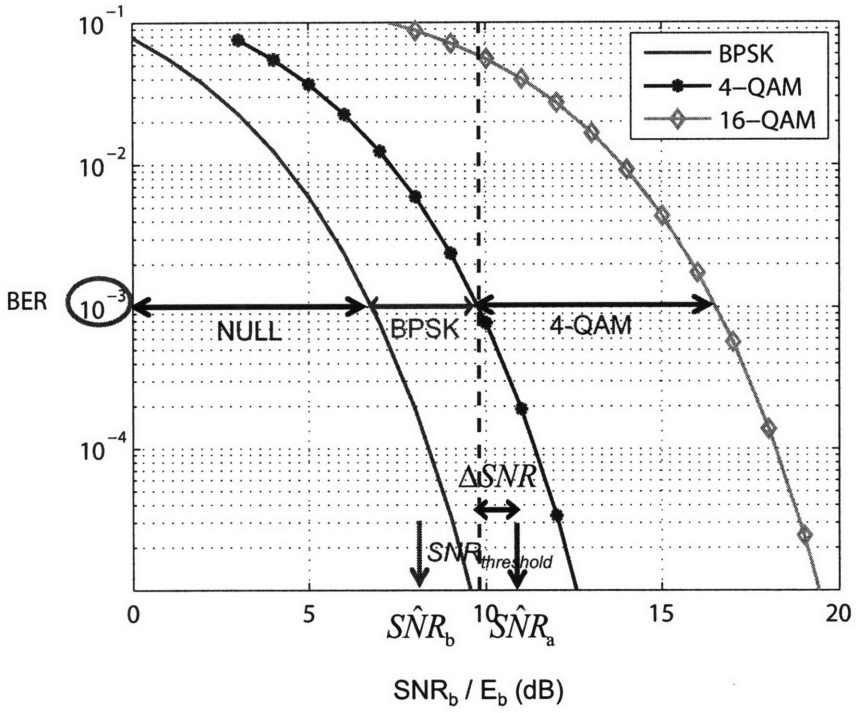

Figure 4-3: Illustration of how ΔSNR is obtained from measured $S\hat{N}R_a$ and $S\hat{N}R_b$ in our protocol to obtain $\{SNR_{margin}\}$.

Figs. 4-7 and 4-8.

The channel fading estimates, $|H|^2$, are the measured values at the channel estimator's output without any normalization. Hence, $|H|^2$ includes the following factors:

1. Normalization of QAM (at transmitter) to get same average power on all modulations and minimize the maximum transmit power.

2. Clipping threshold factor (according to Equation 2.24).

3. Factor of $N_{FFT} = 128$ from IFFT/FFT implementation.

4. Analog filters in the signal path.

5. Multipath wireless channel.

6. Signal attenuations from ISI due to CFO and SFO.

Modulation	K_{MOD}
BPSK	1/1.1504
4-QAM	1/1.627
16-QAM	1/1.2127
64-QAM	1/1.065

Table 4.1: Normalization factor of each modulator output symbol to obtain same average power.

In the absence of the data converters, the RF Front End, and the wireless channel, when the output of digital transmitter (sending 100 BPSK sub-carriers) is fed directly into the digital receiver, $|H|^2$ includes factors from (1) 1/1.1504=0.8692, (2) 0.0261, and (3) 128 only, resulting in:

$$|H^2| = 20\ log_{10}(0.8692 \times 0.0261 \times 128) = 9.25\ dB. \tag{4.2}$$

The normalization (1) of the output of QAM symbols, X, is given by

$$X = (I + jQ) \times K_{MOD}\ , \tag{4.3}$$

where I and Q are the In-phase and Quadrature-phase components respectively. This normalization is done according to (Table 4.1):

$$K_{MOD} = \frac{1}{\sqrt{\frac{\text{avg. power of QAM with max power of 1}}{\text{avg. power of 256-QAM with max power of 1}}}}\ , \tag{4.4}$$

such that all modulations have an average output power equal to the average power of a 256-QAM with maximum power of 1. However, since at the receiver, the QAM demodulator assumes that modulations have an average power of 1, this factor appears in the channel estimates.

In the figures of SNR estimates, the horizontal lines refer to the minimum SNR, SNR_{min}, necessary to support a particular modulation scheme at a target BER of 10^{-3}, reported in Table 3.2. The number of sub-carriers assigned to each modulation are shown in the parenthesis. As stated earlier, we use the same transmit RF power

over all sub-carriers, and hence differences in the SNRs reflect differences in sub-channel fading characteristics, as verified by measurements.

Overall, the figures shows high frequency diversity over the wide 100 MHz bandwidth, justifying the use of sub-carrier adaptive modulation in wideband OFDM systems. The figures also show the result of our modulation assignment algorithm. For instance, in LOS location E, there are 4 null sub-carriers, 3 BPSK sub-carriers, 25 4-QAM sub-carriers, 38 16-QAM sub-carriers and 21 64-QAM sub-carriers. This result indicates the gain from adaptive modulation which enables sending 64-QAM sub-carriers on 23% of the sub-carriers, which would have not been possible if the same modulation is picked for all sub-carriers. In the NLOS location J, the adaptive modulation scheme assigns 15 sub-carriers to null, 8 sub-carriers to BPSK, 52 sub-carriers to 4-QAM, 17 sub-carriers to 16-QAM, and no sub-carriers to 64-QAM, which is due to location J being at the maximum link distance and hence having relatively low SNR on all sub-carriers. The benefit of sub-carrier adaptive modulation is apparent at location J as well since it enables sending 16-QAM on some of the sub-carriers despite the overall low average SNR.

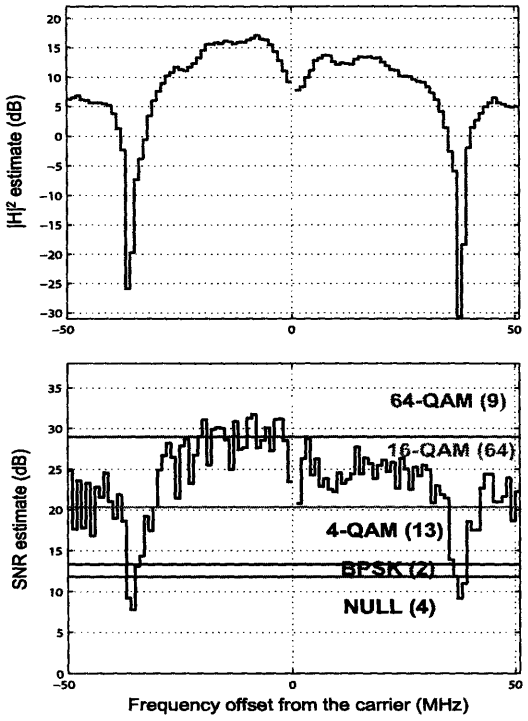

(a) NLOS Loc A

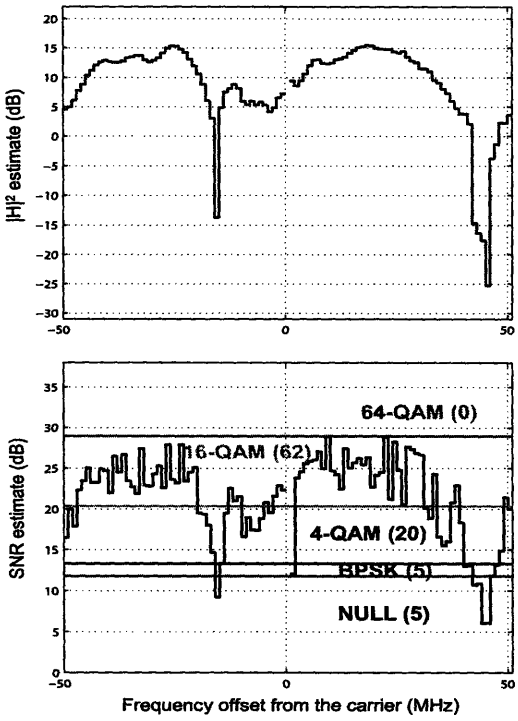

(b) NLOS Loc B

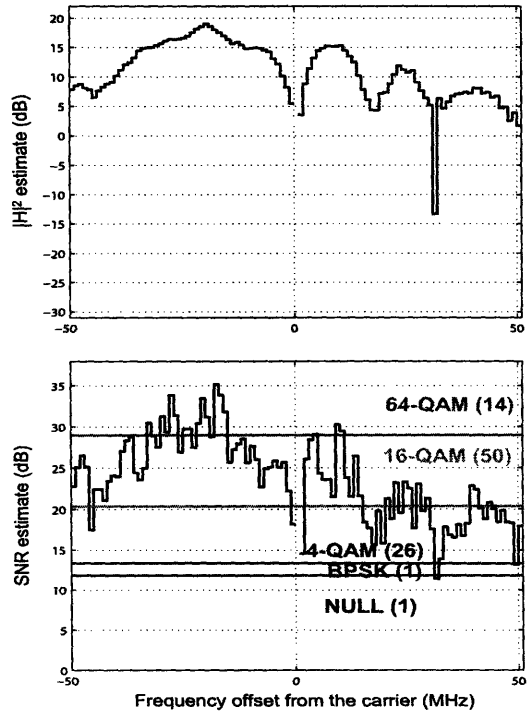

(c) NLOS Loc C

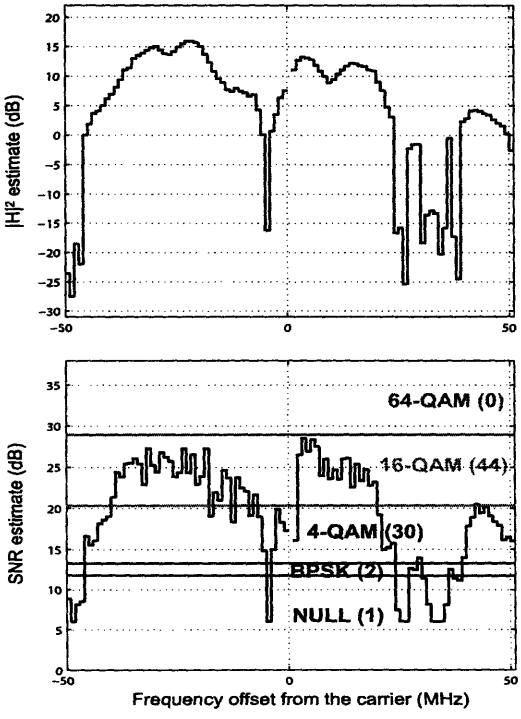

(d) NLOS Loc D

Figure 4-4: Channel power estimate $|H|^2$ vs. frequency (top) and SNR estimate vs. frequency (bottom) for NLOS locations A, B, C, and D.

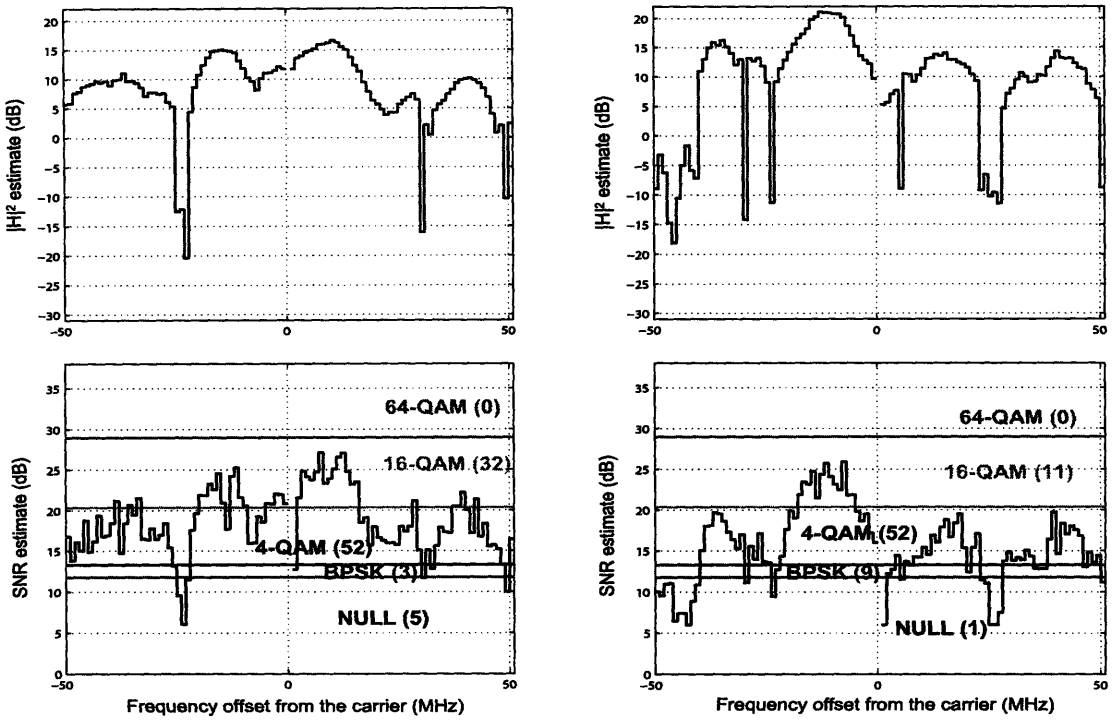

(a) NLOS Loc E

(b) NLOS Loc F

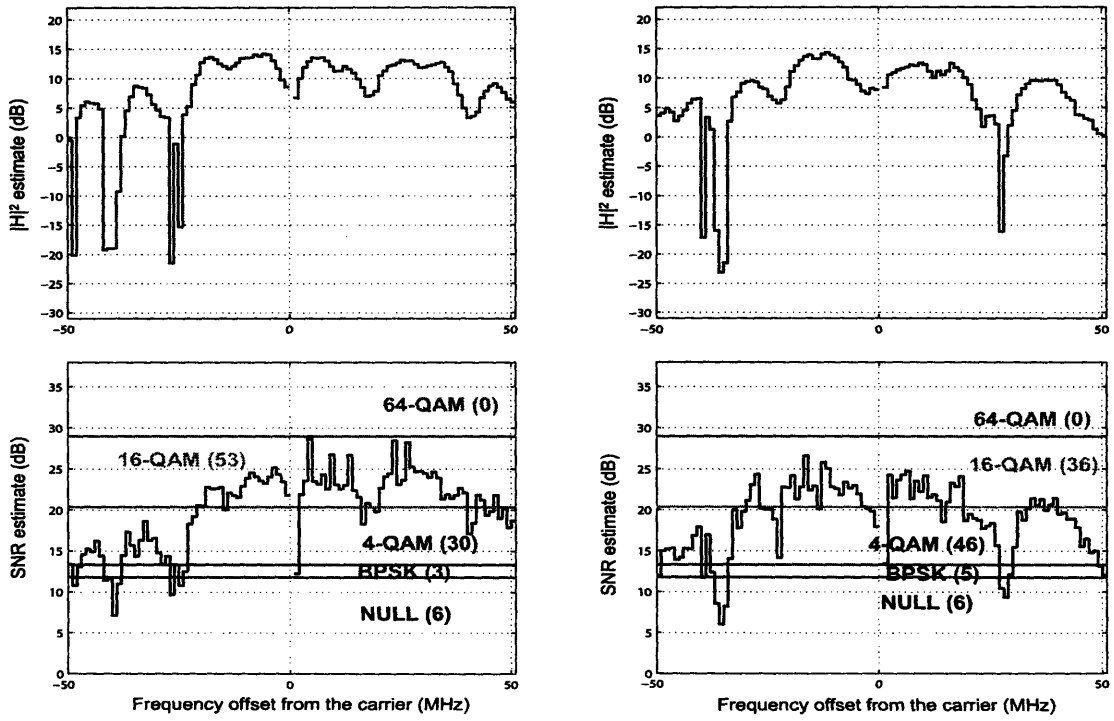

(c) NLOS Loc G

(d) NLOS Loc H

Figure 4-5: Channel power estimate $|H|^2$ vs. frequency (top) and SNR estimate vs. frequency (bottom) for NLOS locations E, F, G, and H.

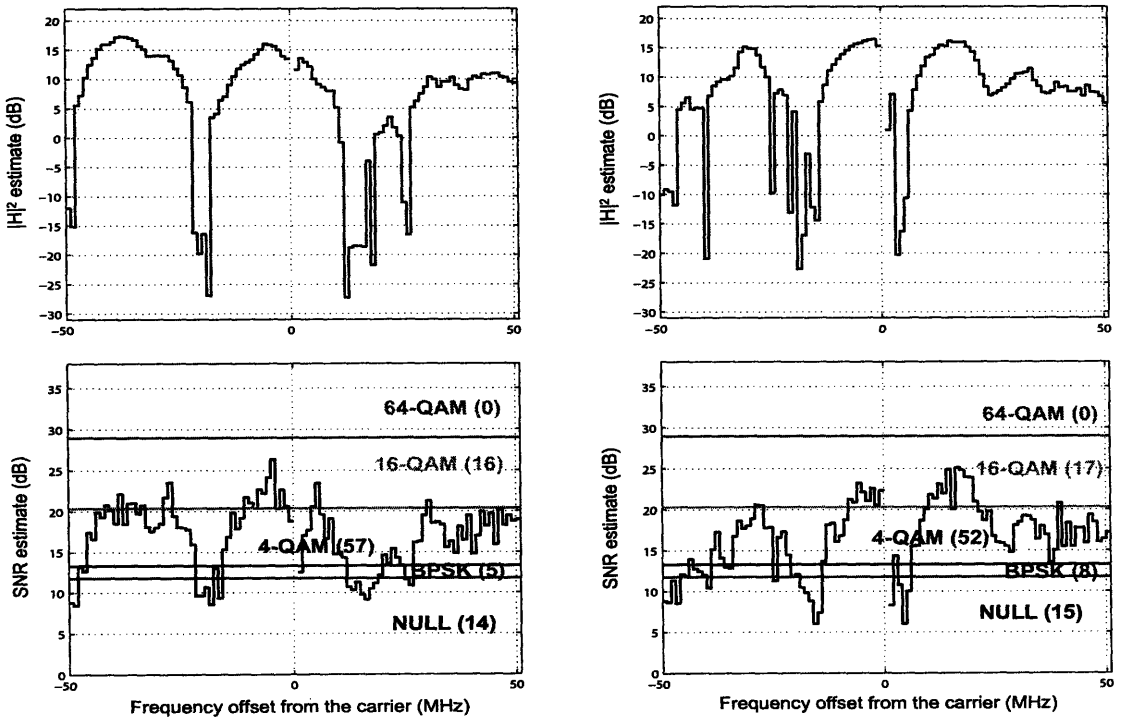

(a) NLOS Loc I

(b) NLOS Loc J

Figure 4-6: Channel power estimate $|H|^2$ vs. frequency (top) and SNR estimate vs. frequency (bottom) for NLOS locations I and J.

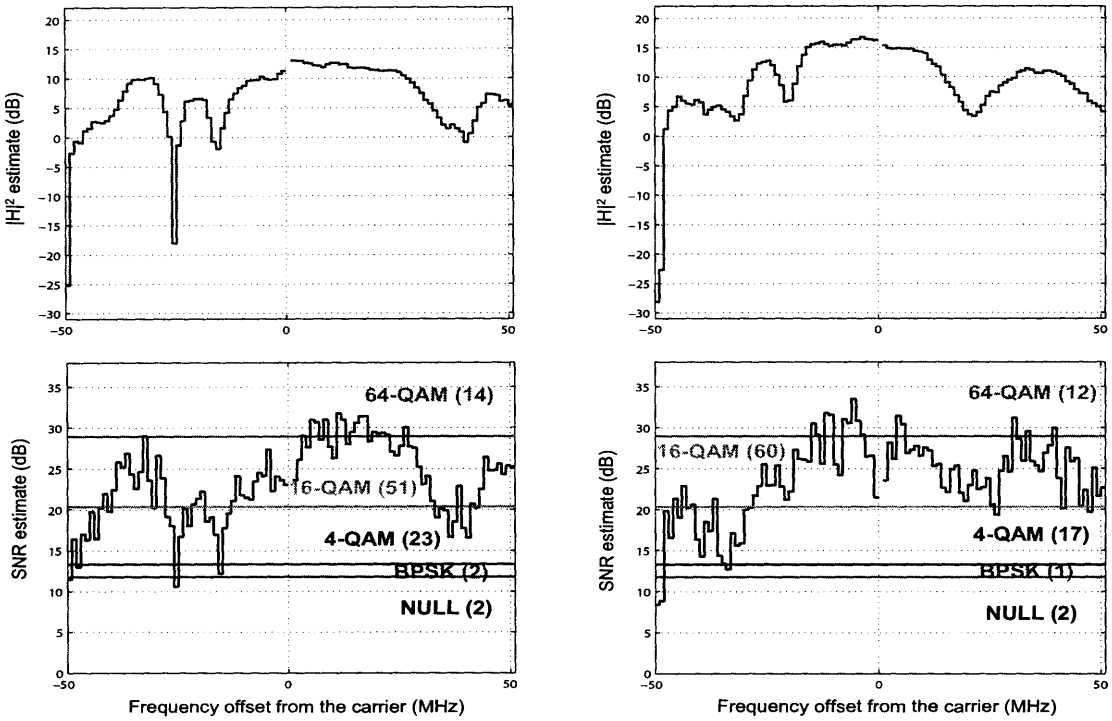

(a) LOS Loc A

(b) LOS Loc B

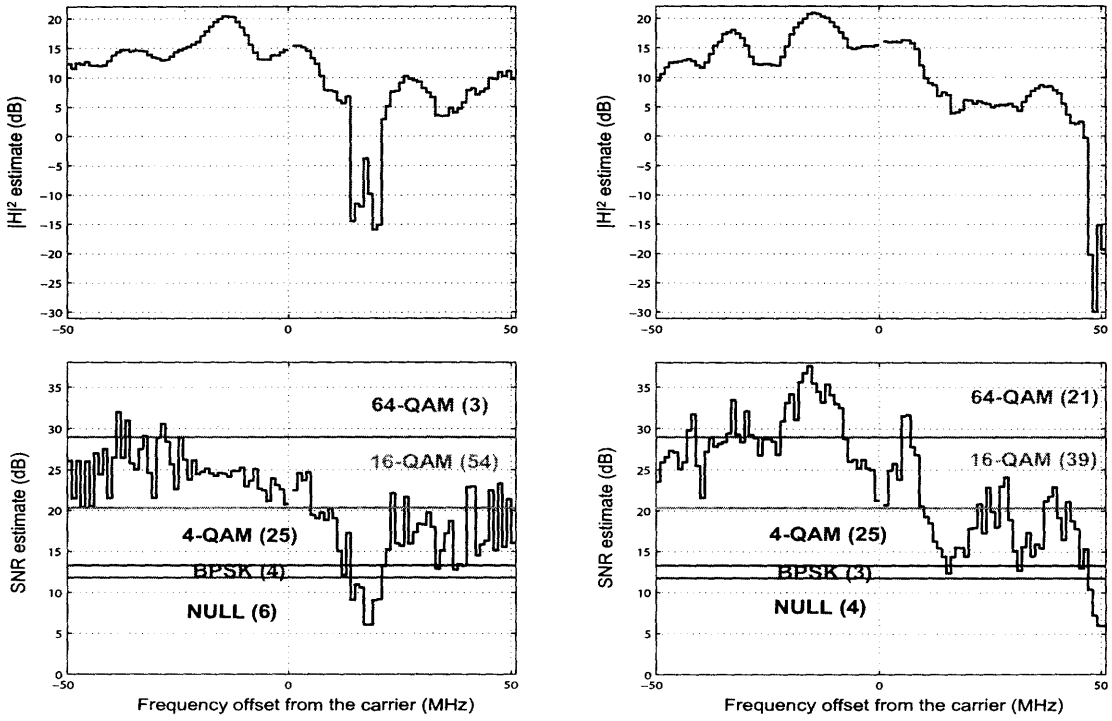

(c) LOS Loc C

(d) LOS Loc D

Figure 4-7: Channel power estimate $|H|^2$ vs. frequency (top) and SNR estimate vs. frequency (bottom) for LOS locations A, B, C, and D.

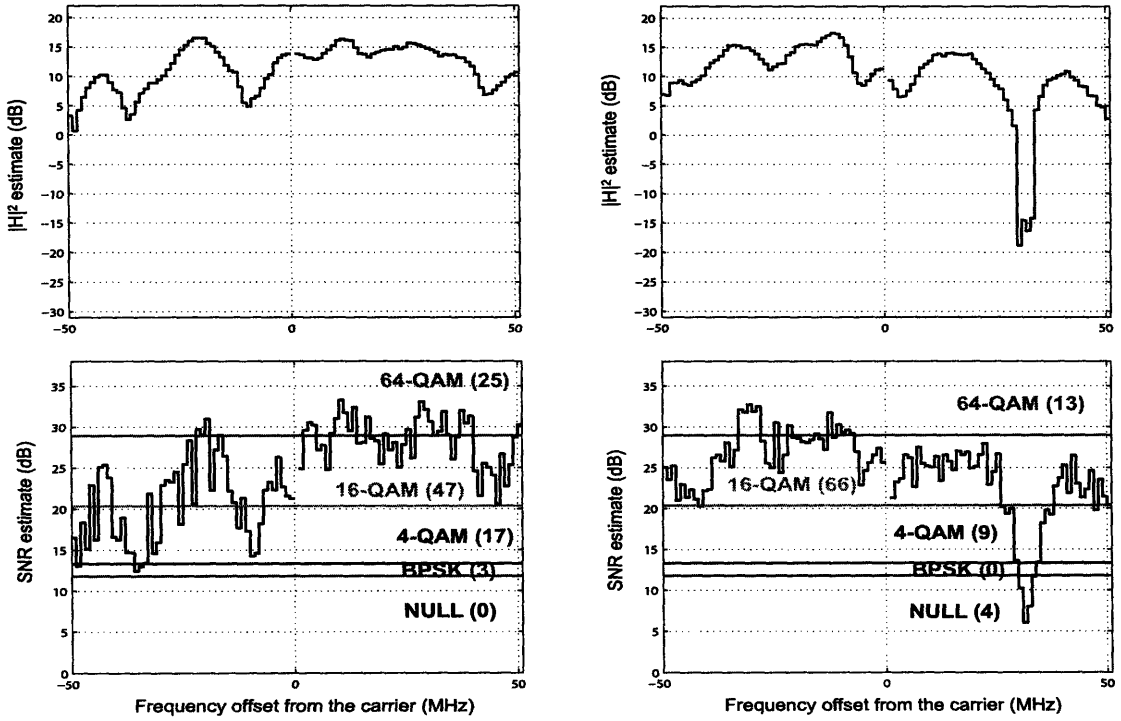

(a) LOS Loc E (b) LOS Loc F

Figure 4-8: Channel power estimate $|H|^2$ vs. frequency (top) and SNR estimate vs. frequency (bottom) for LOS locations E and F.

4.3 Analysis

Figs. 4-4 to 4-8 verify that different sub-carriers in a wideband channel experience different SNRs, and thus should employ different modulation schemes. Based on the channel and SNR measurements taken, the subsequent section will provide an in-depth analysis on the following:

- WiGLAN Data Rate Gain from Sub-carrier Adaptive Modulation.
- Comparison of WiGLAN data rate gain to the optimum Water-filling method.
- WiGLAN throughput with Adaptive Modulation overhead.
- Effect of SNR_{margin} on throughput.
- Fading over time.

4.3.1 WiGLAN Data Rate Gain from Sub-carrier Adaptive Modulation

To quantify the measured performance gain from sub-carrier Adaptive Modulation, we define the attainable data rate, R, as:

$$R = \frac{N_{BPS}}{T_{FFT}} \tag{4.5}$$

We ignore the CP because its value is not related to the use of sub-carrier Adaptive Modulation and will be significantly smaller if we use a more robust time synchronization algorithm (as discussed in Section 3.5). Section 4.3.3 explores the influence of CP and other overheads on the data rate.

We take 10 measurements for each LOS and NLOS location, and for each measurement, compute the data rate with sub-carrier Adaptive Modulation, R_{ADAPT}, and compare it with the data rate when a single modulation scheme is used across all the sub-carriers that can support that scheme for the target BER, $R_{nonADAPT}$. For a conservative comparison, we find the maximum data rate when sending BPSK,

4-QAM, 16-QAM or 64-QAM on all sub-carriers, and use the maximum $R_{nonADAPT}$ in calculating the data rate gain as:

$$GAIN = R_{ADAPT}/R_{nonADAPT} \tag{4.6}$$

Note that this is an extremely conservative computation of GAIN as compared to practical systems such as OFDM WLAN standard 802.11a. Moreover, using maximum $R_{nonADAPT}$ in computation of GAIN, quantifies the data rate gain from *Sub-carrier* adaptation over OFDM *Symbol* adaptation (which uses the same modulation over all sub-carriers). In other words, $R_{nonADAPT}$ is a form of adaptation, and hence, we expect higher gains over non-adaptive modulation in practice.

Fig. 4-9 demonstrates that sub-carrier Adaptive Modulation consistently improves performance over single adaptation in every location, providing average gains of $1.15-1.47$ in NLOS scenarios and $1.16-1.27$ in LOS scenarios. Further, the figure shows that the standard deviation is relatively small indicating stable gains. Finally, NLOS scenarios tend to show higher gains which can be attributed to the higher frequency diversity.

Table 4.2 shows the data rates and modulation decisions for a typical measurement in each LOS and NLOS location. We see that while the best non-adaptive modulation varies depending on the location (the shaded cells), sub-carrier Adaptive Modulation always outperforms the best non-adaptive modulation. The data rate gain with respect to the best non-adaptive modulation is on average $1.30\times$ for link distances of 1.0 to 10.8 meters in NLOS environment and $1.27\times$ for link distances of 1.0 to 5.3 meters in LOS environment.

NLOS Tx Loc Dist (m)	R_{ADAPT} *(Mbps)*	$R_{nonADAPT}$ *(Mbps)*				*GAIN*			
		BPSK	*4-*	*16-*	*64-*	*BPSK*	*4-*	*16-*	*64-*
A (1.0)	**338**	88	172	**292**	54	3.84	1.97	**1.16**	6.26
B (2.8)	**293**	87	164	**248**	0	3.37	1.79	**1.18**	–
C (4.5)	**337**	91	180	**256**	84	3.70	1.87	**1.32**	4.01
D (6.3)	**238**	76	148	**176**	0	3.13	1.61	**1.35**	–
E (4.0)	**235**	87	**168**	128	0	2.70	**1.40**	1.84	–
F (7.3)	**157**	72	**126**	44	0	2.18	**1.25**	3.57	–
G (5.7)	**275**	86	166	**212**	0	3.20	1.66	**1.30**	–
H (7.2)	**241**	87	**164**	144	0	2.77	**1.47**	1.67	–
I (8.9)	**183**	78	**146**	64	0	2.35	**1.25**	2.86	–
J (10.8)	**180**	77	**138**	68	0	2.34	**1.30**	2.65	–
Avg.	**248**					2.96	1.56	1.89	1.03

LOS Tx Loc Dist (m)	R_{ADAPT} *(Mbps)*	$R_{nonADAPT}$ *(Mbps)*				*GAIN*			
		BPSK	*4-*	*16-*	*64-*	*BPSK*	*4-*	*16-*	*64-*
A (1.0)	**336**	90	176	**260**	84	3.73	1.91	**1.29**	4.00
B (1.8)	**347**	90	178	**288**	72	3.86	1.95	**1.20**	4.82
C (4.6)	**288**	86	164	**228**	18	3.35	1.76	**1.26**	16.00
D (5.3)	**335**	88	170	**240**	126	3.81	1.97	**1.40**	2.66
E (3.6)	**375**	92	178	**288**	150	4.08	2.11	**1.30**	2.50
F (3.1)	**360**	0	176	**316**	78	–	2.05	**1.14**	4.62
Avg.	**340**					3.14	1.96	1.27	5.77

Table 4.2: Typical adaptive and non-adaptive data rates, and gains for NLOS(top) and LOS(bottom) measurements. The shaded boxes represent the single modulation that achieves the highest non-adaptive data rate.

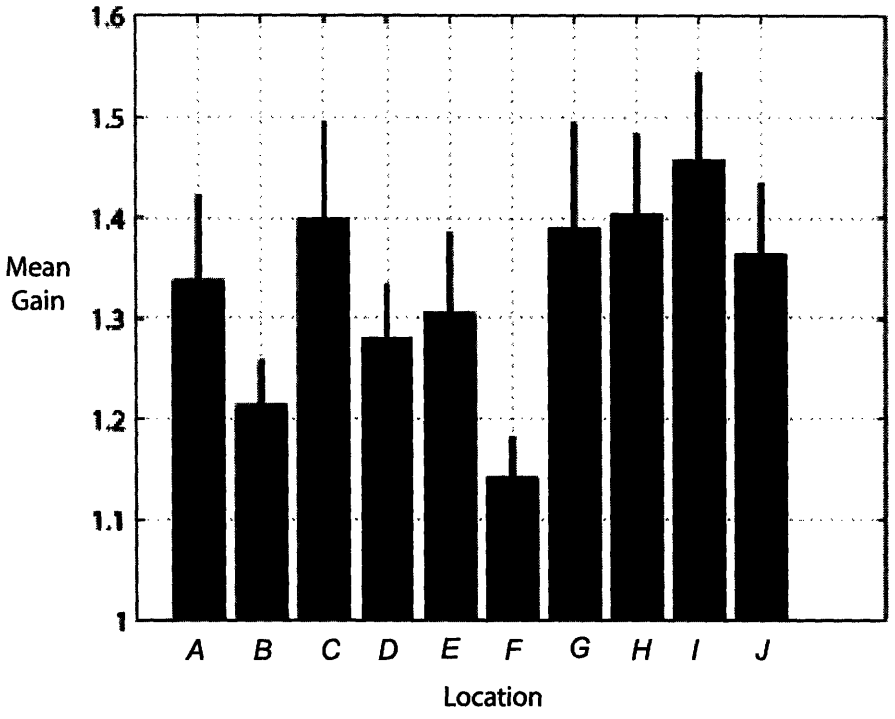

(a) NLOS

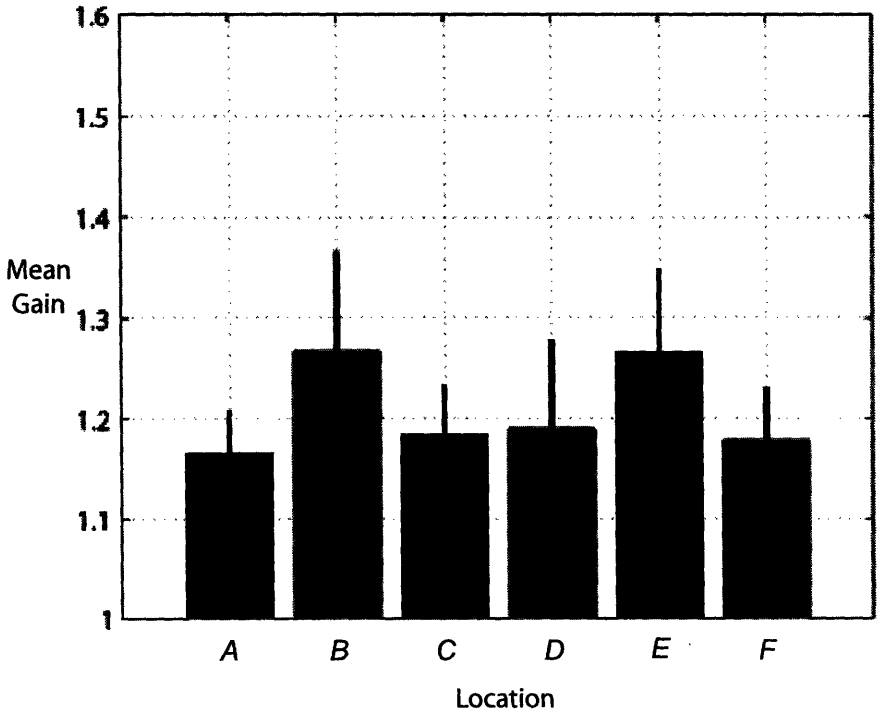

(b) LOS

Figure 4-9: Mean and standard deviation of GAIN across 10 measurements in each transmitter-receiver location in (a) NLOS and (b) LOS scenarios. The solid line indicates one standard-deviation below and above the mean value.

4.3.2 Comparison of WiGLAN Data Rate Gain to Water-filling

When the CSI is available to both the transmitter and receiver, as it is in sub-carrier Adaptive Modulation system, the capacity is achieved if the power per sub-carrier as well as the modulation is optimally adapted to the sub-channel fading conditions [8]. The optimal power allocation is the **water-filling** power allocation defined below.

Definition 4.3.1. The capacity of a multicarrier system with N independent sub-channels of bandwidth B, sub-channel gain $\{|H_k|^2, k = 0, \cdots, N-1\}$, Noise power spectral density N_0, and a total power constraint P_{total}, is given by [8]:

$$C = max_{P_k:\sum P_k = P_{total}} \sum_{k=0}^{N-1} B \; log_2 \left(1 + \frac{|H_k|^2 P_k}{N_0 B}\right) , \tag{4.7}$$

which is the exact capacity when the $\{|H_k|^2\}$ are independent, *i.e.* when the sub-channels bandwidths are greater than the channel's coherence bandwidth. Otherwise, the $\{|H_k|^2\}$ are correlated, in which case this capacity is an upper bound (tight bound in practice) on the true capacity. The power allocation P_k that maximizes this expression is a *water-filling* over frequency given by:

$$\frac{P_k}{P_{total}} = \begin{cases} \frac{1}{\gamma_c} - \frac{1}{\gamma_k}, & \gamma_k \geq \gamma_c \\ 0, & \gamma_k < \gamma_c \end{cases} \tag{4.8}$$

for some cutoff fade depth γ_c, where $\gamma_k = |H_k|^2 P_{total}/N_0 B$ is the SNR of k_{th} sub-carrier assuming that it is allocated the entire power budget. The cutoff value is obtained by substituting the power adaptation formula into the power constraint. The capacity then becomes:

$$C = \sum_{k;\gamma_k \geq \gamma_c} B \; log_2 \left(\frac{\gamma_k}{\gamma_c}\right) \tag{4.9}$$

Applying the variable-rate variable-power M-QAM modulation scheme to the sub-

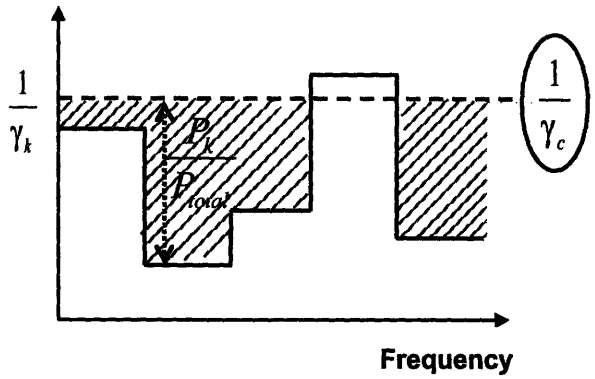

Figure 4-10: Optimal power allocation per sub-channel according to water-filling: in each sub-channel, k, if $\frac{1}{\gamma_k} \leq \frac{1}{\gamma_c}$, power of amount $\frac{P_k}{P_{total}}$ is allocated, where $\gamma_k = \frac{|H_k|^2 P_{total}}{N_0 B}$.

carriers, the total data rate is as Equation 4.9 with the optimal power allocation $\frac{KP_i}{P_{total}}$ according to Equation 4.8, where $K = -1.5/ln(5 \cdot BER)$ for target BER in each sub-channel [8].

As shown in Fig. 4-10, the water-filling terminology refers to the fact that the line $1/\gamma_k$ sketches out the bottom of a bowl, and power is poured into the bowl to a constant power level of $1/\gamma_c$. The amount of power allocated for a given γ_k equals $1/\gamma_c - 1/\gamma_k$, the amount of water between the bottom of the bowl $(1/\gamma_k)$ and the constant water line $(1/\gamma_c)$. The intuition behind water-filling is to take advantage of good channel conditions: when channel conditions are good (γ_k large), more power and a higher data rate are sent over the channel. As channel quality degrades (γ_k small), less power and rate are sent over the channel. If the sub-carrier SNR falls below the cutoff value, the channel is not used [8].

Fig. 4-11 compares the WiGLAN raw data rate to the water-filling data rate for the channel measurements in Table 4.2. The data rate with water-filling power allocation is obtained according to Equation 4.9 with the parameters set to the following:

- $B = 1\ MHz$ (sub-channel bandwidth).
- $\gamma_k = S\hat{N}R_k$ (sub-carrier measured SNR).
- $K = \frac{-1.5}{ln(5 \times 10^{-3})}$ with uncoded BER $= 10^{-3}$.

- P_{total} = 92 (total power budget corresponding to the 92 maximum available data sub-carriers).

- γ_c, cut-off fade depth, is obtained by solving $\sum_{k;\gamma_k \geq \gamma_c}(\frac{1}{\gamma_c} - \frac{1}{\gamma_k}) = K$. γ_c is initialized assuming $\gamma_c < \gamma_k$ for all k. If $\gamma_c > \min(\gamma_k)$, the weakest sub-channel is not used, and γ_c is re-calculated using above equation until $\gamma_c < \gamma_k$ for all used k.

Through water-filling, we obtain the maximum additional data rate increase possible, *i.e.* $(\frac{R_{waterfilling} - R_{ADAPT}}{R_{waterfilling}})$, as shown in percentages in Fig. 4-11. This indicates that on average, our uncoded OFDM with sub-carrier Adaptive Modulation is *43%* and *38%* away from the capacity rate in NLOS and LOS locations respectively.

Hence, with the average spectral efficiency of our sub-carrier Adaptive Modulation scheme being 2.96 bits/s/Hz in NLOS locations and 3.82 bits/s/Hz in LOS locations, our scheme performs 4.1 dB and 4.6 dB less than the optimal "water-filling" method respectively. Table 4.3 indicates how these are obtained, where the spectral efficiency, ρ, for the "water-filling" method is found from spectral efficiency of Adaptive Modulation and the data rate gain calculated above. The capacity-achieving SNR is calculated according to:

$$\rho = log_2(1 + SNR) \tag{4.10}$$

Although the calculated SNR is for a capacity-achieving system, it is reasonable to use the SNR difference for performance assessment of our uncoded system.

Scenario	*Average* ρ		*SNR (dB)* (Equation 4.10)		*SNR loss* (dB)
	ADAPT	"water-filling"	ADAPT	"water-filling"	
NLOS	2.96	2.96 × (1.43)	8.31	12.50	4.19
LOS	3.82	3.82 × (1.38)	11.18	15.76	4.58

Table 4.3: Measured average spectral efficiency, ρ_{ADAPT}, using sub-carrier Adaptive Modulation. The spectral efficiency of "water-filling" is ρ_{ADAPT} × 1.g where g is the average percentage increase in data rate from "water-filling." SNR loss(dB) = $SNR_{waterfilling} - SNR_{ADAPT}$.

Furthermore, to compare the SNR gain from our Adaptive Modulation scheme

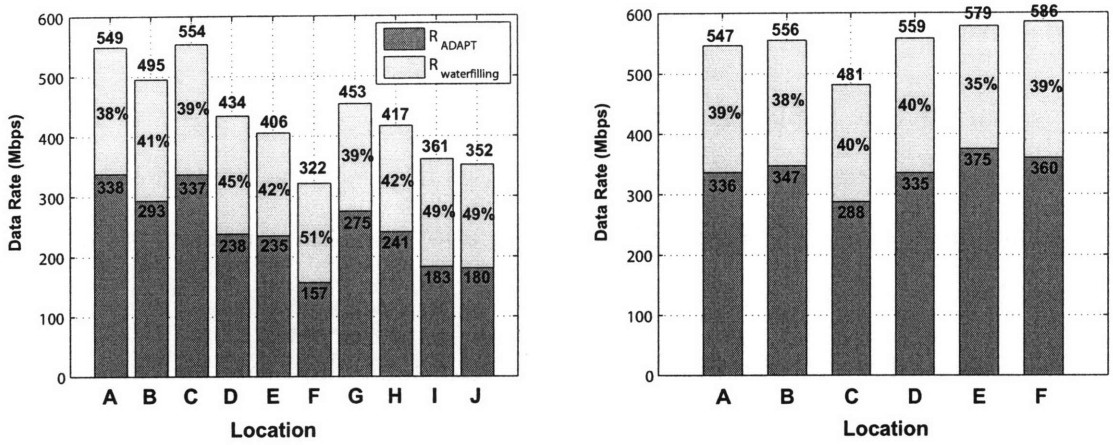

(a) NLOS (b) LOS

Figure 4-11: Comparison of measured raw data rate from sub-carrier Adaptive Modulation (dark color) (see Table 4.2) vs. data rate from water-filling (light color) for locations in (a) NLOS and (b) LOS scenarios. Data rate increases from water-filling are shown in percentages.

over non-adaptation scheme, Table 4.4 shows the spectral efficiency when BPSK or 4-QAM is used on all sub-carriers that can support them, obtained from the spectral efficiency of our Adaptive Modulation scheme with the gains in Table 4.2. We only indicate results for BPSK and 4-QAM since these are closer to the gains when a fixed modulation is used across *all* sub-carriers.

Scenario	*ρ (bits/s/Hz)*		*SNR (dB)* (Equation 4.10)		*SNR gain (dB)*	
	BPSK	*4-QAM*	*BPSK*	*4-QAM*	*BPSK*	*4-QAM*
NLOS	2.96/2.96	2.96/1.56	0	4.35	8.31	3.96
LOS	3.82/3.14	3.82/1.96	1.22	4.57	9.96	6.61

Table 4.4: Measured average spectral efficiency $\rho_{nonADAPT} = \rho_{ADAPT}/gain$ where the gain is from Table 4.2. SNR gain(dB) = $SNR_{ADAPT} - SNR_{nonADAPT}$.

4.3.3 WiGLAN Throughput with Adaptive Modulation Overhead

In the raw data rate of Section 4.3.1, we ignored the effect of overhead from sub-carrier Adaptive Modulation, as well as the preamble and cyclic prefix that are sent in the data packet. The effective data rate, R_{eff}, or throughput, of WiGLAN with sub-carrier Adaptive Modulation is calculated as:

$$R_{eff} = \frac{R \times T_{data}}{T_{data} + T_{overhead}}, \tag{4.11}$$

where

- R is the data rate during the payload obtained from $R = N_{BPS}/T_{SYM}$ ($T_{SYM} = T_{FFT} + T_{CP}$).
- T_{data} is the time duration of the payload.
- $T_{overhead}$ is the overhead time needed for synchronization between transmitter and receiver and for sub-carrier Adaptive Modulation.

The overhead due to sub-carrier Adaptive Modulation protocol in Chapter 3 is introduced by the synchronization packets sent in steps 1 and 2 and their corresponding computational processing latency. Fig. 4-12 indicates the break-down of this overhead at the transmitter and receiver of steps 1 and 2. This figure indicates the overhead in terms of number of samples, where the sampling period is $T_s = 1/(128MHz) = 7.8125$ ns. The overhead in units of time is calculated as below:

- *Step1-tx:* processing overhead of $T_{1-tx} = 324 \times T_s = \mathbf{2.53}$ μs to generate Step 1 packet.
- *Step1-rx:* $T_{1-rx} = 1228 \times T_s$ (processing overhead) $+ T_{packet}$, where

$$T_{packet} = T_{CP} + (5 + M) \times T_{FFT} \tag{4.12}$$

For $T_{CP} = 51 \times T_s$ and $M = 32$, $T_{1-rx} = \mathbf{47}$ μs.

- *Step2-tx:* processing overhead of $T_{2-tx} = 762 \times T_s = \mathbf{5.95}$ μs to generate Step 2 packet.

- *Step2-rx:* $T_{2-rx} = 3051 \times T_s$ (processing overhead) $+ T_{packet}$, where

$$T_{packet} = T_{CP2} + 7 \times T_{FFT} + N_{Step2} \times (T_{CP2} + T_{FFT}) \tag{4.13}$$

  For $T_{CP2} = 26 \times T_s$ and $N_{Step2} = 19$ (Number of OFDM CSI symbols), $T_{2-rx} =$ **53.9** μs.

Hence, the **synchronization overhead from sub-carrier Adaptive Modulation** is ***109.37*** μs.

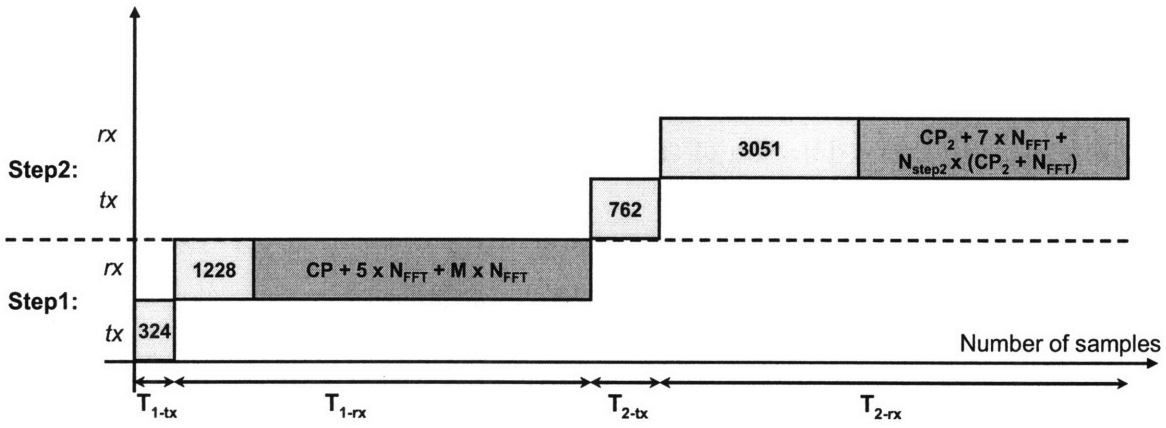

Figure 4-12: Breakdown of overhead from sub-carrier Adaptive Modulation protocol. The numbers indicate the number of samples, where the sampling period is $T_s = 1/(128MHz)$.

According to Equation 4.11, R_{eff} is optimized when T_{data} is large. However, T_{data} is limited by the channel coherence time, at which time the sub-carrier Adaptive Modulation protocol has to be re-initialized. The overhead can be minimized by using a networking protocol that incurs the synchronization overhead once for as many as data packets within the channel coherence time. Hence, the throughput gain of sub-carrier Adaptive Modulation is appreciated best when the channel is static for a relative long time, as in the indoor environment, where the channel coherence time is about $T_{coh} \approx 10\ ms$ (see Section 3.4). Applying this networking protocol in the indoor environment, the number of OFDM data symbols that can be sent within T_{coh}

is:

$$\text{Number of OFDM data symbols} = \left\lfloor \frac{10\ (ms) - 109.37\ (\mu s)}{T_{SYM} = 1.4\ (\mu s)} \right\rfloor = 7064\ , \qquad (4.14)$$

and the throughput is:

$$\text{Throughput} = \frac{N_{BPS} \times \text{Number of OFDM data symbols}}{T_{coh}} = \frac{N_{BPS} \times 7064}{10\ (ms)} \qquad (4.15)$$

Fig. 4-13a shows that for CP = 0.4 μs, the overhead due to combined sub-carrier Adaptive Modulation and Cyclic Prefix is 29%. Hence, the throughput of WiGLAN including these overheads is **71%** of the raw data rates obtained in the Section 4.3.1. However, as mentioned previously, our CP length is higher than the reasonable value of 0.25 μs (*i.e.* CP should be no more than 25% of useful OFDM symbol length) because we use two separate oscillators to generate the carrier and sampling clock frequencies and we do not have fine timing algorithms. Since the success of Adaptive Modulation requires precise time synchronization, we increased the length of CP to tolerate the high timing errors.

By implementing finer timing algorithms, as it is done in standards such as 802.11a [44], and by using a single oscillator, we can reduce the size of CP to 0.25 μs. In this case, as Fig. 4-13b indicates, the throughput improves (by about 10%) to 80% of the raw data rates.

4.4 Effect of SNR_{margin} on Throughput

As discussed in Section 3.5, there are two components in SNR_{margin} that affect the throughput: mismatches in channel and noise variance estimations, which are controlled by the number of OFDM pilot symbols L and M respectively. Our measurements indicate that with only $L = 2$ OFDM pilot symbols, channel estimations in Step 1 and Step 3 are in close match, about 0.5 dB in most cases and up to 4 dB in deep fades. Also, increasing L affects the throughput more severely than increasing

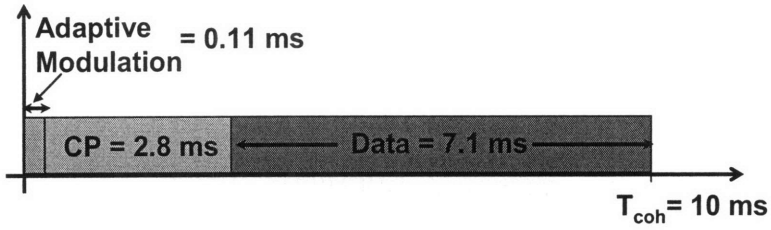

(a) CP = 0.4 μs

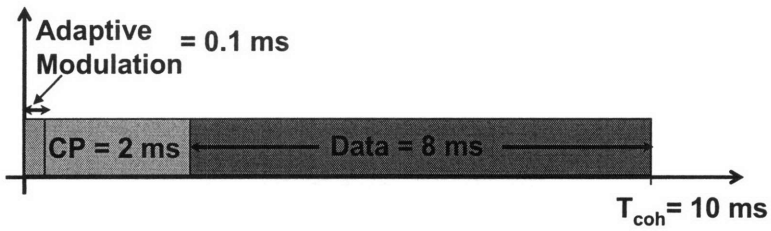

(b) CP = 0.25 μs

Figure 4-13: Within Channel coherence time, T_{coh}, of $10ms$, the overhead due to sub-carrier Adaptive Modulation protocol is 1.1%. The overhead due to Cyclic Prefix is (a) 28% for CP = 0.4 μs and (b) 20% for CP = 0.25 μs.

M. Hence, we examine effect on throughput from choosing different M, defined as

$$\text{Throughput} = N_{BPS} \times (1 - R_{M,overhead}) , \tag{4.16}$$

where $R_{M,overhead}$ is the reduction in data rate according to Equation 3.28.

Each M requires a different SNR_{margin}. Fig. 4-14 shows effect of SNR_{margin} on throughput using mismatch z and $R_{M,overhead}$ from Table 3.1 for choosing various M. The x-axis is the additional ΔSNR_{margin} that results from decreasing M by powers of 2 (as indicated by dots), starting from $M = 8192$ where $\Delta SNR_{margin} = 0.2\ dB$ up to $M = 2$ where $\Delta SNR_{margin} = 30\ dB$. The SNR_{margin} required for each modulation is then $(SNR_{margin} - 2.8) + \Delta SNR_{margin}$, with values of SNR_{margin} from Table 3.2. The four curves in Fig. 4-14 are obtained using SNR measurements in NLOS locations A, D, F, J in Table 4.2. In all locations, the throughput increases sharply by a factor 3 for first 0.1 dB increase in SNR_{margin}, and by 50% and 20% for the next increases of 0.1 dB. The throughput reaches its peak at $\Delta SNR_{margin} = 1$ dB (M = 256) at locations A, D, F and $\Delta SNR_{margin} = 0.7$ dB (M = 512) at location J. The reason for the increase in throughput despite increasing SNR_{margin} is the decrease in high overhead

from large M. In other words, there is a maximum M that increases the throughput by reducing SNR_{margin} before the overhead dominates and decreases the throughput. After the peak, decreasing M further results in decreasing the throughput. At this point, the throughput rolls down to zero ($\Delta SNR_{margin} = 30$ dB) at a rate significantly slower than the initial increase slope.

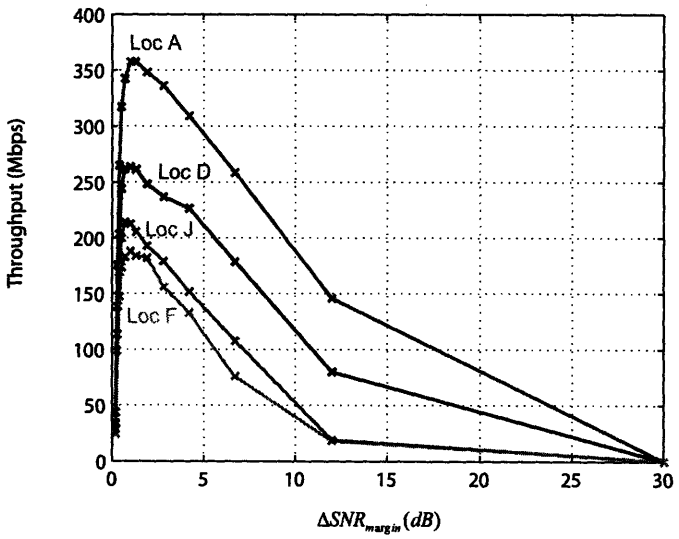

Values at *maximum* Throughput

Loc	Max Throughput	M	$\Delta SNR_{margin}(dB)$
A	357.5	256	1
D	263.6	256	1
J	214.0	512	0.7
F	187.9	256	1

Figure 4-14: Effect of additional SNR_{margin} from decreasing M (from 8192 to 2) on the throughput - for NLOS locations A, D, E, J.

4.5 Fading over Time

Fig. 4-16a and 4-16b indicate BER as a function of time. The uncoded BER values correspond to the measured BER values of coded data bits before being decoded in a coded WiGLAN system (as it will be explained in the next Chapter). The uncoded BER values are reported as such due to the mechanism that is in place to capture more bits (which is required to show fading over time) in the coded WiGLAN system and not in the uncoded system.

In the measurement of Fig. 4-16a, 79,573 OFDM data symbols are captured. The allocation of sub-carriers to modulations are: BPSK (none), 4-QAM (7 sub-carriers), 16-QAM (59), and 64-QAM (24), which results in 394 bits per OFDM symbol. Similarly, in measurement of Fig. 4-16a, 105,472 OFDM data symbols are

captured. Here we have BPSK (1 sub-carrier), 4-QAM (25), 16-QAM (59) and no 64-QAM sub-carriers, giving rise to 287 bits per OFDM symbol.

The increase in BER after 86 ms in Fig. 4-16a is due to the accumulation of uncompensated sample drifts from the SFO, $\zeta = \frac{T'-T}{T}$, where T and T' denote sampling period of transmitter's DAC and receiver's ADC respectively. Assuming the start of the 0^{th} OFDM symbol is perfectly detected at the receiver, the drift of i^{th} OFDM symbol is $-i\zeta N_{SYM}$ as shown in Fig. 4-15. With WiGLAN sampling clock accuracy of 100 PPM, the maximum drift that can occur is 1 sample for every $1/(200 \times 10^{-6}) = 5000$ samples which is about 28 OFDM symbols (1 OFDM symbol = 51 (CP) + 128 = 179 samples). In this case, a drift of 1 OFDM symbol results after 5,012 OFDM symbols. However, this amount varies in each measurement based on the detected start of OFDM symbol and the amount of SFO experienced. Our measurements verified that in worst scenarios, the significant increase in BER was seen after more than 5,035 OFDM symbols.

However, in measurement of Fig. 4-16b, the BER stays relatively stable over 147.6 ms indicating that the channel coherence time can be long in an indoor environment when people are not walking around.

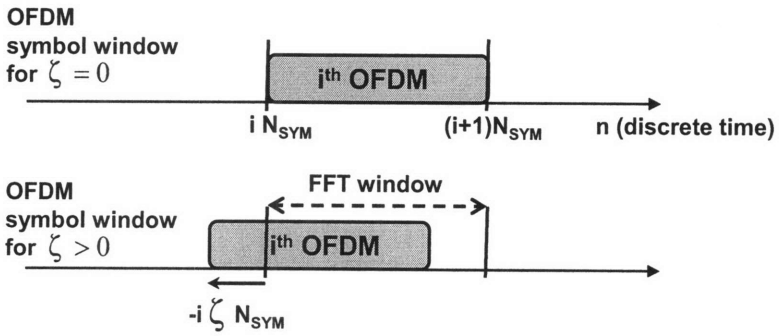

Figure 4-15: OFDM symbol drift due to sampling frequency offset $\zeta = \frac{T'-T}{T}$ [40].

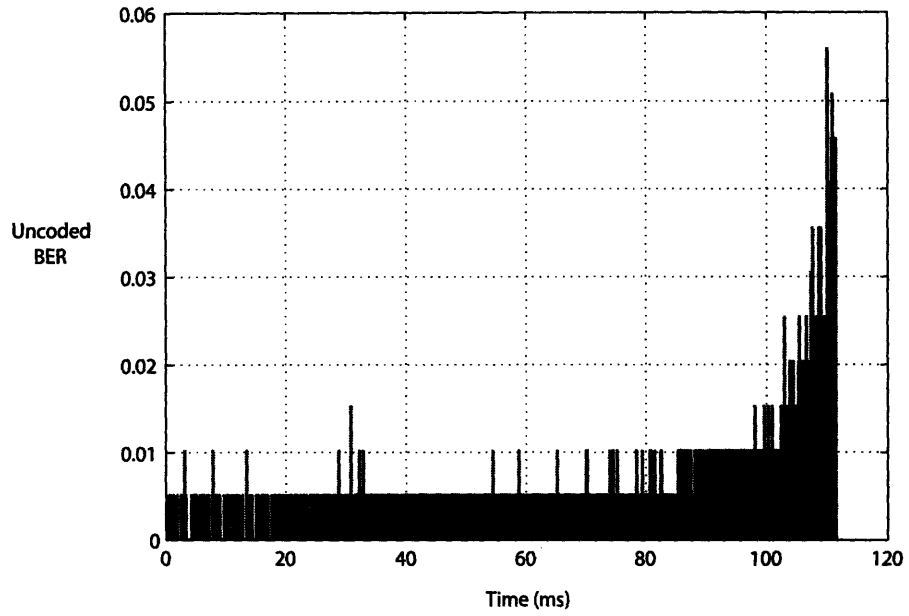

(a)

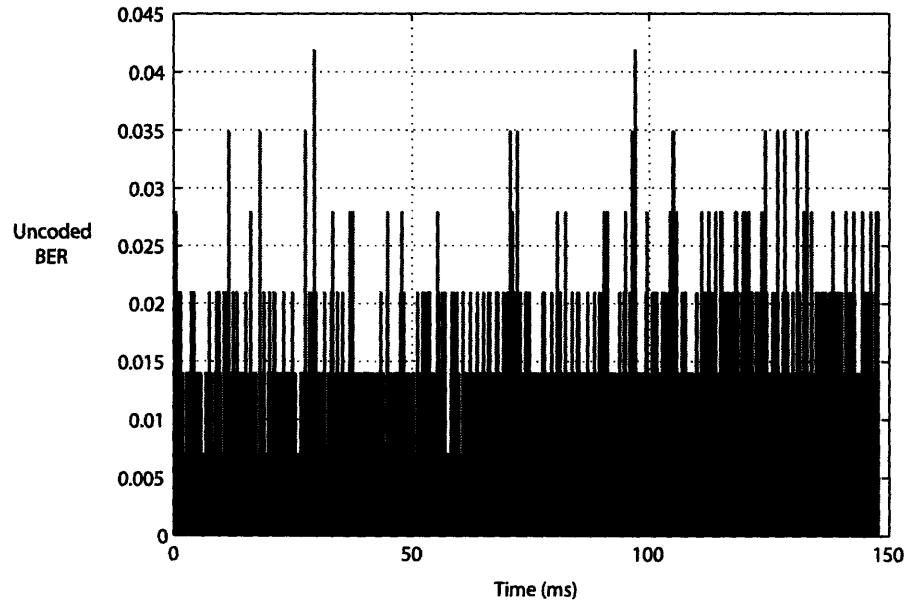

(b)

Figure 4-16: Uncoded BER vs. Time(ms) for two measurements with: (a) 79,573 OFDM data symbols (b) 105,472 OFDM data symbols.

Chapter 5

Sub-carrier Adaptive Coding Design with Adaptive Modulation

In this chapter, we will first introduce the main parameters in design of a Forward Error Correction (FEC) code. Next, we will discuss the desirable characteristics of FEC codes in an OFDM system with sub-carrier Adaptive Modulation and Coding (AMC). Finally, in the third section, we will present the design and implementation of the an adaptive FEC encoder and decoder for the WiGLAN system.

5.1 Error Correction Coding Design Parameters

When designing an error correction code, the following parameters are determined in order to meet the system objectives:

- *BER*
- *Signal Energy*, quantified by SNR
- *Data Rate*, based on modulation and code rate and quantified by spectral efficiency (*i.e.* number of data bits/s/Hz)

In WiGLAN system, the first objective of sub-carrier AMC is to minimize the average BER by achieving an equal BER on all sub-carriers. So in the code design,

a **fixed coded BER** is set for all sub-carriers. We choose BER = 10^{-5} since it is a reasonable target BER in packet-oriented wireless LAN systems.

The second objective of sub-carrier AMC is to maximize the system throughput. To achieve this, for each operating **SNR**, the code design picks a modulation/coding pair that achieves the **highest spectral efficiency** while meeting the target coded BER. For a feasible implementation, we pick one family of codes and choose among a finite set of coding rates within that family.

To understand the aforementioned code design procedure, we will go through an example scenario here. We will first define the following parameters that characterize an error correction code [56]:

- $R_c = k/n$: is the code rate of an n-bit codeword with k information bits.
- d_{free}: is the free distance of the code, which is the minimum Hamming distance between any two of its codewords. The Hamming distance between two codewords is the number of bits in which they differ: *e.g.* the Hamming distance between codewords c_1 = '0101' and c_2 = '1111' is 2.
- G_c: is the coding gain defined as the reduction in SNR that results from coding (with respect to the uncoded system) to achieve a specific BER. The *asymptotic* coding gain, G_{asym} is the coding gain at very large SNR values that provides a quick performance metric for a code with rate R_c and minimum Hamming distance d_{free}, defined as:

$$G_{asym}(dB) = 10\ log_{10}(R_c \times d_{free}) \tag{5.1}$$

5.1.1 Example of Coding Design

Suppose we choose a *Punctured Convolutional code* with

- rates = {1/2, 2/3, 3/4, 5/6, 13/14}, obtained from
- *puncturing* - *i.e.* deleting bits periodically according to a puncturing pattern of

- the "mother" code, which is a rate-1/2 binary convolutional code with (see Fig. 5-1):
  - generator polynomial (in octal notation): $(171, 133)_8$, and
  - constraint length (*i.e.* number of memory elements plus one): $\nu = 7$.

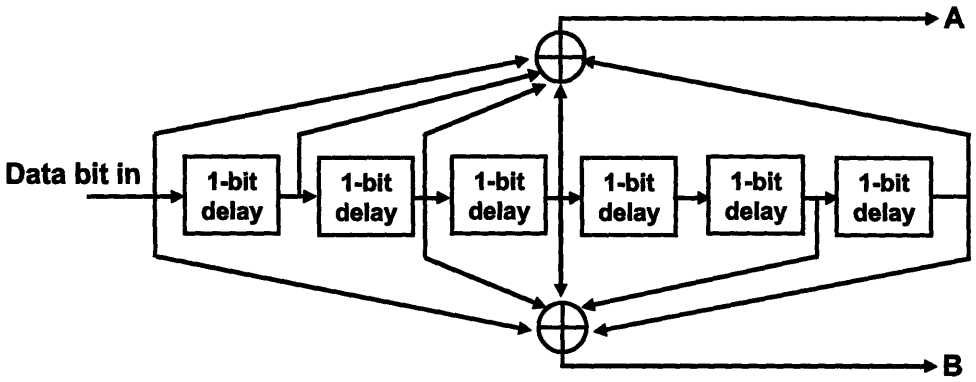

Figure 5-1: Rate-1/2 convolutional encoder with generator polynomial $(171, 133)_8$ and $\nu - 1 = 6$ delay (memory) units.

Fig. 5-2 shows how rate-5/6 puncturing is done on the output bits of the rate-1/2 convolutional encoder. For every 5-bit input to the rate-1/2 encoder, 10 coded bits are generated, out of which 4 bits are punctured (or deleted) according to the shaded pattern. Thus puncturing gives a 6-bit output for every 5-bit input, resulting in 5/6 coding rate. At the decoder, "dummy" bits (*e.g.* '0') are inserted in place of punctured bits and are fed into a decoder that decodes rate-1/2 codewords.

In the above punctured convolutional code, the mentioned code rates are chosen since as shown by [57], they give the highest asymptotic coding gains among all punctured code rates (of form $(n-1)/n$) up to 13/14. Table 5.1 indicates d_{free} and G_{asym} for these code rates obtained from puncturing the above rate-1/2 binary convolutional code.

Fig. 5-3 shows coded spectral efficiency vs. SNR at all modulation/code-rate combinations. For each modulation/code-rate pair with constellation size M and code-rate R_c, the coded spectral efficiency is:

$$\text{coded spectral efficiency} = log_2(M) \times R_c \text{ (bits/s/Hz)}, \tag{5.2}$$

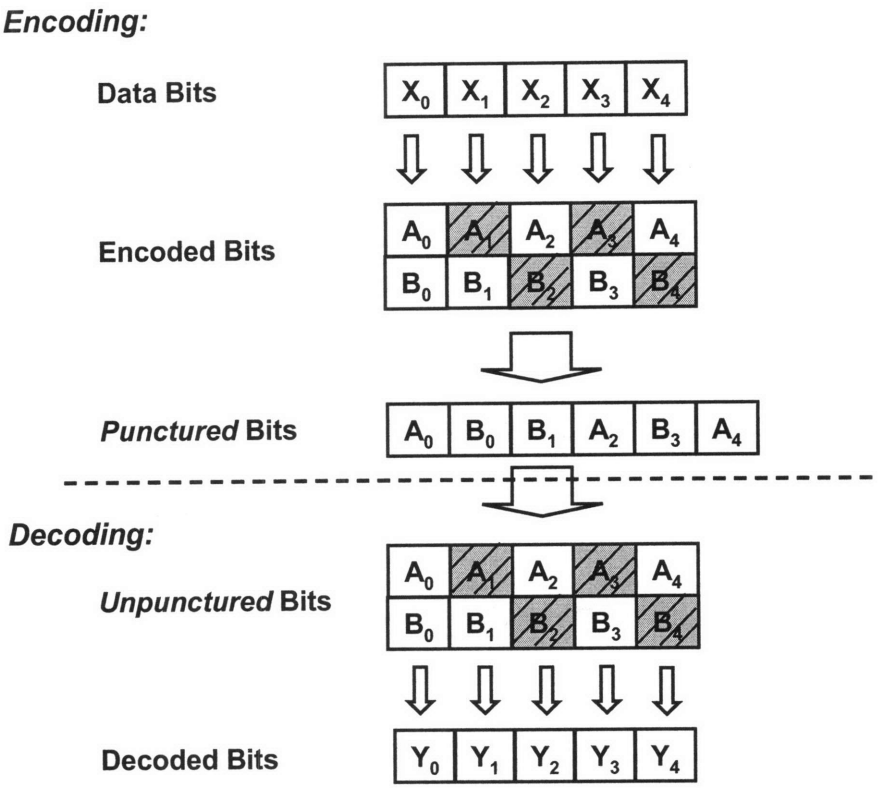

Figure 5-2: Puncturing at rate 5/6: At the encoder, shaded bits are stolen. At the decoder, "dummy" bits are inserted in their place.

at coded SNR:

$$SNR_{coded}(dB) = SNR_{uncoded}(dB) - G_{asym}(dB)\,, \tag{5.3}$$

where $SNR_{uncoded}$ is the SNR value at BER $= 10^{-5}$ of the uncoded system. For comparison to the maximum attainable coded spectral efficiency at each SNR value, the Shannon limit, $log_2(1 + SNR)$, is also plotted with a solid line.

Finally, the sub-carrier AMC algorithm chooses the mod./code pair that provides the highest spectral efficiency for each sub-carrier SNR estimate. For instance, since {64-QAM, rate-1/2} (3 bits/s/Hz) has a lower spectral efficiency than {16-QAM, rate-13/14} (3.7 bits/s/Hz) over their overlapped supporting SNR region, {64-QAM, rate-1/2} pair is discarded from the set of pairs to be considered.

R_c	d_{free}	$G_{asym}(dB)$ (Equation 5.1)
1/2	10	7
2/3	6	6
3/4	5	5.7
5/6	4	5.2
13/14	3	4.4

Table 5.1: Asymptotic coding gain, G_{asym}, for punctured convolutional codes of rate, R_c, and free-distance, d_{free}, obtained from rate-1/2 binary convolutional code ($\nu = 7$, $(171, 133)_8$) [57].

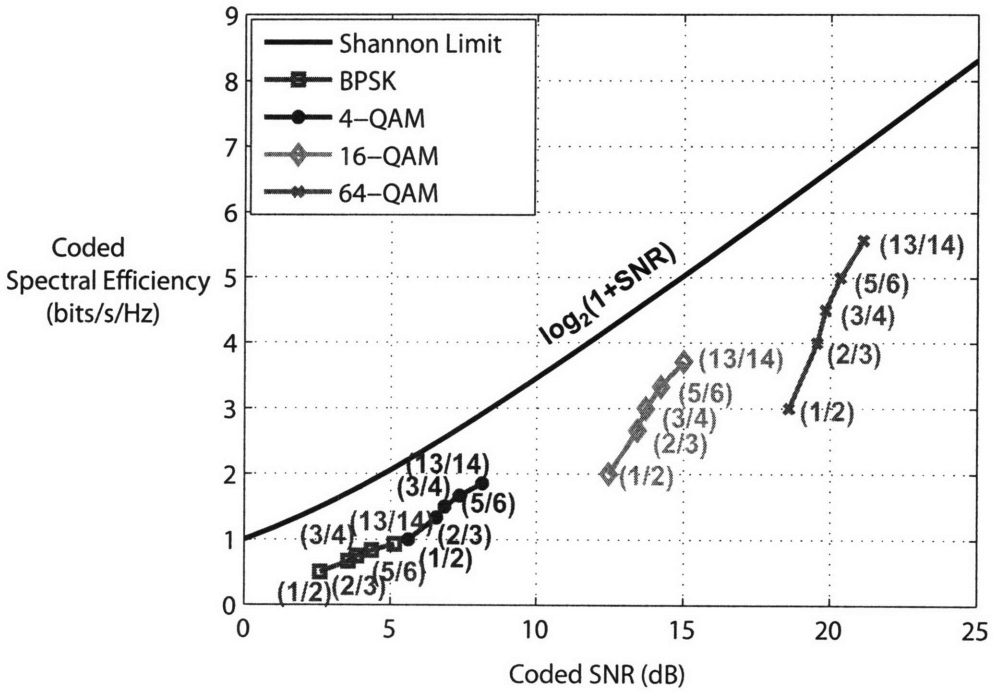

Figure 5-3: Coded spectral efficiency vs. Coded SNR for modulations/code-rate pairs shown. The code rates are shown in the parenthesis. $SNR_{coded}(dB) = SNR_{uncoded}(dB) - G_{asym}(dB)$(Table. 5.1) at BER = 10^{-5}.

5.2 Error Correction Coding in Sub-carrier AMC

As mentioned in the previous section, to find various codes for a system with adaptive coding, we pick a code family and subsequently choose codes with different error correction capabilities within that code family. For a high data rate sub-carrier AMC OFDM system, the following characteristics are desirable in the error correction code:

- *High code-rate*: to achieve a high data rate.
- *Low latency*: limited by the channel coherence time since the estimated CSI are only valid during this duration.
- *Flexible*: to obtain various coding gains from a single encoder and decoder in real-time.
- *Feasible implementation*: to use in practical systems.
- *Robust to errors*: from time and frequency synchronization and channel estimation, as exist in practice.

Depending on the code family, codes of various performance can be obtained by varying the code rate, puncturing (for convolutional and turbo codes), block lengths (for block codes), and interleaving.

In addition, the FEC encoder can be done at various locations in the OFDM system before the QAM-modulator. Fig. 5-4 categorizes all combinations in three types:

- *Type-I:* a separate FEC block is dedicated to each sub-carrier.
- *Type-II:* there is only one FEC block before serial-to-parallelization (S/P) block. Hence, the coded bits are spread over all sub-carriers.
- *Type-III:* there is a dedicated FEC block to all sub-carriers with same modulation type or one FEC block for each same modulation/code-rate combination.

In terms of implementation feasibility, *Type I*, which allows adaptation of code per sub-carrier, is the least favorable since with a single or at most 2 Viterbi decoders at the receiver, the decoder must run at an integer multiple of N_{FFT} times faster than the data rate to maintain the data rate. The reason for limiting the number Viterbi decoders to one or two is because they occupy a large percentage of the transceiver's total resources. *Type II* is one of the most popular coding methods in current OFDM systems [20, 32, 33], where coding is adapted to the time variations of channel rather than its frequency-selectivity. However, this type suffers from inability to adapt the code to the sub-carriers or block of sub-carriers for performance improvement. **Type III** provides a reasonable implementation complexity, and at the same time enables adaptation to a block of sub-carriers to increase the data rate. This type of coding is used in WiMAX [2], and it is chosen as the adaptive coding strategy in sub-carrier AMC in WiGLAN. Next, we will examine one of the most popular codes used in OFDM systems that meets the desirable code criteria mentioned earlier in this section.

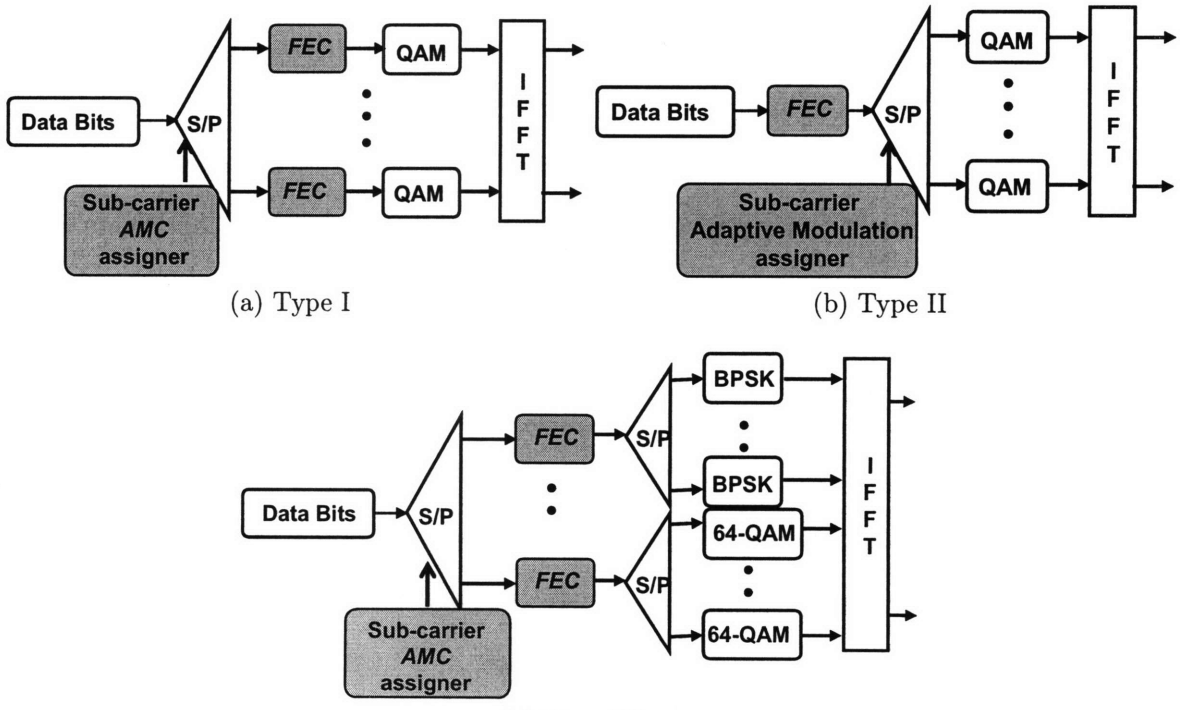

(a) Type I

(b) Type II

(c) Type III

Figure 5-4: Different placements of FEC encoder in an OFDM system.

5.2.1 Punctured Convolutional Codes

Punctured convolutional codes are well-suited for code adaptation, owing to their good performance and flexibility to achieve different code rates. They are used in OFDM wireless standards such as IEEE 802.11a [20], 802.11n [1], and 802.16e (mobile WiMAX) [2]. As we saw in sub-section 5.1.1, they implement high-rate codes (*e.g.* rates of (n-1)/n) from a low-rate code (e.g. rate-1/2 or 1/n) by periodically deleting (or *puncturing*) selected code bits at the output of the low-rate convolutional encoder. Similarly, the bits are decoded by a single Viterbi decoder that uses the trellis of the low-rate code and computes the metrics based on the puncturing patterns by inserting dummy '0' bits to replace the punctured bits. As a result, it avoids the high computational complexity associated with high-rate decoders since the branch complexity of decoding trellis increases exponentially with k for a code with rate k/n [27]. Hence, only one encoder/decoder pair is needed to generate the different code rates.

Another specific type of such code that is especially well-suited to adaptive coding is the *Rate-Compatible Punctured Convolutional codes (RCPC).* RCPC obtains various code rates from a single rate 1/n convolutional code by using puncturing patterns that satisfy a rate-compatibility criterion, with the basic requirement that lower-rate codes should transmit the same coded bits as all higher-rate codes [58]. This allows more real-time adaptation of various rates.

Regarding the performance, puncturing a code reduces the free distance, d_{free}, of the original rate 1/n code. By computer search, good puncturing patterns are generated that result in a d_{free} that is equal to or 1 bit less than the best same high-rate convolutional code without puncturing.

Convolutional codes are predominantly decoded by the Viterbi algorithm, especially in wireless applications, and other decoding methods are practically non-existent [44]. This is due to the Viterbi algorithm being a maximum-likelihood (ML) decoding rule for the trellis defined by a convolutional code [59], which provides the best estimate of the transmitted codeword. In addition, great performance on mem-

Coding Rate	**1/2**	**3/4**	**5/6**
d_{free}	10	5	4
A	1	101	10101
B	1	110	11010
AB	A_1B_1	$A_1B_1B_2A_3$	$A_1B_1B_2A_3B_4A_5$

Table 5.2: Map of deleting bits for punctured codes of rates 3/4 and 5/6 with corresponding free-distances d_{free}, derived from rate-1/2 convolutional code (ν = 7, $(171, 133)_8$) [57].

oryless channels can be obtained for codes with small constraint length, *e.g.* $\nu \leq 10$, when the Viterbi decoder is practically implementable.

Furthermore, soft-decision decoding is the recommended method to use with Viterbi decoding since it provides 2 dB coding gain over hard-decision decoding at no cost of communications resources. The 2 dB difference in performance is a fundamental result that applies in general to coded digital communications over the AWGN channel [27].

5.3 WiGLAN Adaptive Coding

5.3.1 Encoder: Punctured Convolutional Code

Due to suitability of punctured convolutional codes (as mentioned in the previous section) for adaptive coding, we have chosen **Punctured Convolutional Code** of rates 1/2, 3/4, and 5/6 obtained by puncturing the rate-1/2 binary convolutional code in Fig. 5-1 according to the puncturing patterns in Table 5.2 [57, 20]. This rate-1/2 convolutional code was chosen since it has the maximum free distance, $d_{free} = 10$, at constraint length $\nu = 7$ [60].

In our prototype, due to memory resource limitations, the code bits are generated as described below:

- Generate the code bits off-line using a punctured convolutional encoder in MATLAB, and load these bits in Read-Only-Memory (ROM) blocks on the FPGA.
- Due to the finite length of the ROM, the code bits are the outputs of a convolu-

tional encoder with *zero-tailing*, in which a sufficient amount of zeros ($= \nu \times k$) are padded to the input bits of the encoder. Hence, for rates 1/2, 3/4, and 5/6 (with $\nu = 7$), 7×1, 7×3, and 7×5 zeros are padded respectively.

- We have chosen ROM blocks of length 1024 1-bit, 2-bit, 4-bit and 6-bit (all coded bits), the outputs of which are fed into BPSK, 4-QAM, 16-QAM and 64-QAM modulators respectively. In general, in a zero-tailing convolutional code, the higher the code block length, the better the performance. We have chosen a relatively high block size based on the ROM resources available on the FPGA. Our simulations indicated negligible performance loss from zero-tailing with these block lengths.

In the context of WiGLAN, we do not use a *time or frequency interleaver*, that is generally used in practice following the encoder or puncturing block (if used). To correct for instantaneous burst errors (for instance if something blocks one of the antennas) during the coherence time period, a time-interleaver would be needed in our system as well. However, we do not need a frequency interleaver since by adapting the modulation and coding to the sub-carriers' fading conditions, bits are not sent in sub-carriers in deep fades.

5.3.2 Decoder: Soft-decision Viterbi

We use soft-decision Viterbi decoding with 8-level (3-bit) quantization, since there is only 0.2-dB performance loss from quantizing the channel outputs to 8 levels compared to unquantized, suggesting that there is not much gain from using more levels [56].

In our prototype, the QAM-demodulator generates 3-bit soft-metrics for each bit, according to Fig. 5-5, where the soft-metric '111' denotes the most reliable bit '1' and the soft-metric '000' denotes the least reliable bit '1' (which is the most reliable bit '0'). Hence, soft-metrics quantify the reliability of each bit being a '1' or a '0'. For an M-QAM constellation with $log_2(M)$ bits per symbol, $log_2(M)$ 3-bit soft-metrics are generated. The soft-metrics are then processed by a Viterbi decoder off-line in

MATLAB to generate the received data bits.

The traceback length, which reduces the impractically long decoding delay, for the Viterbi decoder is set to $TB = 72$, which is $> 10 \times \nu$. This is a rule of thumb for an insignificant performance loss for punctured codes relative to the optimum Viterbi algorithm [27].

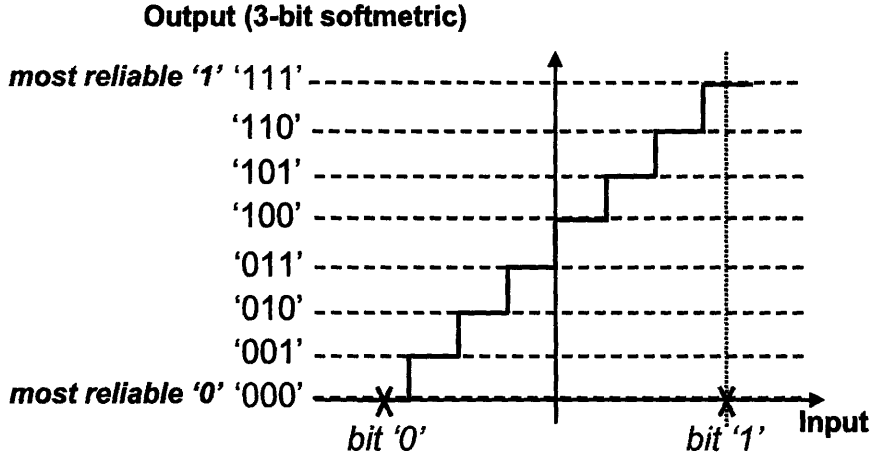

Figure 5-5: Generation of 3-bit soft-metric for each bit by the QAM demodulator.

5.3.3 Adaptive Coding Design

Once we have chosen a fixed coded BER $= 10^{-5}$ and a family of codes - punctured convolutional codes with zero-tailing with rates $\{1/2, 3/4, 5/6\}$, our sub-carrier AMC design is completed by:

- First, we obtain the minimum SNR, $SNR_{threshold}$, required for each modulation/code-rate at the coded BER $= 10^{-5}$ from the BER vs. SNR curves in an AWGN channel.

- Second, we plot the spectral-efficiency vs. Coded SNR for all mod./code-rate pairs, where Coded SNR(dB) $= SNR_{threshold}(dB) + SNR_{margin}(dB)$.

- Third, we choose the mod./code-rate pairs with the highest spectral efficiency at each SNR to use in the sub-carrier AMC algorithm.

We obtain the BER vs. SNR curve for each mod./code-rate pair by running Monte-Carlo Simulations for a range of SNRs, where randomly generated and zero-padded data blocks are fed into a punctured convolutional encoder followed by a modulator, an AWGN channel, a demodulator and a hard-decision Viterbi decoder. The data bits and decoded bits are then fed into a BER calculator to find the BER. At each SNR point, a value of BER is obtained by running the simulation until either 100 bit errors or 10^8 total bits are received. This provides sufficient confidence on the BER values up to 10^{-6}. Since SNR estimates in Step 1 of Adaptive Modulation protocol are SNR-per-bit, SNR_b, normalized by QAM-symbol Energy-per-bit E_b, we normalize SNR of these curves by Energy-per-bit for each modulation, where $E_b = log_2(M)$. The resulting curves are shown in Figs. 5-6a–5-6d for BPSK, 4-QAM, 16-QAM, and 64-QAM respectively. From these figures, Table 5.3 tabulates the minimum SNR, $SNR_{threshold}$, required to meet the target BER of 10^{-5} with soft-decision decoding. Since soft-decision decoding improves the performance by 2 dB from hard-decision decoding, $SNR_{thresholds}$ are obtained from:

$$SNR_{threshold}(dB) = \text{SNR(dB) (@ BER} = 10^{-5} \text{ in Fig. 5-6) - 2(dB)} \tag{5.4}$$

Using $SNR_{threshold}$ values in this table, for each mod./code-rate pair, the coding gain at $BER = 10^{-5}$ is the reduction in SNR from the uncoded scenario. For all modulations, the coding gains are within 5.3–6.3 dB for rate-1/2, 4.4–4.8 dB for rate-3/4, and 3.5–3.6 dB for rate-5/6.

Modulation	$SNR_{threshold}$ *(dB) @* $BER = 10^{-5}$			
	r=1/2	**r=3/4**	**r=5/6**	**uncoded**
BPSK	4.25	5.20	6.06	9.58
4-QAM	7.43	8.20	9.07	12.60
16-QAM	13.83	14.67	16.19	19.46
64-QAM	19.26	20.79	21.93	25.57

Table 5.3: Minimum SNR, $SNR_{threshold}$, required to meet BER = 10^{-5} (with soft-decision decoding) for code rates 1/2, 3/4, 5/6, and the uncoded system.

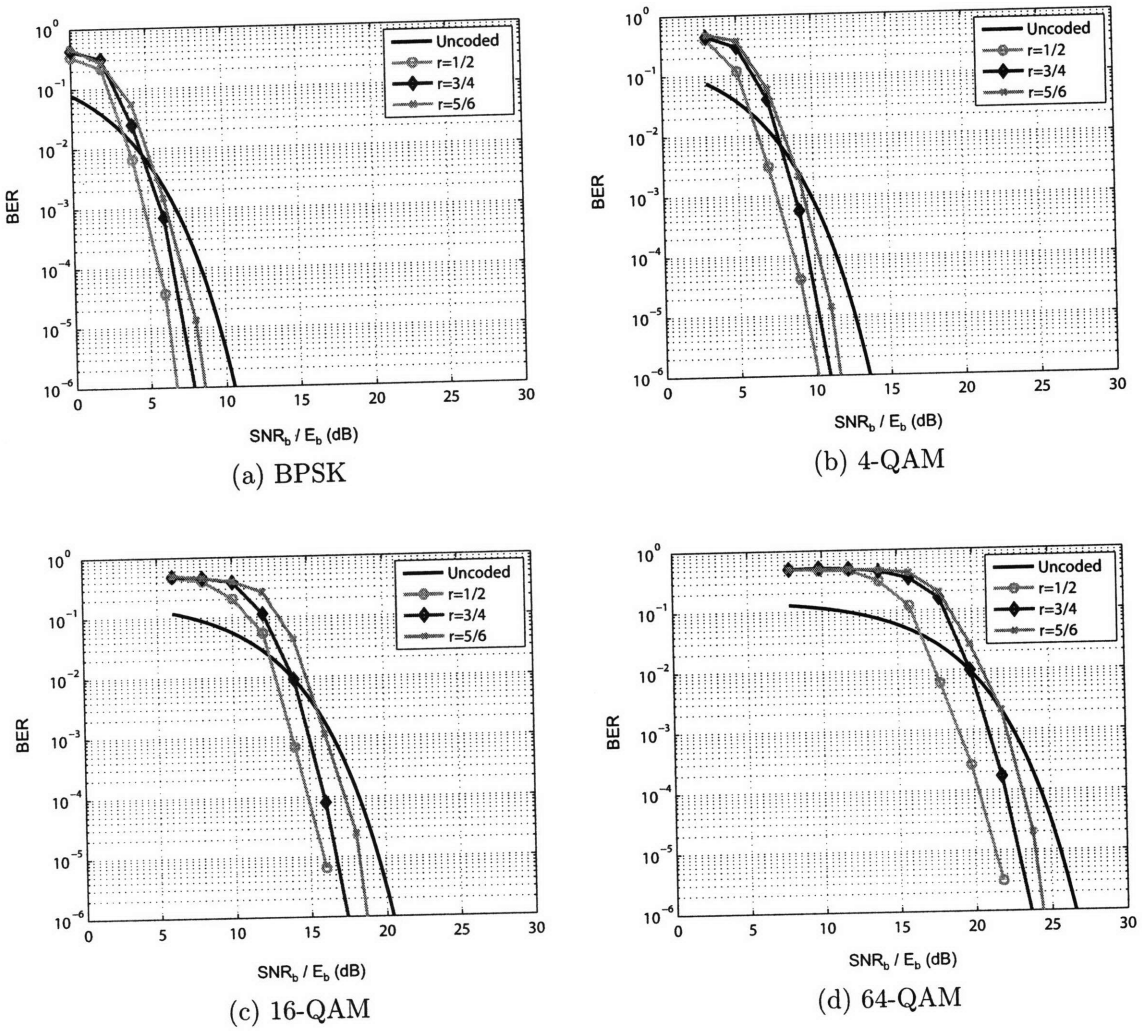

(a) BPSK

(b) 4-QAM

(c) 16-QAM

(d) 64-QAM

Figure 5-6: Plots of BER vs. SNR (normalized by modulation bit-energy E_b) from Monte Carlo Simulations with an AWGN channel using Punctured Convolutional encoder with zero-tailing and hard-decision Viterbi decoder. The results are shown for different modulations in sub-figures (a) BPSK, (b) 4-QAM, (c) 16-QAM, (d) 64-QAM. In each sub-figure, the uncoded theoretical BER vs. SNR is shown as well (same as Fig. 3-2).

Modulation	SNR_{min} *(dB)*		
	r=1/2	**r=3/4**	**r=5/6**
BPSK	9.25	10.20	11.06
4-QAM	10.93	11.70	12.57
16-QAM	17.63	18.47	19.99
64-QAM	25.66	27.19	28.33

Table 5.4: $SNR_{min}(dB) = SNR_{threshold}(dB)$(Table 5.3)$+SNR_{margin}(dB)$(Table 3.2).

Second, we plot the spectral efficiency vs. Coded SNR in Fig. 5-7. For each mod./code-rate pair, Coded SNR is (as tabulated in Table. 5.4):

$$\text{Coded SNR}(dB) = SNR_{threshold}(dB) \text{ (Table 5.3)} + SNR_{margin}(dB) \text{ (Table 3.2)}, \tag{5.5}$$

where SNR_{margin} is added to account for variations in SNR estimate (see Section 3.5).

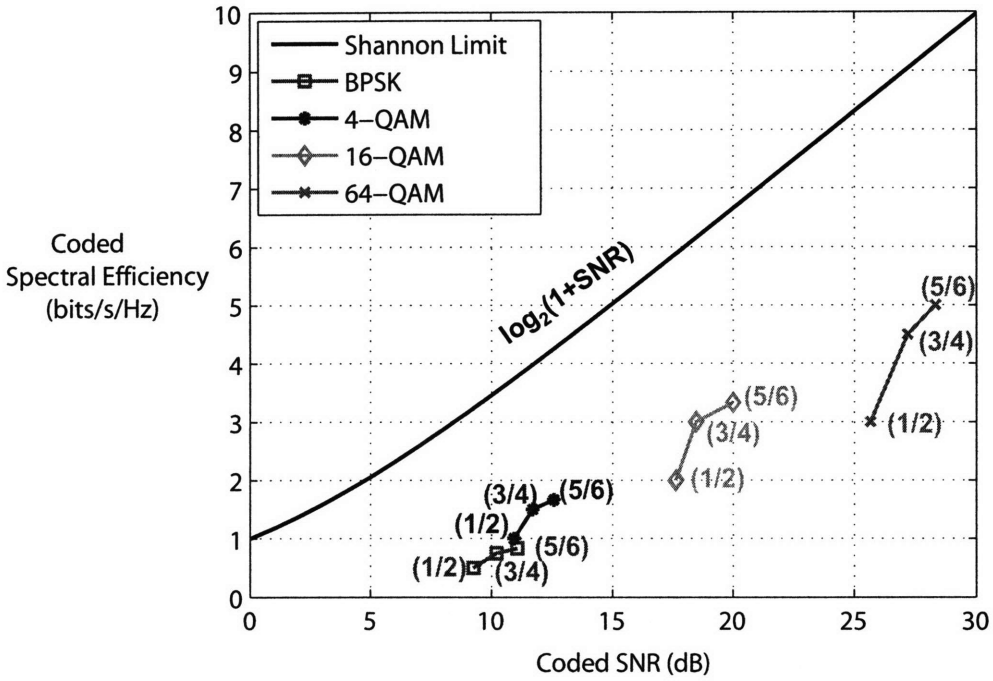

Figure 5-7: Coded spectral efficiency vs. Coded SNR for 12 modulation/code-rate pairs. The code rates are shown in the parenthesis. Coded SNR is SNR_{min} in Table 5.4.

Finally, as shown in Fig. 5-7, {64QAM, rate-1/2} (3 bits/s/Hz) has a lower spectral efficiency than {16-QAM, rate-5/6} (3.3 bits/s/Hz) over their overlapped supporting

SNR regions, and {BPSK, rate-5/6} (0.83 bits/s/Hz) has a lower spectral efficiency than {4-QAM, rate-1/2} (1 bit/s/Hz). Hence, we eliminate {64-QAM, rate-1/2} and {BPSK, rate-5/6} from our set of mod./code-rate candidate pairs to be used by the sub-carrier AMC. Thus, in Step 1, depending on which of the 11 SNR regions (defined by the 10 remaining mod./code-rate pairs in Fig. 5-7) each sub-carrier SNR estimate falls into, the corresponding modulation and code-rate are assigned to that sub-carrier.

Chapter 6

Sub-carrier Adaptive Modulation and Coding (AMC) Measured Results

In this chapter measured results from sub-carrier AMC will be presented. The first section will present the measurement setup. The second section will show the measured raw data rate. Finally, the third section will analyze the collected data.

6.1 Measurement Test Setup

Measurements are taken in NLOS location A in Fig. 4-1 following steps 1 to 3 as mentioned in Chapter 1. The packets sent in these steps are the same as those used in measurements for sub-carrier Adaptive Modulation in Fig. 4-2 except that in Step 3, the data bits are coded and pre-loaded in ROMs prior to each experiment (as explained in Section 5.3.1). The receiver processes this packet and generates 3-bit soft-metrics for each code bit. The soft-metrics are subsequently fed into a Viterbi decoder in MATLAB to decode and generate the data bits.

To measure coded BER of 10^{-5}, we need to capture at least 3×10^6 coded bits for each modulation [61]. To capture such large number of bits, we cannot use the PCI (Peripheral Component Interconnect) to transfer the bits directly from the FPGA to

the PC since the data rate transfer (on average 320 Mbps) is higher than than what the PC can handle (8–10 Mbps). Instead, we buffer the bits and use Xilinx ChipScope tool to transfer the bits to the PC. However, this limits us to capture not much more than 524,288 bits which is not sufficient for our experiment.

To capture more bits, the receiver sends out only the soft-metrics of QAM symbols received in error. As Fig. 6-1 shows, this is done in the digital receiver by:

- *QAM-mod*: re-generates the transmitted QAM symbols using the modulation assignments and the transmitted coded bits (since we know what we had sent).
- *QAM-demod*: generates the received QAM symbols and their soft-metrics. The maximum length of soft-metric is 18 bits for 64-QAM: *i.e.* 18 bits = (3-bit soft-metric) $\times$ (6 bits).
- *Compare/Error Word Generator*: compares the transmitted and received QAM symbols for each sub-carrier and generates a 32-bit Error Word if they are not equal. The structure of Error Word is shown in Fig. 6-1. The Error Word contains the OFDM symbol and sub-carrier number of the erroneous QAM symbol with its soft-metric. Since we have a limited number of bits to represent OFDM symbol number (we choose 5 bits), a counter is used that keeps track of OFDM symbol number and sends out an Error Word with Type=0 every 32 OFDM symbol.

Finally after the Error Words are captured from the FPGA, the entire received soft-metrics are generated in MATLAB using soft-metrics in Error Words of Type 1 or 2 and transmitted soft-metrics. The resulting soft-metric sequence is decoded by a Viterbi decoder in MATLAB.

The amount of bits captured is hence limited by the BER. In the most error-free experiment, we have been able to capture up to 30,270,464 code bits.

Measurements are taken for each of the following 3 coding schemes using FEC placement as Type III in Fig. 5-4c:

- Non-adaptive fixed rate-1/2: Use 4 separate rate-1/2 convolutional encoders, one for each modulation type: BPSK, 4-QAM, 16-QAM, and 64-QAM.

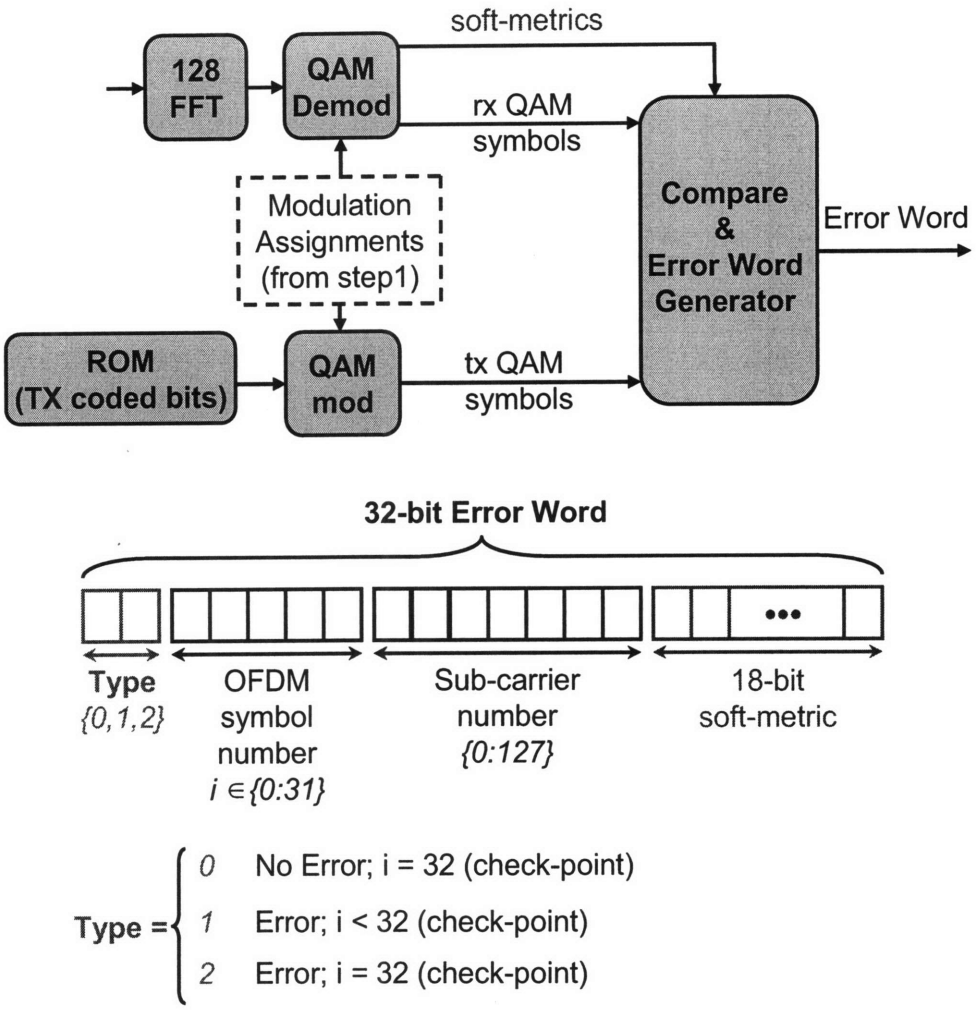

Figure 6-1: WiGLAN block diagram (at digital receiver) showing how a 32-bit Error Word is generated for each QAM symbol received in error.

- Non-adaptive fixed rate-3/4: Use 4 separate rate-3/4 punctured convolutional encoders.

- Non-adaptive fixed rate-5/6: Use 4 separate rate-5/6 punctured convolutional encoders.

As described in Section 5.3.3, our **sub-carrier AMC** chooses a modulation/code-rate combination (from a set of size 10) for each sub-carrier based on the SNR region its SNR estimate falls in Fig. 6-2. For instance, if a sub-carrier SNR estimate is in SNR-region for rate-5/6 16-QAM (as indicated in Fig. 6-2), the data on that sub-carrier is coded with rate-5/6 and modulated with 16-QAM.

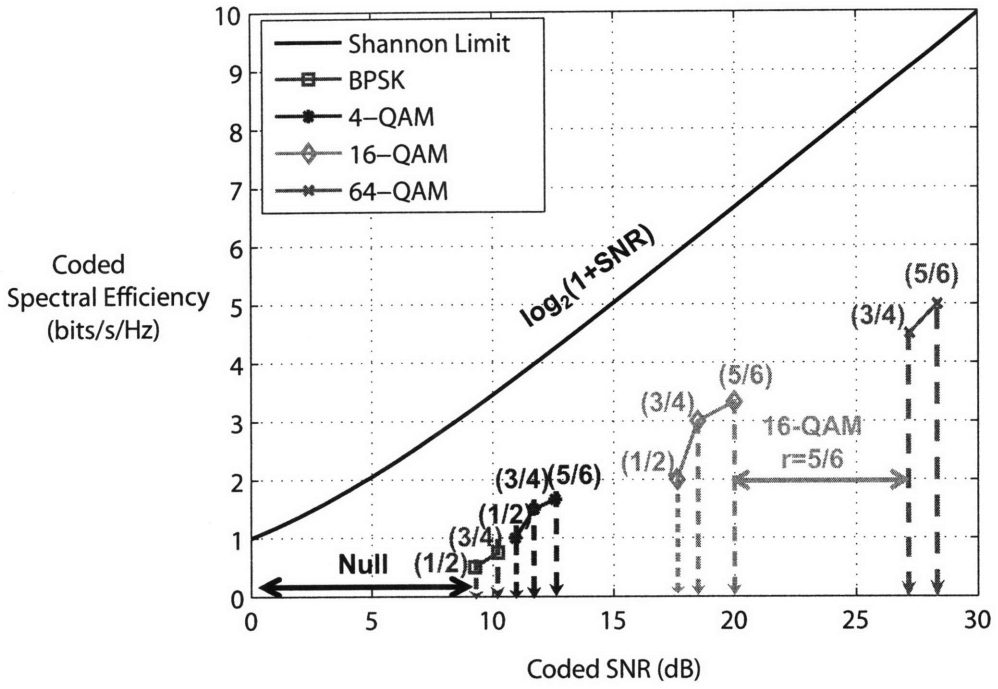

Figure 6-2: Coded spectral efficiency vs. Coded SNR for modulations/code-rate pairs used by our sub-carrier ACM. The code rates are shown in the parenthesis. Coded SNR is SNR_{min} in Table 5.4.

6.2 Measured Results

For each fixed code-rate scheme mentioned above, 10 measurements are taken in the NLOS location A. Fig. 6-3 shows the measured average number of data bits per OFDM symbol, over the 10 measurements for each coding scheme. As shown in the figure, at this location, coding with fixed rate-3/4 and 5/6 give similar raw data rates. Coding with fix rate-1/2 reduces the raw data rate by about 28% from fixed rate-3/4 and 5/6.

The average system BERs for uncoded (*i.e.* before decoding) and coded bits are shown in Table 6.1. As indicated, the target coded BER of 10^{-5} is met. Hence, the channel over each set of same-modulation sub-carriers behaved similar to the AWGN channel since they achieved the target BER using $SNR_{thresholds}$ for an AWGN Channel (Fig. 5-6).

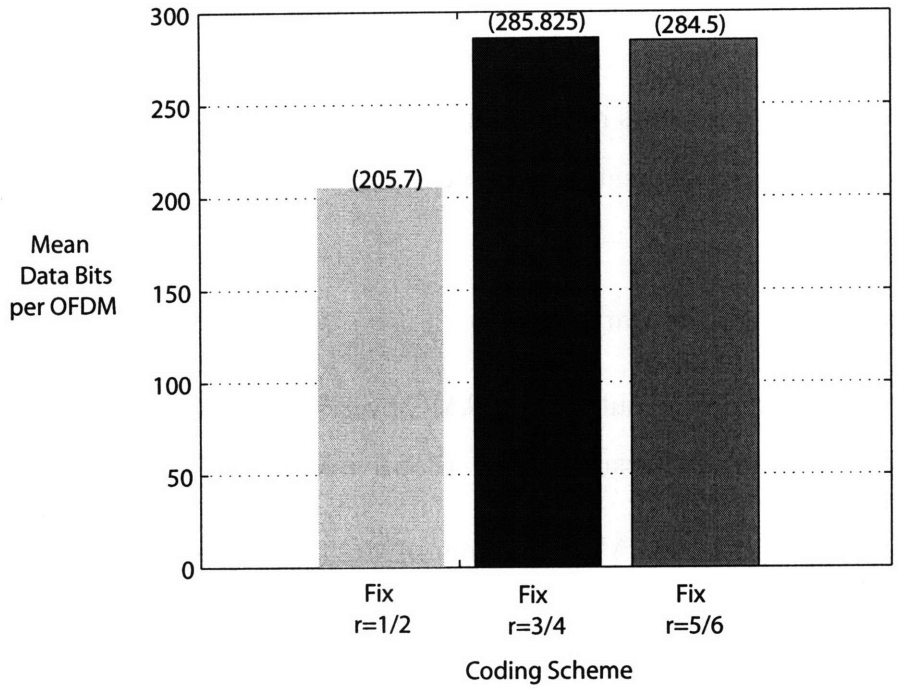

Figure 6-3: Mean (over 10 measurements) of data bits per OFDM symbol using Fix rate-1/2, 3/4 and 5/6 coding with sub-carrier Adaptive Modulation in NLOS location A.

Code-rate	*Uncoded BER*		*Mean Coded BER*
	mean	*std*	
Fix rate-1/2	1.3×10^{-3}	8.97×10^{-4}	$0/(3.39 \times 10^{6})$
Fix rate-3/4	1.6×10^{-3}	2×10^{-3}	$0/(5.99 \times 10^{6})$
Fix rate-5/6	1.3×10^{-3}	6.9×10^{-3}	$0/(3.76 \times 10^{6})$

Table 6.1: System uncoded (*i.e.* before decoding) and coded BER from measurements with Fix rate-1/2, 3/4 and 5/6 codings in NLOS location A.

6.3 Analysis

The measured raw data rates for sub-carrier AMC (in Fig. 6-3) can be reproduced from the corresponding measured SNR estimates of Step 1 and applying appropriate SNR_{min} in Table 5.4 to find the modulation assignment for each sub-carrier. Hence, based on the SNR measurements in Chapter 4 (10 NLOS locations A to J, and 6 LOS locations A to F), the subsequent sections will provide an in-depth analysis on the following:

- Effect of Coding on the Data Rate.
- Raw data rate gain from sub-carrier AMC over Fix rate-1/2, Fix rate-3/4, and Fix rate-5/6 codings with sub-carrier Adaptive Modulation.
- Raw data rate gain from AMC over non-AMC (non-adaptive Modulation and Coding).
- Implementation complexity and overhead from AMC.
- AMC scheme with reduced signalling (CSI) overhead.

6.3.1 Effect of Coding on Data Rate

Coding affects the data rate in two ways:

1. Sub-carrier Modulation Assignment, that is based on SNR_{min} (minimum SNR level at target BER) of modulation/code-rate combinations.
2. Code Rate.

Fig. 6-4a shows measured results (in NLOS location A) of the number of sub-carriers assigned to each modulation when sub-carrier AMC, and non-adaptive Fix rate-1/2, 3/4 and 5/6 codes (with adaptive modulation) are used. As shown, the number of sub-carriers assigned to each modulation is similar among all coding schemes. However, the number of 64-QAM sub-carriers is the most with Fix rate-1/2 coding and the least with Fix rate-5/6 coding. This is expected since SNR_{min} at {64-QAM, rate-1/2} is

the lowest (25.66 dB) and at {64-QAM, rate-5/6} is the highest (28.33 dB) among all the coding schemes, as seen in Table 5.4.

From modulation assignment, the Number of Coded Bits per OFDM symbol N_{CBPS} - *i.e.* before multiplying by the code rate, can be obtained from:

$$N_{CBPS} = N_{BPSK} + 2\ N_{4QAM} + 4\ N_{16QAM} + 6\ N_{64QAM}\ , \tag{6.1}$$

where N_{mod} denotes number of sub-carriers assigned to modulation type, *mod*. Fig. 6-4b shows the results for the various coding schemes. As with the modulation assignment, N_{CBPS} is similar for all coding schemes. We also observe that Fix rate-1/2 code gives the highest N_{CBPS} due its highest number of 64-QAM sub-carriers. However, to obtain the raw data rate, the code rate must be taken into account. The code rate reduces N_{CBPS} for Fix rate-1/2 to 1/2 of N_{CBPS} while those of Fix rate-3/4 and 5/6 to only 3/4 and 5/6 of N_{CBPS} respectively. The reduction in data rate from code rate is shown by shaded areas in Fig. 6-4b.

Hence, the code rate dominates the effect of $\{SNR_{min}\}$ in determining the data rate in our sub-carrier ACM system.

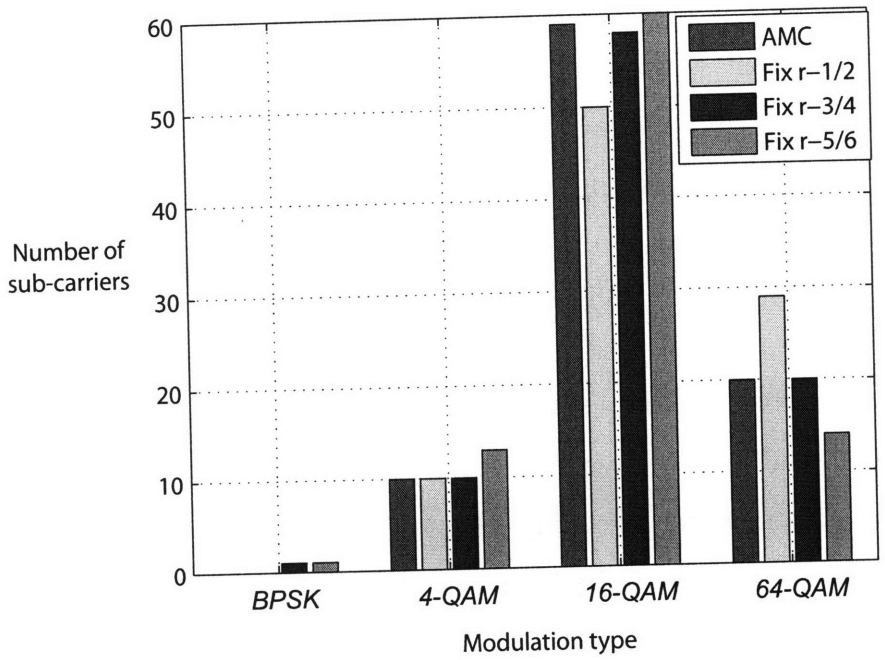

(a) Effect of Modulation Assignment

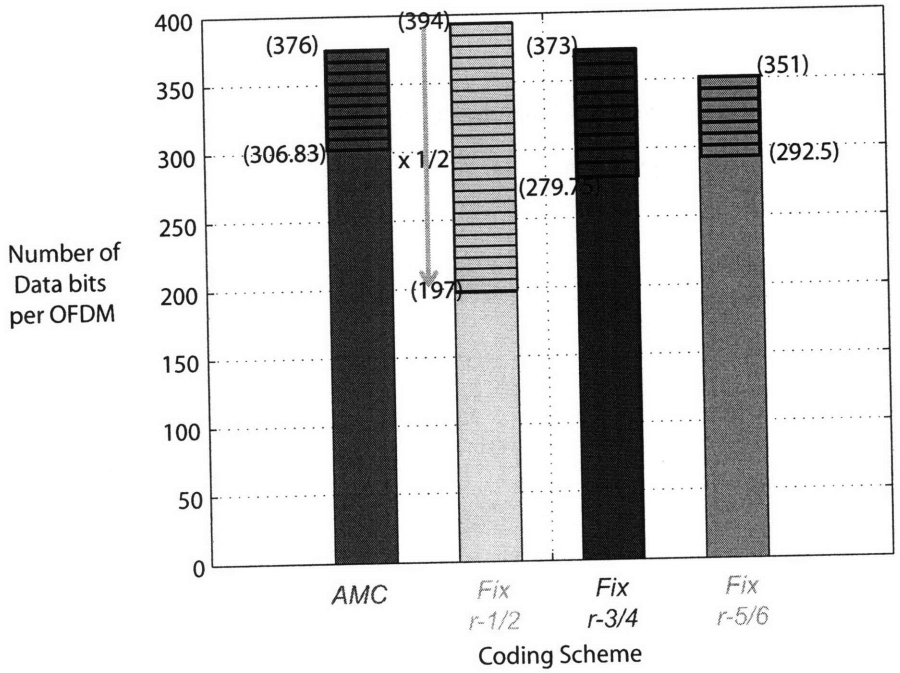

(b) Effect of Code Rate

Figure 6-4: Coding determines the data rate through: (a) Modulation Assignment and (b) Code Rate. (a) Measured number of sub-carriers assigned to each modulation for coding schemes (leftmost bar to rightmost bar): AMC, Fix rate-1/2, 3/4 and 5/6. (b) Measured number of Data bits per OFDM (shown in the parenthesis) before and after accounting for the code-rate. With code-rate, the data rate is reduced by the shaded area.

6.3.2 Data Rate Gain from AMC over Adaptive Modulation with Non-adaptive Coding

Fig. 6-5a shows the raw data rate, N_{BPS} as tabulated in Table 6.2, for 4 coding schemes - AMC, and non-adaptive codes with fixed rate 1/2, 3/4 and 5/6 - in NLOS locations (A-J). Fig. 6-5b shows N_{BPS} for LOS locations. The measurements indicate an average N_{BPS} of 238.1 Mbps (over 10 measurements) and 308.3 Mbps (over 6 measurements) in NLOS and LOS environments respectively.

NLOS Tx Location	*Number of assigned sub-carriers*										N_{BPS}
	BPSK		*4-QAM*			*16-QAM*			*64-QAM*		
	1/2	**3/4**	**1/2**	**3/4**	**5/6**	**1/2**	**3/4**	**5/6**	**3/4**	**5/6**	
A	0	0	1	1	8	1	4	54	6	14	306.83
B	0	2	0	2	12	2	7	56	6	2	273.17
C	0	0	1	0	9	11	5	41	6	19	311.67
D	0	0	3	0	15	6	10	40	4	1	226.33
E	2	0	2	0	39	9	6	33	0	0	214.00
F	3	2	6	2	45	4	10	11	0	0	161.67
G	1	2	2	2	18	4	8	51	1	2	253.50
H	0	1	0	5	18	7	16	42	0	0	240.25
I	3	4	3	2	27	12	18	19	0	0	196.83
J	2	3	2	6	29	11	13	19	0	0	186.92

Table 6.2: Measured sub-carrier AMC assignment in 10 NLOS locations A-J. From the modulation assignment and code-rates, number of data bits per OFDM, N_{BPS}, is obtained as indicated in the last column.

We observe that over all locations with various SNR profiles, Fix rate-1/2 coding scheme consistently gives the lowest data rate, as reasoned in the previous section due to its low coding rate. Furthermore, the data rate from AMC is always higher than Fix rate-3/4 and Fix rate-5/6 codings. We quantify the data rate gain from AMC scheme over Adaptive Modulation with Non-adaptive Coding scheme by:

$$Gain = \frac{N_{AMC} - N_{nonADAPTcode}}{N_{nonADAPTcode}}, \tag{6.2}$$

where N_{AMC} and $N_{nonADAPTcode}$ denote N_{BPS} with AMC and non-Adaptive coding scheme respectively. Fig. 6-6 indicates the average gain (over 10 NLOS locations in

Fig. 6-5a) from AMC over non-adaptive coding with fixed rates-1/2, 3/4 and 5/6. The mean gain is about **52%** over Fix rate-1/2 coding and **10%** and **11%** over Fix rate-3/4 and 5/6 codings respectively. However, this quantifies the additional gain from code adaptation in an adaptive modulation system. To evaluate the full gain from sub-carrier AMC, AMC must be compared to a scheme with non-adaptive coding and modulation, as described in the next section.

6.3.3 Data Rate Gain from AMC over non-AMC

Finally, similar to Section 4.3.1, we obtain the data rate gain from AMC over the best non-Adaptive Modulation and Coding scheme (non-AMC). In other words, the non-AMC scheme chooses one modulation type and code-rate for all sub-carriers and the best non-AMC is the one with the highest N_{BPS} (data rate).

For the measurements in Fig. 6-5a (NLOS scenario) and Fig. 6-5b (LOS scenario), our AMC scheme provides an average gain of **34%** and **40%** over the best non-AMC technique. Fig. 6-7 demonstrates that our AMC scheme consistently improves performance over no adaptation in every single location, providing average gains of 29%–61% in NLOS scenarios and 32%–48% in LOS scenarios. Furthermore, the figure shows that the standard deviation is relatively small indicating stable gains. Finally, NLOS scenarios tend to show higher gains which can be attributed to the higher frequency diversity.

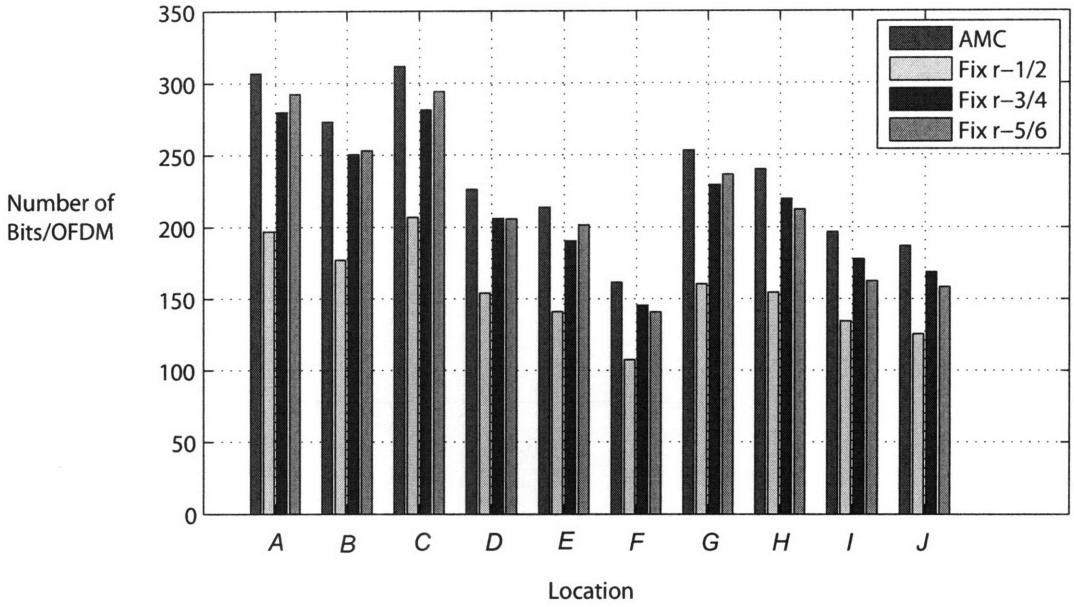

(a) NLOS

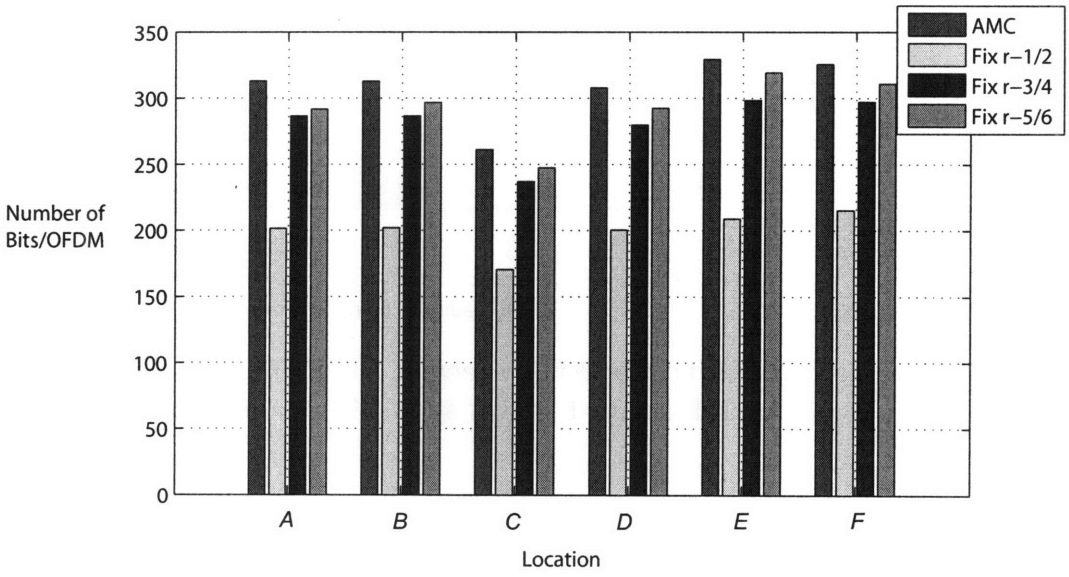

(b) LOS

Figure 6-5: Measured number of Bits per OFDM symbol, N_{BPS}, for four coding schemes in NLOS and LOS locations. The four coding schemes are (from leftmost bar to rightmost bar in each location): AMC, Fix rate-1/2, Fix rate-3/4, and Fix rate-5/6.

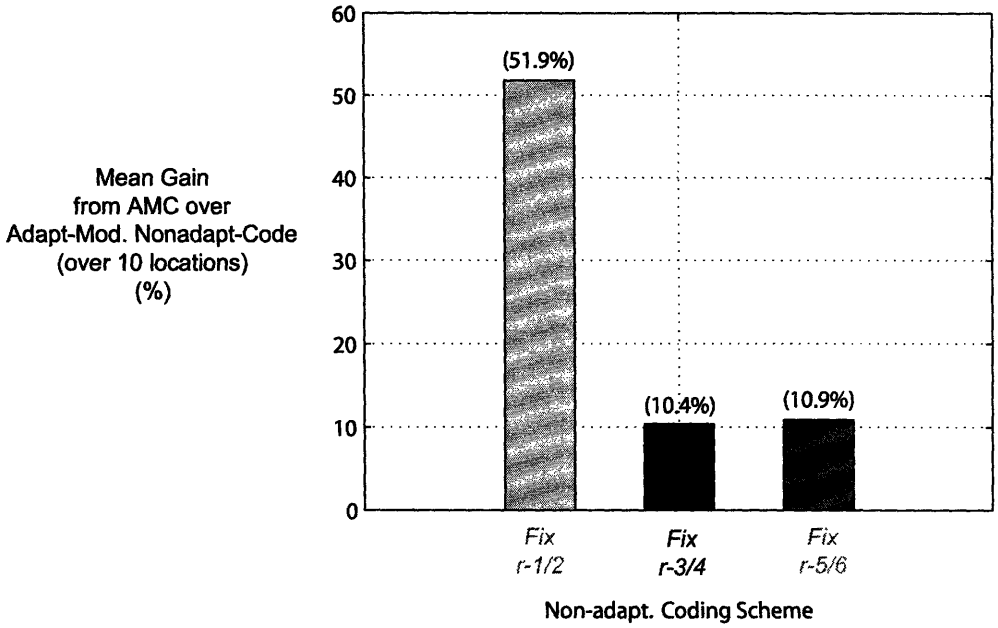

Figure 6-6: Measured mean data rate Gain (across 10 NLOS locations) from AMC over non-adaptive code with Fix rate-1/2, 3/4 and 5/6 (with adaptive modulation).

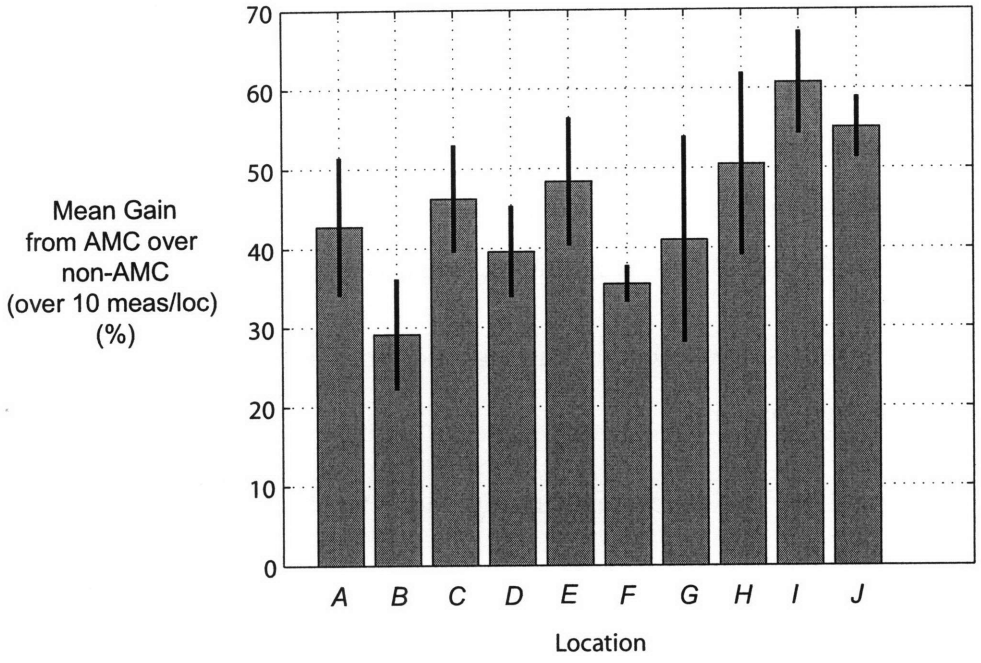

(a) NLOS

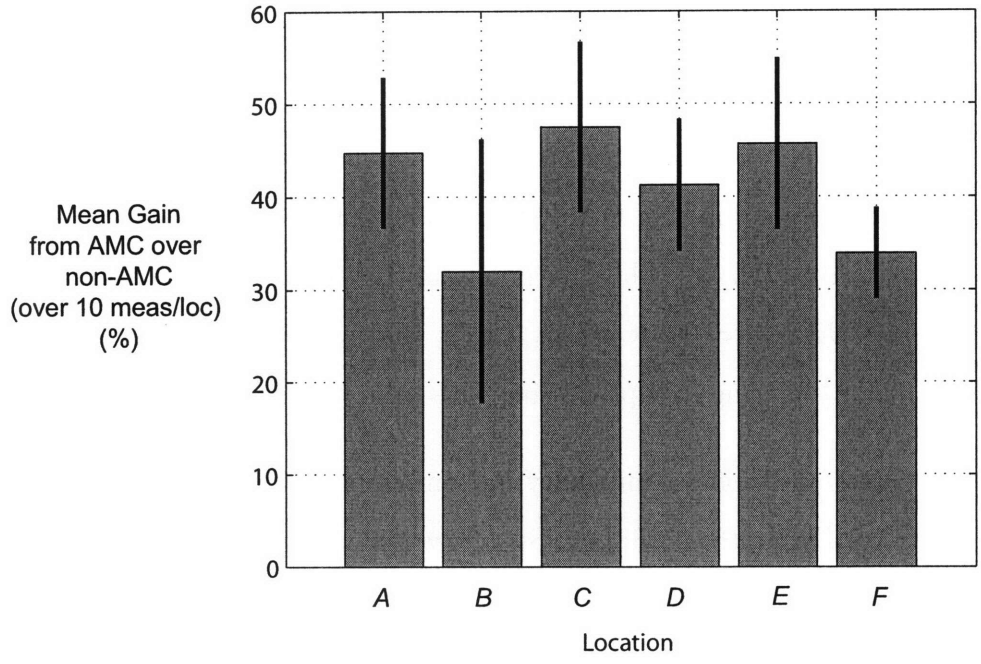

(b) LOS

Figure 6-7: Measured mean data rate Gain from AMC over the best non-AMC in (a) NLOS and (b) LOS locations. The mean is obtained over 10 measurements for each location. The solid line indicates one standard-deviation below and above the mean value.

6.3.4 AMC Implementation Complexity and Overhead

The implementation complexity and overhead from AMC vs. Adaptive Modulation with Non-adaptive Coding are described below.

(a) Implementation complexity:

The additional implementation complexity from adaptive coding vs. non-adaptive coding in WiGLAN system is insignificant when the following design rules are used:

- Time share a single encoder and decoder to achieve various coding rates for different sub-carriers.
- Use type III FEC placement in Fig. 5-4c for both AMC and non-adaptive schemes (such as Fix rate-1/2).
- Choose the Block Length of convolutional code such that extra buffering is avoided in AMC compared to fixed rate coding schemes. Let BL_{ACM} be the block length for codes used in the 10-mode AMC scheme, and $BL_{nonADAPT}$ be the block length for non-adaptive codes (with 4 modulation types). When all mod./code-rate pairs are used by sub-carriers within an OFDM symbol, for the AMC, the number of QAM symbols need to be processed for each OFDM symbol is $10 \times BL_{ACM}$ while for non-adaptive coding it is $4 \times BL_{nonADAPT}$. By choosing $BL_{ACM} = 0.4 \times BL_{nonADAPT}$, the two schemes will require an equal amount of buffering and processing rate from the encoder and decoder.

In this case, the additional complexity is from the extra 6 comparisons that is performed by *SNR Estimator* module in Step 1, which is insignificant. Thus, in terms of FPGA logic utilization, our sub-carrier AMC technique occupies 9.95% of the total transceiver gates as detailed in Section 3.6.

(b) Overhead:

The overhead from the AMC technique can be broken down to:

1. *Signalling overhead* in Step 2 from the additional mod./code-rate modes.
2. *Decoding overhead* in Step 3.

As mentioned in Section 3.3, in Step 2, the modulation/code-rate modes for the 128 sub-carriers are encoded by BCH(15,5) and CRC(48,32), and are sent by 92 BPSK sub-carriers to the transmitter. In the case of non-adaptive coding, 3 bits represent the 6 modulation modes (including 2 modes for Pilot and Null sub-carriers), which can be sent with 19 OFDM data symbols (as derived in Equation 3.14). In our AMC scheme, where we have 12 modes, 4 bits are needed instead. Hence, the number of OFDM data symbols, N_{Step2}, needed to send the encoded 4-bit per sub-carrier is 26 (using Equation 3.14), which is an additional 7 OFDM data symbols (8.4 μs) compared to the non-adaptive coding scheme. Using the analysis in Section 4.3.3, since the number of OFDM data symbols that can now be sent over the channel coherence time, $T_{coh} = 10$ ms, is reduced by 6, as obtained below:

$$\left\lfloor \frac{8.4\ (\mu s)}{T_{SYM} = 1.4\ (\mu s)} \right\rfloor = 6\ , \tag{6.3}$$

the additional signalling overhead in AMC translates to a loss in throughput by:

$$\text{Loss in Throughput} = \frac{6\ (\mu s)}{10\ (ms)} = 0.06\% \tag{6.4}$$

Regarding the decoding overhead, generally, in a coded system, delay is dominated by the time interleaver after the encoder that breaks up the correlation in the coded bits in the time-domain to avoid occurrence of burst errors. In addition, delay is of concern when using more powerful capacity-approaching codes such as Turbo and LDPC codes. However, for our coding scheme, where we do not use any interleaver, as mentioned in Section 5.3.1, the overhead delay is due to the processing delay from the encoder and decoder, which depends heavily on their implementation. In fact, the processing delay is expected to be dominated by the Viterbi decoder since it is much more complex that the convolutional encoder and depends on the amount of pipelining and parallelization done. In addition, using traceback length TB in the Viterbi decoder results in a delay of TB times the bit-rate of the decoder.

6.3.5 AMC with Reduced Signalling Overhead

We propose another sub-carrier AMC scheme (with Type III placement in Fig. 5-4), that does not increase the signalling overhead in Step 2 since 3 bits will be sufficient to denote the set of 6 candidate modulation/code-rate pairs, as the following:

[{BPSK, 3/4}, {4-QAM, 5/6}, {16-QAM, 3/4}, {16-QAM, 5/6}, {64-QAM, 3/4}, {64-QAM, 5/6}]

Here, we omitted codes of rate-1/2 since the low code-rate results in an insignificant increase in data rate. In addition, {4-QAM, 5/6} gives only an additional 0.1 bits/s/Hz within 0.87 dB SNR over {4-QAM, 3/4} (see Fig. 6-2), and hence using only {4-QAM, 5/6} will result in an insignificant loss in data rate. Fig. 6-8 compares the raw data rate, N_{BPS}, between the previous 10-mode AMC scheme and the above 6-mode AMC technique for the NLOS locations A-J. On average (over 10 locations), the 6-mode AMC results in a raw data rate loss of 2.26% with respect to the 10-mode AMC scheme. In the LOS scenario, the average (over 6 locations) data rate loss is 0.48%.

However, based on the analysis in the previous section, using 6-mode AMC scheme reduces the overhead from signalling in Step 2 by only 0.06% with respect to the 10-mode AMC scheme). Hence, the net effect of 6-mode AMC on the throughput (which includes the overhead from adaptive modulation and coding algorithm) is a loss of amount 2.2% and 0.42% with respect to the 10-mode AMC in NLOS and LOS locations respectively.

These results indicate that the 10-mode AMC, with full code adaptation, results in the highest throughput over other variants of AMC with a reduced level of code adaptation since the overhead from full adaptation is insignificant compared to the data rate gain.

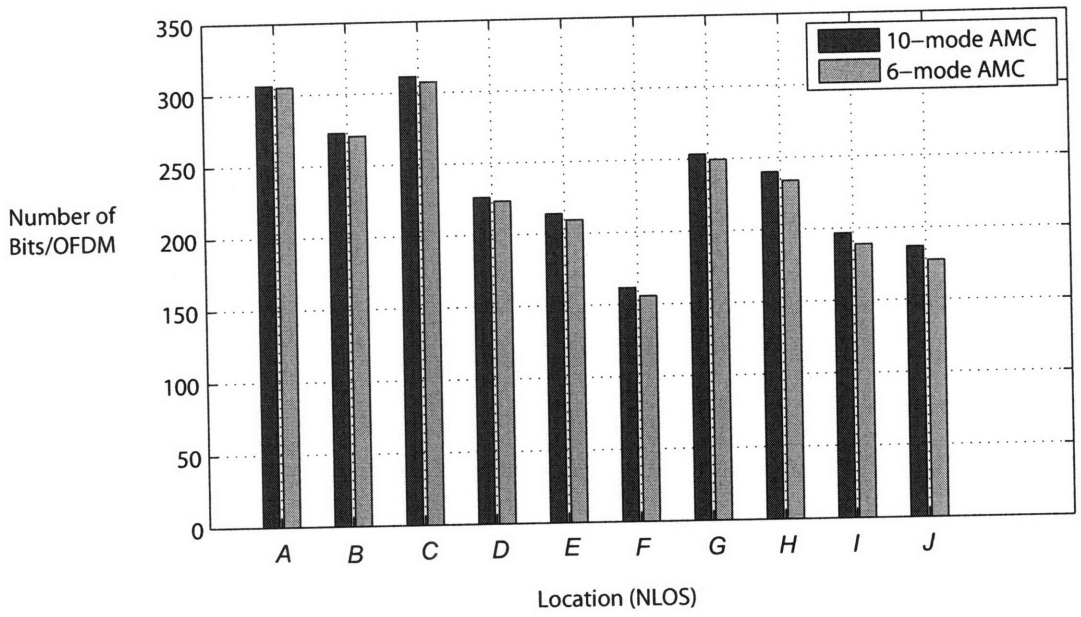

Figure 6-8: Measured number of Data bits per OFDM symbol using a 10-mode AMC (left bar) and a 6-mode AMC (right bar).

Chapter 7

Conclusions and Future Research

In this chapter, a summary of the thesis contributions is presented, and future research directions are suggested.

7.1 Conclusions

In this work, we demonstrate the case for sub-carrier Adaptive Modulation and Coding (AMC) in wideband wireless OFDM systems. Wideband wireless channels exhibit high frequency diversity. An OFDM system exploits this high frequency diversity by adapting the modulation and coding of each sub-carrier to its sub-channel fading conditions. The sub-carrier AMC chooses the modulation/code-rate pair that achieves the highest spectral efficiency at a target BER.

To determine the design challenges and quantify performance gains from real-time sub-carrier AMC, a wideband OFDM transceiver prototype is built for the WiGLAN system, and measurements are taken in a real environment.

The WiGLAN digital baseband modem is implemented on a Xilinx Virtex 4 FPGA and interfaced through the DAC and ADC with a custom-made RF Front End. Table 7.1 shows a summary of WiGLAN system specifications. The entire digital transceiver design uses 439,988 2-input NAND gates clocked at 128 MHz on the FPGA. Chapter 3 shows that the AMC scheme occupies **9.95%** of the total gates in the transceiver design. This indicates that the AMC implementation incurs a low

Parameter	*Value*
Carrier frequency	5.247 GHz
Sampling frequency	128 MHz
Sub-carrier frequency spacing	1 MHz
Number of data sub-carriers	92
Number of pilot sub-carriers	8
IFFT/FFT period	1 μs
Cyclic Prefix	0.4 μs
OFDM symbol period	1.4 μs
Coded BER	10^{-5}
Modulation per bin	BPSK, 4-, 16-, 64-QAM
Error Correction Scheme	Punctured Convolutional Encoder Code rate = {1/2, 3/4, 5/6} 3-bit Soft-decision Viterbi Decoder
Max Link Distance	10 m

Table 7.1: WiGLAN System Specifications.

additional complexity.

Using our prototype transceiver nodes, measurements are taken in an indoor environment. We found that the success of the AMC technique requires accounting correctly for the unavoidable SNR mismatches that exist between SNR estimation step and the data transmission step. While there is an inherent SNR mismatch due to the accuracy of SNR estimation, other sources of SNR mismatch include RF Front End non-idealities and compensation capabilities of time and frequency synchronization algorithms in the baseband receiver. An efficient AMC scheme calls for a precise timing acquisition, which can be obtained by using fine symbol timing algorithms and minimizing the amount of uncompensated SFO by using a single and accurate oscillator to generate the carrier and sampling clocks. In our prototype, due to lack of the above two solution designs, the higher timing error is tolerated by using a CP that is 40% of the useful OFDM symbol period, which is higher than the reasonable amount (25%). Chapter 4 presents a protocol to measure sufficient levels of SNR_{margin} to account for the SNR mismatches.

Chapters 4 and 6 report measurement results when the WiGLAN nodes (with a maximum transmit RF power of 7.5 dBm) are used with uncoded sub-carrier Adaptive

Modulation and AMC schemes respectively. The analysis shows that the sub-carrier AMC WiGLAN system with target coded BER = 10^{-5}, achieves:

- Average raw data rates - *i.e.* (Number of Bits per OFDM)/(1 μs) - of 308.3 Mbps and 237.1 Mbps across a variety of LOS (1.0 to 5.8 meters) and NLOS locations (1.0 to 10.8 meters).

- Average gains of **34%** and **40%** over the best non-adaptive scheme respectively. The higher gain in NLOS locations is due their higher frequency diversity. The best non-adaptive scheme chooses a single modulation type and code rate for all capable sub-carriers that meet the target BER, and it chooses the mod./code that gives the highest data rate. Hence, as the best non-adaptive technique is still adaptive to some extent, the reported gains from AMC are conservative results. Thus, higher gains are expected with respect a true non-adaptive scheme that does not have knowledge of the sub-carrier SNRs.

- Average spectral efficiency of 3.42 and 2.7 bits/s/Hz in LOS and NLOS locations respectively. Thus, using the average data rate gains above, the average spectral efficiency from the best non-adaptive scheme is 2.55 and 1.93 bits/s/Hz in LOS and NLOS scenarios.

- Average SNR gain of **3 dB** over the best non-adaptation scheme. This is obtained by plugging the average spectral efficiency ρ values in the capacity formula $\rho = log_2(1 + SNR)$ to find SNR and taking the difference. Although the absolute SNR values are capacity-approaching values, their difference reasonably quantifies the performance gain.

We note that in a LOS scenario, the AMC SNR gain of 3 dB can increase the throughput by 34% or it can be used to increase the link distance by 41% using the Path Loss-Distance relation [39]:

$$\text{Path Loss} \propto (\text{Distance})^n \tag{7.1}$$

where n, the path-loss exponent, is chosen 2 for LOS. In fact, 3 dB gain of SNR cannot be achieved from increasing the output power of a linear PA since even a 1 dB improvement is exceedingly difficult and the PA is driven into its saturation region. Instead, getting an SNR gain of 3 dB requires using capacity-approaching codes such as Turbo or LDPC codes.

Furthermore, adapting the modulation type alone (AM) provides higher gains than adapting coding only (AC). In other words, most of the gain of AMC is from adaptive modulation. Fig. 7-1 shows the total number of bits per OFDM using AMC, and the best AM, AC, and non-adaptive schemes for locations in NLOS and LOS environments. Similar to the best non-adaptive scheme, the best AM or AC is the modulation-only or coding-only adaptation that gives the highest data rate. The data rate gain from the best AC and AM over the best non-adaptive scheme is on average 11% and 29% respectively in NLOS environment, and it is 9% and 28% respectively in LOS environment.

When the overhead from AMC synchronization setup time between the transmitter and receiver is taken into account, the raw data rates will be reduced by **1.1%**. This assumes that data packets are sent until the channel coherence time of 10 ms, when the CSI has to be refreshed. The overheads due to AM and AC schemes are close to that of the AMC scheme. Finally, including AMC synchronization overhead as well as the CP and preamble per packet, the data throughput is 71% and 80% of the raw data-rate for CP of 0.4 μs and 0.25 μs (in the better design) respectively.

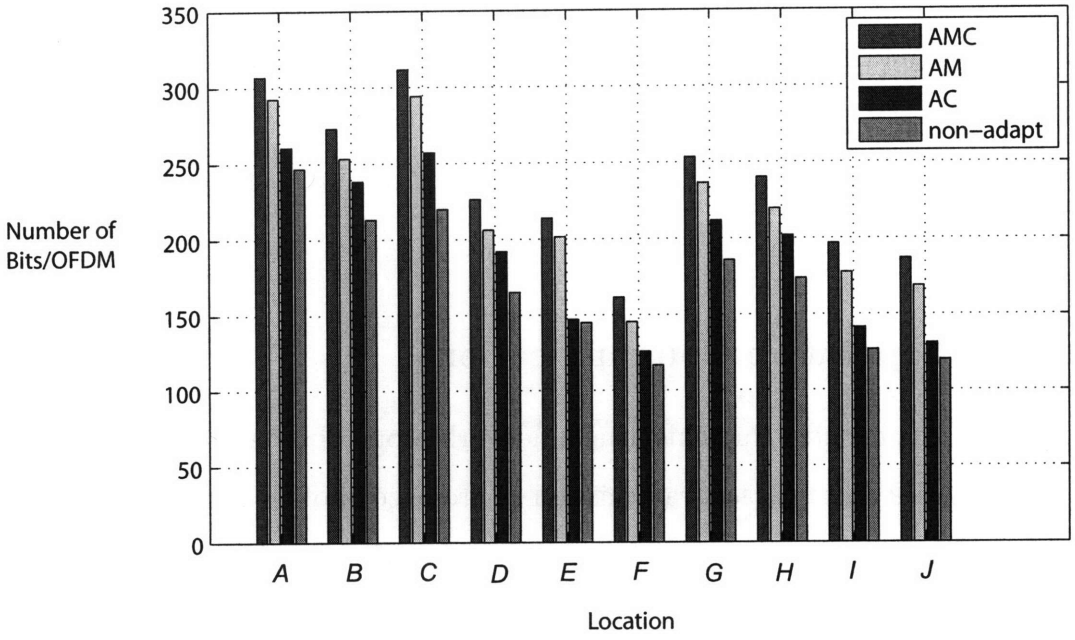

(a) NLOS

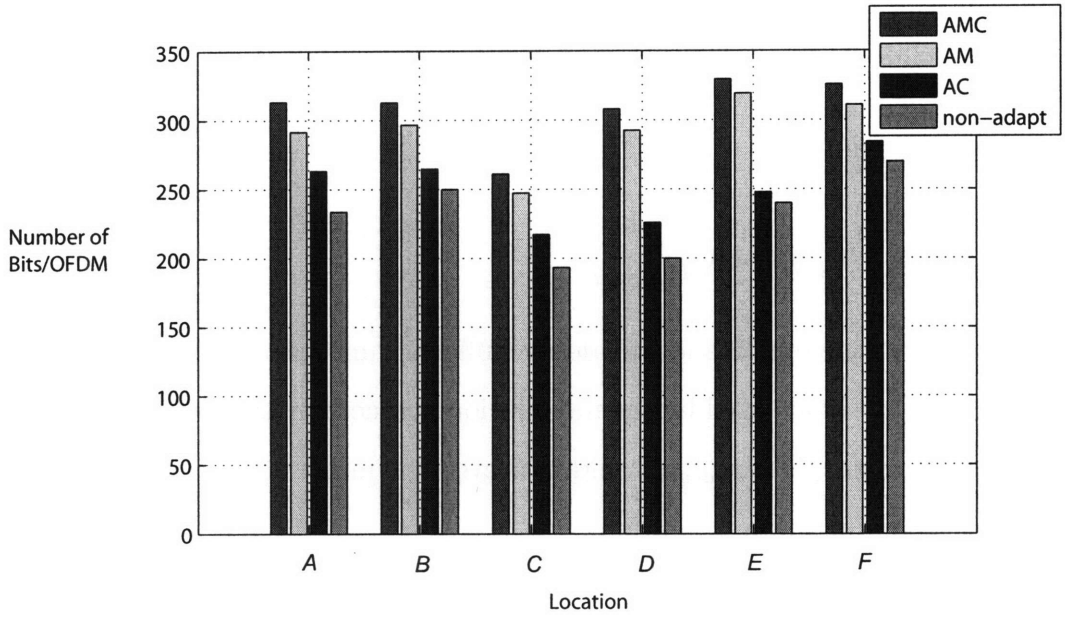

(b) LOS

Figure 7-1: Number of bits per OFDM for various adaptation schemes for each location in (a)NLOS and (b)LOS scenarios. Leftmost bar to rightmost bar: number of bits per OFDM from AMC, and the best AM, AC, and non-adaptive schemes.

7.2 Future Research

In this work, we proved the value of implementation of a real-time AMC technique in providing insights on practical design issues and attainable performance gains in a real system. Similarly, using this system in investigation of other techniques can provide valuable contribution. Some of the research opportunities that can be exploited are described in the following sub-sections.

7.2.1 Cooperative Communications

Future research includes implementing a network protocol layer on the AMC-capable WiGLAN nodes that enables transmission in presence of other wireless LAN systems in the environment in a cooperative manner. In other words, since the WiGLAN system's bandwidth (128 MHz) is higher than other wireless LAN standards (20 or 40 MHz), during SNR estimation phase, the WiGLAN transceiver identifies the bandwidths already in use by another wireless system and sends data on the available sub-carriers. Prof. Dina Katabi's group at MIT is currently investigating this cooperative communications using WiGLAN transceiver nodes.

7.2.2 Analysis of SNR_{margin}

Our work showed the importance of adding sufficient amounts of SNR_{margin} in calculation of SNR thresholds used by the modulation and coding assigner. We proposed a methodology to find $\{SNR_{margin}\}$, and indicated the major sources of noise affecting it with corresponding design solutions.

To fully utilize the potential of AMC in increasing the throughput, a *minimum* amount of SNR_{margin} is desirable. Hence, more work is needed to precisely characterize all the sources of SNR mismatch from hardware and algorithm non-idealities. For instance, we characterized the effect of our channel and noise-variance estimators on SNR mismatch. However, we did not quantify the relationship between our timing and frequency synchronization algorithms and SNR mismatch levels. It is expected that these noise sources affect SNR mismatch levels in a coupled fashion.

Such analysis can first be done through a simulation tool that carefully models all the noise sources on actual hardware, where the effect of each noise source independently and together can be quantified. Finally, the results should be verified in the real environment.

Such analysis would not only determine the minimum SNR_{margin} levels, but it would also provide tolerance levels on the accuracy of hardware components, such as the sampling and carrier frequency oscillators, and the baseband algorithms. The resulting design will enable AMC to achieve its maximum attainable throughput.

7.2.3 Power Adaptation

In our AMC scheme, the transmit RF power level was maintained constant across all sub-carriers - regardless of the modulation. As mentioned in Chapter 3, Wu [49] proposed a power re-allocation policy that provided gains in data rate of 13.2% when the power of 8 NULL sub-carriers was re-allocated to the sub-carriers that would guarantee a modulation level upgrade. This indicates that simple, yet intelligent, power adaptation policies can be implemented that would further improve the performance of AMC with no power adaptation. The data rate gain from power adaptation depends on the operating SNR, where higher gains are expected at lower SNR values. This is because at high SNR regime, spectral efficiency, ρ, is related to capacity-approaching SNR as $\rho \approx log_2(SNR)$. Hence, a factor 2 increase in SNR (or 3-dB) increases the data rate by 1 bit/s/Hz. On the other hand, at low SNR regime, $\rho \approx SNR$, and hence, a factor of 2 increase SNR increases the data rate by 2 bit/s/Hz.

7.2.4 Capacity-approaching Error Correction Codes

As we mentioned, most of the current work on FEC codes in OFDM systems is on design of capacity-approaching codes, such as LDPC codes, most suitable for such systems. For instance, LDPC codes are optimum error correction methods in the Wireless LAN 802.11a and 802.11n standards and Mobile Wireless Broadband

Access standard, WiMAX. Some of desirable characteristics from LPDC codes in adaptive OFDM systems include *high code rate*, *flexibility*, *implementation feasibility*, and *robustness* to channel estimation errors.

The benefit of these stronger codes is that their higher coding gains enable assignment of more sub-carriers to higher level modulations, which result in an increased throughput. In such coded systems, modulation levels higher than 64-QAM up to 1024-QAM or higher might become possible [34].

In the context of AMC scheme in an OFDM system, the improvement in performance from *adapting* LDPC codes in a *feasible* fashion remains to be investigated. For instance, one might find that due to the already high coding gains from such codes, the adaptation would provide negligible increase in throughput.

Appendix A

Acronyms

ADC Analog-to-Digital Converter

ADSL Asymmetric Digital Subscriber Line

AMC Adaptive Modulation and Coding

ARQ Automatic Repeat reQuest

AWGN additive white Gaussian noise

BCH Bose, Ray-Chaudhuri, Hocquenghem

BER Bit Error Rate

BPSK Binary Phase-Shift Keying

CFO Carrier Frequency Offset

COFDM Coded OFDM

CP Cyclic Prefix

CRC Cyclic Redundancy Check

CSI Channel State Information

DAB Digital-Audio-Broadcasting

DAC Digital-to-Analog Converter

DFT Discrete Fourier Transform

DMB Digital-Multimedia-Broadcasting

DMT Discrete-Multi-Tone

DSL Digital Subscriber Line

DVB Digital-Video-Broadcasting

FDD Frequency Division Duplexing

FEC Forward Error Correction

FFT Fast Fourier Transform

FPGA Field Programmable Gate Array

HDSL High bit-rate DSL

HIPERLAN High Performance LAN

HT High Throughput

ICI Inter-Carrier Interference

IF intermediate-frequency

IFFT Inverse Fast Fourier Transform

ISI Inter-Symbol Interference

LAN Local Area Network

LDPC Low-Density Parity-Check

LOS Line-of-Sight

LS Least Squares

LSB Least Significant Bits

LTI linear and time-invariant

ML Maximum Likelihood

NLOS Non Line-of-Sight

OFDM Orthogonal Frequency Division Multiplexing

OFDMA Orthogonal Frequency Division Multiple Access

MIMO Multiple-Input Multiple-Output

PA Power Amplifier

PAPR Peak-to-Average Power Ratio

PCB printed circuit boards

PDF probability distribution function

PPM parts-per-million

QAM Quadrature Amplitude Modulation

RF radio-frequency

RCPC Rate-Compatible Punctured Convolutional codes

RTL Register Transfer Level

ROM Read-Only-Memory

SFO Sampling Frequency Offset

SNR Signal-to-Noise Ratio

TCM Trellis Coded Modulation

TDD Time Division Duplexing

VDSL Very high-speed DSL

VGA variable gain amplifier

WiGLAN Wireless Giga-bit Local Area Network

Bibliography

[1] I. P802.11n/D1.06, *Draft Amendment to Standard for Information Technology - Telecom. and Information Exchange Between Systems - Local and Metropolitan Area Networks - Specific Requirements - Part 11: Wireless LAN Medium Access Control (MAC) and Physical Layer (PHY) Specifications: Enhancements for Higher Throughput*, November 2006.

[2] P802.16-2004/Cor2/D4, *Draft Standard for Local and Metropolitan Area Networks. Part 16: Air Interface for Fixed and Mobile Broadband Wireless Access Systems: Corrigndum 2*, 22 May 2007.

[3] D. Tse and P. Viswanath, *Fundamentals of Wireless Communication.* United Kingdom: Cambridge University Press, 2005.

[4] C. E. Shannon, "A mathematical theory of communication," *Bell System Technical Journal*, vol. 27, pp. 379–423, 623–656, July - October 1948.

[5] E. Crozier and A. Kelin, "Wimax's technology for los and nlos environments," *WiMAX Forum.*

[6] P. S. Chow, J. C. Tu, and J. M. Cioffi, "Performance evaluation of a multichannel transceiver system for ADSL and VHDSL services," *IEEE Journal on Selected Area in Communications*, vol. 9, no. 6, pp. 909–919, August 1991.

[7] J. S. Chow, J. C. Tu, and J. M. Cioffi, "A discrete multitone transceiver system for HDSL applications," *IEEE Journal on Selected Areas in Communications*, vol. 9, no. 6, pp. 895–908, August 1991.

[8] A. Goldsmith, *Wireless Communications.* New York: Cambridge University Press, 2005.

[9] J. F. Hayes, "Adaptive feedback communications," *IEEE Transactions on Communications Technology*, vol. 16, no. 1, pp. 29–34, 1968.

[10] J. K. Cavers, "Variable-rate transmission for rayleigh fading channels," *IEEE Transactions on Communications*, vol. 20, no. 1, pp. 15–22, February 1972.

[11] I. Kalet, "The multitone channel," *IEEE Transactions on Communications*, vol. 27, pp. 119–124, February 1989.

[12] A. Cyzlwik, "Adaptive OFDM for wideband radio channels," in *Proceedings of IEEE Global Telecommunications Conference*, 18-22 November 1996, pp. 713–718.

[13] P. S. Chow, J. M. Cioffi, and J. A. C. Bingham, "A practical discrete multitone transceiver loading algorithm for data transmission over spectrally shaped channels," *IEEE Transactions on Communications*, vol. 43, no. 234, pp. 773–775, February/March/April 1995.

[14] R. G. Gallager, *Information Theory and Reliable Communication.* New York, NY: Wiley, 1968.

[15] D. Hughes-Hartogs, *Ensemble Modem Structure for Imperfect Transmission Media*, U.S. Patents no. 4,679,227 (July 1987), 4,731,816 (March 1988), and 4,833,706 (May 1989).

[16] J. A. Bingham, "Multicarrier modulation for data transmission: An idea whose time has come," *IEEE Communications Magazine*, vol. 28, no. 5, pp. 5–14, May 1990.

[17] R. F. Fischer and J. B. Huber, "A new loading algorithm for discrete multitone transmission," in *Proceedings of IEEE Global Telecommunications Conference (GlobeCom)*, vol. 1, 18-22 November 1996, pp. 724–728.

[18] L. Piazzo, "Fast algorithm for power and bit allocation in OFDM systems," *IEEE Electronic Letters*, vol. 35, no. 25, pp. 2173–2174, 9 December 1999.

[19] L. Van der Perre, S. Thoen, P. Vandenameele, B. Gyselinckx, and M. Engels, "Adaptive loading strategy for a high speed OFDM-based WLAN," in *Proceedings of IEEE Global Telecommunications Conference (GlobeCom)*, vol. 4, 8-12 November 1998, pp. 1936–1940.

[20] I. S. 802.11a 1999, *Supplement to IEEE Standard for Information Technology - Telecomm. and Information Exchange Between Systems - Local and Metropolitan Area Networks - Specific Requirements - Part 11: Wireless LAN Medium Access Control (MAC) and Physical Layer (PHY) Specifications: High-speed Physical Layer in the 5 GHz Band*, 1999.

[21] J. G. Andrews, A. Ghosh, and R. Muhamed, *Fundamentals of WiMAX: Understanding Broadband Wireless Networking*, T. Rappaport, Ed. Upper Saddle River, NJ: Prentice Hall Communications Engineering and Emerging Technologies Series, 2007.

[22] T. Starr, J. M. Cioffi, and P. J. Silverman, *Understanding Digital Subscriber Line Technology*, T. Rappaport, Ed. Upper Saddle River, NJ: Prentice Hall Communications Engineering and Emerging Technologies Series, 1999.

[23] M. Wouters, G. Vanwijnsberghe, P. V. Wesemael, T. Huybrechts, and S. Thoen, "Real time implementation on FPGA of an OFDM based wireless LAN modem extended with adaptive loading," in *Proceedings of the 28th European Solid-State Circuits Conference*, 24-26 September 2002, pp. 531–534.

[24] J. Veillcux, P. Fortier, and S. Roy, "An FPGA implementation of an OFDM adaptive modulation system," in *Proceedings of the 3rd International IEEE-NEWCAS Conference*, 19-22 June 2005, pp. 353–356.

[25] J. Zheng, "Analysis of coded OFDM system over frequency-selective fading channels," Master's thesis, Texas A&M Univeristy, August 2003.

[26] W. Y. Zou and Y. Wu, "COFDM: an overview," *IEEE Transactions on Broadcasting*, vol. 41, no. 1, pp. 1–8, March 1995.

[27] J. G. Proakis, *Digital Communications*, 4th ed. New York, NY: McGraw-Hill, 2001.

[28] S. K. Lai, R. S. Chen, K. B. Lataief, and R. D. Murch, "Adaptive trellis coded MQAM and power optimization for OFDM transmission," in *Proceedings of IEEE Vehicular Technology Conference*, vol. 1, 16-20 May 1999, pp. 290–294.

[29] Y. J. Zhang and K. B. Lataeif, "Single- and multi-user adaptive pragmatic trellis coded modulation for OFDM system," in *Proceedings of IEEE Wireless Communications and Networking Conference*, vol. 1, 16-20 March 2003, pp. 9–14.

[30] G. Ungerboeck, "Channel coding with multilevel/phase signals," *IEEE Transactions on Information Theory*, vol. 28, no. 1, p. 55, 1982.

[31] V. K. N. Lau and M. D. Macleod, "Variable-rate adaptive trellis coded QAM for flat-fading channels," *IEEE Transactions on Communications*, vol. 49, pp. 1550–1560, September 2001.

[32] *ITU (G.992.1) Series G: Transmission Systems and Media, Digital Systems and Networks. Digital transmission systems - Digital sections and digital line system - Access Networks. Asymmetric digital subscriber line (ADSL) transceivers*, ITU-T, June 1999.

[33] *ITU-T (G.993.2) Series G: Transmission Systems and Media, Digital Systems and Netowrks. Digital sections and digital line system - Access networks - Very high speed digital subscriber line transceivers 2 (VDSL2)*, ITU-T, February 2006.

[34] Y. Li and J. Moon, "Increasing data rates through iterative coding and antenna diversity in OFDM-based wireless communication," in *Proceedings of IEEE Conference on Global Telecommunications (GlobeCom)*, vol. 5, November 2001, pp. 3130–3134.

[35] V. Mannoni, D. Declercq, and G. Gelle, "Optimized irregular low-density parity-check codes for multicarrier modulations over frequency-selective channels," *EURASIP Journal on Applied Signal Processing*, vol. 204, no. 10, pp. 1546–1556, 2004.

[36] H. Futaki and T. Ohtsuki, "Performance of low-density parity-check (LDPC) coded OFDM systems," in *Proceedings of IEEE International Conference on Communications (ICC)*, vol. 3, 2002, pp. 1696–1700.

[37] E. Eleftheriou and S. Olcer, "Low-density parity-check codes for digital subscriber lines," in *Proceedings of IEEE International Conference on Communications (ICC)*, vol. 3, 2002, pp. 1752–1757.

[38] E. Eleftheriou, S. Olcer, and H. Sadjadpour, "Application of capacity approaching coding technique to digital subscriber lines," *IEEE Communications Magazine*, vol. 42, no. 4, pp. 88–94, April 2004.

[39] T. S. Rappaport, *Wireless Communications: Principles & Pratice.* New Jersey: Prentice Hall, Inc., 1996.

[40] J. K. Tan, "An adaptive orthogonal frequency division multiplexing baseband modem for wideband wireless channels," Master's Thesis, Massachusetts Institute of Technology, Department of Electrical Engineering and Computer Science, May 2006.

[41] S. S. Ghassemzadeh, R. Jana, C. W. Rice, W. Turin, and V. Tarokh, "Measurement and modeling of an ultra-wide bandwidth indoor channel," *IEEE Transactions on Communications*, vol. 52, no. 10, pp. 1786–1796, 2004.

[42] Xilinx, *Virtex-4 User Guide*, 10 September 2004.

[43] C. J. Meyer, "Measuring the peak-to-average power of digitally modulated signals," Boonton Electronics, Application Note AN-50, 1 April 1993.

[44] J. Terry and J. Heiskala, *Wireless OFDM LANs: A Theoretical And Practical Guide.* Indianapolis, IN: Sams Publishing, 2002.

[45] T. M. Schmidl and D. C. Cox, "Low-overhead, low-complexity [burst] synchronization for OFDM," in *Proceedings of IEEE International Conference on Communications*, vol. 3, Dallas, TX, June 1996, pp. 1301–1306.

[46] M. Speth, S. A. Fechtel, G. Fock, and H. Meyr, "Optimum receiver design for wireless broadband systems using OFDM-part I," *IEEE Transactions on Communications*, vol. 47, no. 11, pp. 1668–1677, November 1999.

[47] N. Matalon, "An implementation of a 5.25 GHz transceiver for high data rate wireless applications," Master's Thesis, Massachusetts Institute of Technology, Department of Electrical Engineering and Computer Science, July 2005.

[48] A. J. Goldsmith and S.-G. Chua, "Variable rate variable power MQAM for fading channels," *IEEE Transactions on Communications*, vol. 45, no. 10, pp. 1218–1230, October 1997.

[49] Y. Wu, "Null power reallocation for data rate improvement in a wireless multicarrier system," Master's Thesis, Massachusetts Institute of Technology, Department of Electrical Engineering and Computer Science, August 2007.

[50] M. Rice and S. B. Wicker, "Adaptive error control for slowly varying channels," *IEEE Transactions for Communications*, vol. 42, no. 234, Part 2, pp. 917–926, February-April 1994.

[51] Y. Teng, T. Nagaosa, K. Mori, and H. Kobayashi, "Grouping adaptive modulation method for burst mode OFDM transmission system," in *Proceedings of IEEE Region 10 Conference on Computers, Communications, Control and Power Engineering (TENCON'02)*, vol. 2, October 2002, pp. 929–932.

[52] A. P. Kannu, T. Sivanadyan, and S. Subramaniam, "Performance of block adaptive modulation schemes for OFDM based WLAN systems," in *Proceedings of*

IEEE International Conference on Personal Wireless Communications, 15-17 December 2002, pp. 6–10.

[53] B. Sklar, *Digital Communications Fundamentals and Applications*, 2nd ed. Upper Saddle River, NJ: Prentice Hall, 2001.

[54] Wikipedia, "Walking - wikipedia, the free encyclopedia," Online, 26 September 2007, available: http://en.wikipedia.org/wiki/Walking.

[55] A. Leon-Garcia, *Probability and Random Processes for Electrical Engineering*, 2nd ed. Addison-Wesley, May 1994.

[56] S. Lin and D. J. Costello, *Error Control Coding*, 2nd ed. Upper Saddle River, NJ: Pearson Education, Inc., 2004.

[57] Y. Yasuda, K. Kashiki, and Y. Hirata, "High-rate punctured convolutional codes for soft decision decoding," *IEEE Transactions on Communications*, vol. 32, no. 3, pp. 315–319, March 1984.

[58] J. Hagenauer, "Rate-compatible punctured convolutional codes (RCPC codes) and their applications," *IEEE Transactions on Communications*, vol. 36, no. 4, pp. 389–400, April 1988.

[59] J. Omura, "On the viterbi deocding algorithm," *IEEE Transactions on Information Theory*, vol. 15, no. 1, pp. 177–179, January 1969.

[60] K. J. Larsen, "Short convolutional codes with maximal free distance for rates 1/2, 1/3, and 1/4 (corresp.)," *IEEE Transactions on Information Theory*, vol. 19, no. 3, pp. 371–372, May 1973.

[61] A. Lesea, "Bit error rate: What is it? what does it mean?" [On-line] Xilinx, Inc. TechXclusives.